
Physiologically Constrained Aerocapture for Manned Mars Missions

James Evans Lyne, Ames Research Center, Moffett Field, California

August 1992



National Aeronautics and
Space Administration

Ames Research Center
Moffett Field, California 94035-1000

ABSTRACT

Aerobraking has been proposed as a critical technology for manned missions to Mars. The variety of mission architectures currently under consideration presents aerobrake designers with an enormous range of potential entry scenarios. Two of the most important considerations in the design of an aerobrake are the required control authority (lift-to-drag ratio) and the aerothermal environment which the vehicle will encounter. Therefore, this study examined the entry corridor width and stagnation-point heating rate and load for the entire range of probable entry velocities, lift-to-drag ratios, and ballistic coefficients for capture at both Earth and Mars.

To accomplish this, a peak deceleration limit for the aerocapture maneuvers had to be established. Previous studies had used a variety of load limits without adequate proof of their validity. Existing physiological and space flight data were examined, and it was concluded that a deceleration limit of 5 G was appropriate.

When this load limit was applied, numerical studies showed that an aerobrake with an L/D of 0.3 could provide an entry corridor width of at least 1 degree for all Mars aerocaptures considered with entry velocities up to 9 km/s. If 10 km/s entries are required, an L/D of 0.4 to 0.5 would be necessary to maintain a corridor width of at least 1 degree. For Earth return aerocapture, a vehicle with an L/D of 0.4 to 0.5 was found to provide a corridor width of 0.7 degree or more for all entry velocities up to 14.5 km/s.

Aerodynamic convective heating calculations were performed assuming a fully catalytic, "cold" wall; radiative heating was calculated assuming that the shock layer was in thermochemical equilibrium. Heating rates were low enough for selected entries at Mars that a radiatively cooled thermal protection system might be feasible, although an ablative material would be required for most scenarios. Earth return heating rates were generally more severe than those encountered by the Apollo vehicles, and would require ablative heat shields in all cases.

ACKNOWLEDGEMENTS

I would like to express my deep appreciation to Professor Michael Tauber for his daily and untiring guidance over the last two years and to Dr. Malcolm Cohen for the frequent support and advice he provided on the physiological aspects of this study. I also am greatly indebted to Dr. Fred DeJarnette for encouraging me to return to graduate school after a long hiatus from engineering and for making my doctoral program as pleasant an experience as I could have hoped for. Professor Wayland Griffith provided excellent advice on the overall direction for my dissertation research very early in the process and helped me to formulate a plan which would involve my interests in both aeronautics and physiology. Bobby Braun of NASA Langley provided frequent and detailed technical advice on numerous issues and helped to correct several errors in the study. All work was supported by a graduate research assistantship from NASA Grant NAGW-1331 to the Mars Mission Research Center at North Carolina State University.

TABLE OF CONTENTS

List of Tables	vii
List of Figures	viii
NOMENCLATURE	xi
I. INTRODUCTION	1
A) Potential Mission Architectures	2
B) Aerobraking Technology	3
i) Constraints on Aerocapture Maneuvers	5
ii) Corridor Width Determinants and Requirements ..	5
iii) The Use of Lift Modulation to Maximize Corridor Width	7
iv) Target Orbit Selection	9
v) Selected Aerobrake Design Considerations	10
vi) Atmospheric Structure	12
vii) Interplanetary Navigation Schemes	13
viii) Launch Opportunities and Atmospheric Entry Velocities	14
II. OBJECTIVES	16
III. ANALYSIS	18
A) Atmospheric Models	18
B) Equations of Motion	20

C) Aerodynamic Heating	21
i) Convective Heating	22
ii) Radiative Heating	23
IV. PHYSIOLOGICAL ASPECTS OF AEROBRAKING	26
A) Introduction	26
B) Acceleration Physiology	27
i) Normal Response to Acceleration	27
ii) Acceleration Tolerance Limits	29
iii) High G Countermeasures	33
C) Physiological Changes Induced By Weightlessness	34
i) Cardiovascular/Fluid Alterations	34
ii) The Bedrest Analog for Microgravity	37
D) Countermeasures for Zero G Deconditioning	38
E) Effects of Microgravity on Acceleration Tolerance	41
i) Ground-Based Studies	41
ii) Flight Data	42
F) Conclusions and Recommendations	44
IV. METHODOLOGY	46
A) Trajectory Calculations and Requirements	46
B) Heating Calculations	49

V. RESULTS 51

 A) Mars Arrival Aerocapture 51

 i) Entry Corridors 52

 ii) Aerodynamic Heating 53

 iii) Impact of Martian Parking Orbit Selection 55

 B) Earth Return Aerocapture 57

VI. CONCLUSIONS AND RECOMMENDATIONS 61

References 64

Tables 1-9

Figures 1-40

Appendix 1: Convective Heating Calculations

Appendix 2: Computer Algorithm Logic

Appendix 3: Listings of Computer Codes

LIST OF TABLES

TABLE 1.	MARTIAN ATMOSPHERIC DENSITY PROFILE CONSTANTS
TABLE 2.	CONSTANTS FOR CONVECTIVE HEATING EQUATION
TABLE 3.	CONSTANTS FOR RADIATIVE HEATING EQUATION
TABLE 4.	RADIATIVE HEATING VELOCITY FUNCTIONS FOR EARTH AND MARS
TABLE 5.	PHYSIOLOGICAL EFFECTS OF G LOADS
TABLE 6.	RANGE OF PARAMETERS FOR AEROCAPTURE STUDY
TABLE 7.	VARIATION OF NOSE RADIUS WITH L/D FOR MARS AEROBRAKES
TABLE 8.	UNDERSHOOT TRAJECTORY PEAK STAGNATION- POINT HEATING RATE FOR VARIOUS TARGET ORBITS
TABLE 9.	OVERSHOOT TRAJECTORY INTEGRATED STAGNATION-POINT HEAT LOAD FOR VARIOUS TARGET ORBITS

LIST OF FIGURES

- FIGURE 1. ENTRY CORRIDOR
- FIGURE 2. REQUIRED MARS AEROBRAKE L/D VS DECELERATION LIMIT
- FIGURE 3. VEHICLE CLASSES FOR PITCH CONTROL
- FIGURE 4. L/D VS BALLISTIC COEFFICIENT
- FIGURE 5. POTENTIAL CAPTURE ORBITS
- FIGURE 6. EFFECT OF ENTRY ALTITUDE ON ENTRY ANGLE
- FIGURE 7. VARIATION OF VEHICLE L/D WITH REYNOLDS NUMBER
- FIGURE 8. HEMISPHERICAL STAGNATION-POINT HEATING RATES IN CARBON DIOXIDE
- FIGURE 9. PHYSIOLOGICAL FORCE AXES
- FIGURE 10. ARTERIAL OXYGEN SATURATION
- FIGURE 11. APOLLO G LOAD DESIGN LIMITATIONS
- FIGURE 12. EXPECTED GEMINI G LOAD PROFILE
- FIGURE 13. APOLLO EARTH ORBITAL REENTRY G PROFILE
- FIGURE 14. CALCULATED SOYUZ T10-B REENTRY G PROFILE
- FIGURE 15. UNDERSHOOT TRAJECTORY LIFT MODULATION
- FIGURE 16. EARTH RETURN ENTRY CAPSULES
- FIGURE 17. TYPICAL MARS AEROCAPTURE TRAJECTORIES
- FIGURE 18. MARS AEROCAPTURE AND SOYUZ REENTRY G PROFILES

- FIGURE 19. MARS AEROCAPTURE HEATING RATE PROFILES
- FIGURE 20. MARS AEROCAPTURE UNDERSHOOT TRAJECTORY ROLL ANGLE HISTORY
- FIGURE 21. MARS AEROCAPTURE CORRIDOR WIDTH VS BALLISTIC COEFFICIENT
- FIGURE 22. CORRIDOR WIDTH VS L/D FOR AEROCAPTURE AT MARS
- FIGURE 23. CORRIDOR WIDTH VS ENTRY VELOCITY FOR AEROCAPTURE AT MARS
- FIGURE 24. MARS AEROCAPTURE UNDERSHOOT TRAJECTORY PEAK STAGNATION-POINT HEATING RATE
- FIGURE 25. MARS AEROCAPTURE OVERSHOOT TRAJECTORY INTEGRATED STAGNATION-POINT HEAT LOAD
- FIGURE 26. MARS AEROCAPTURE CORRIDOR WIDTH VS PARKING ORBIT PERIOD
- FIGURE 27. MARS AEROCAPTURE CORRIDOR WIDTH VS ENTRY VELOCITY
- FIGURE 28. CORRIDOR WIDTH VS ENTRY VELOCITY BALLISTIC COEFFICIENT = 500 kg/m^2
- FIGURE 29. TYPICAL EARTH RETURN AEROCAPTURE TRAJECTORIES
- FIGURE 30. G LOADS FOR EARTH RETURN AEROCAPTURE AND SOYUZ REENTRY
- FIGURE 31. EARTH RETURN UNDERSHOOT TRAJECTORY BANK ANGLE PROFILE
- FIGURE 32. EARTH RETURN HEATING RATE PROFILES
- FIGURE 33. CORRIDOR WIDTH VS ENTRY VELOCITY FOR EARTH RETURN AEROCAPTURE

- FIGURE 34. EARTH RETURN CORRIDOR WIDTH FOR VARIOUS CAPTURE ORBITS
- FIGURE 35. CORRIDOR WIDTH VS L/D FOR EARTH RETURN AEROCAPTURE
- FIGURE 36. PEAK STAGNATION-POINT HEATING RATE VS ENTRY VELOCITY FOR THE EARTH RETURN UNDERSHOOT TRAJECTORY
- FIGURE 37. PERCENT OF PEAK HEATING DUE TO RADIATION FOR THE EARTH RETURN UNDERSHOOT TRAJECTORY
- FIGURE 38. STAGNATION-POINT PEAK HEATING RATE VS BALLISTIC COEFFICIENT FOR EARTH RETURN UNDERSHOOT TRAJECTORY
- FIGURE 39. STAGNATION-POINT INTEGRATED HEAT LOAD VS BALLISTIC COEFFICIENT FOR THE EARTH RETURN OVERSHOOT TRAJECTORY
- FIGURE 40. STAGNATION-POINT INTEGRATED HEAT LOAD VS ENTRY VELOCITY FOR THE EARTH RETURN OVERSHOOT TRAJECTORY

NOMENCLATURE

a	coefficient in radiative heating expression
A	entry vehicle reference area, m^2
b	coefficient in radiative heating expression
C_D	entry vehicle drag coefficient
C_1	coefficient in convective heating expression
C_2	coefficient in convective heating expression
C_3	coefficient in radiative heating expression
D	drag, Newtons
e	orbital eccentricity
F_A	aerodynamic force, Newtons
$f(V)$	function of velocity in radiative heating expression
g	acceleration due to gravity
g_0	acceleration due to gravity at the planet's surface
G	acceleration due to gravity at Earth's surface
h	altitude, m
h_0	reference altitude in expression for atmospheric density, m
h_1	freestream enthalpy, J/kg
h_T	total enthalpy, J/kg
h_w	wall enthalpy, J/kg

L	lift, Newtons
m	mass, kg
N	G load
q_c	stagnation-point convective heat transfer rate, W/cm^2
q_r	stagnation-point radiative heat transfer rate, W/cm^2
q_s	stagnation-point heat transfer rate, W/cm^2
r_n	entry vehicle nose radius
R_o	planetary radius
t	time after atmospheric entry, seconds
T_w	wall temperature, K
V	velocity, m/s
V_{ESCP}	planetary escape velocity
x,y,z	physiological axes for G loads

GREEK SYMBOLS

β	Atmospheric scale height, m^{-1}
Δ_γ	increment in entry angle in successive trajectory calculations (See Appendix 2)
ϵ	surface emissivity
ϕ	vehicle bank angle
ϕ_v	the bank angle when the vehicle velocity falls below the

	velocity threshold (See Appendix 2)
γ	Flight path angle, degrees
γ_E	atmospheric entry angle
γ_i	the initial, user-supplied entry angle (See Appendix 2)
γ_U	the undershoot angle
ρ	Atmospheric density, kg/m^3
ρ_0	Reference density value used in expression for atmospheric density, kg/m^3
ρ_1	Freestream density, kg/m^3
σ	Stefan-Boltzmann constant, $5.67 (10^{-12}) \text{ W / cm}^2 / \text{K}^4$

ACRONYMS

AFE	Aeroassist Flight Experiment
AOTV	Aeroassisted Orbital Transfer Vehicle
DSN	Deep Space Network
GLOC	G-Induced Loss of Consciousness
LBNP	Lower Body Negative Pressure
PALE	Pelvis and Leg Elevation
SMS	Space Motion Sickness
TPS	Thermal Protection System

INTRODUCTION

Manned missions to Mars have been a topic of great interest to both the scientific community and the general public since well before the beginning of the space age. The possibility of such a mission provided a great deal of inspiration to early leaders of the U.S. space program including Wernher von Braun (Ref. 1). Serious efforts to plan a Mars mission have been conducted by NASA intermittently over the last thirty years and have lead to an enormous range of potential mission designs and objectives. Several recent high-level reports including those of the National Commission on Space (Ref. 2), the Synthesis Group (Ref. 3), the Augustine panel (Ref. 4) and Dr. Sally Ride (Ref. 5) have examined issues of national space policy and concluded that a Mars mission should be given high priority. However, the recommendations of these reports regarding the most appropriate overall architecture for a Mars excursion have conflicted considerably. As a result, we are still in an embryonic phase of mission planning.

Nevertheless, the reasons for engaging in a manned excursion to Mars are diverse and compelling. It has long been recognized that the nation benefited considerably from the technology developed during the Apollo program. Another major space initiative would almost certainly generate similar valuable technological innovations. However, the potential for gaining a clearer understanding of the development and evolution of our home planet is an even stronger impetus for such an endeavor. Mars is by far the most similar of the planets to Earth; in addition, it is believed that the early

atmospheres of the two planets were quite similar, being principally composed of carbon dioxide and nitrogen. Moreover, the canyon systems on Mars suggest that large quantities of water were present in the past. Examining the divergent evolutions of these two planets should help scientists to gain a better understanding of the potential future development of Earth's atmosphere. This is particularly critical at this time of concern over possible atmospheric and climactic changes induced on Earth by human activity (Ref. 6).

POTENTIAL MISSION ARCHITECTURES

An enormous variety of overall designs have been proposed for manned excursions to Mars. The shortest of these are the sprint or opposition class missions which have total durations of 1 to 1.5 years and surface stays at Mars of 30 to 60 days (Ref. 3,7). At the other extreme are ambitious surface-exploration type architectures (often referred to as conjunction class missions) with total durations of up to three years and surface stays which may exceed 500 days (Ref. 8,9). Interplanetary trajectories may either be direct or include the use of a Venus swingby on the outbound or return leg (Ref. 10,11). This type of maneuver can be used to influence transit times, shorten mission duration, or decrease propellant requirements (thus decreasing the initial mass required in low Earth orbit). However, a Venus swingby would bring the spacecraft into closer proximity to the sun and increase the risk of unacceptably high levels

of radiation exposure to the crew in the event of a solar flare. Since these events cannot be accurately predicted, this is a serious disadvantage for architectures employing a swingby maneuver.

Several options have been proposed for the propulsion system. These include conventional chemical fuel engines, nuclear electric, nuclear thermal, and solar electric systems (Ref. 3,12,13). Vehicle deceleration may be accomplished either propulsively or with the use of aerodynamic drag. Obviously, the final choice of mission scenario must depend upon many considerations including cost, technical complexity, scientific rewards, and human factors issues.

AEROBRAKING TECHNOLOGY

One of the most important parameters in determining the cost of a mission to Mars is the initial weight which is required in low Earth orbit (LEO). Most early studies of Mars excursions involved the use of propulsive braking to slow the spacecraft upon arrival at Mars. However, this requires that the fuel for such a maneuver be taken into space as payload. The use of atmospheric drag rather than propulsion to decelerate a spacecraft upon arrival at its target planet was extensively studied by Chapman and others using analytic methods during the late 1950's (Ref. 14-17). Recent studies have shown that the use of this technique, known as aerobraking, could reduce the initial mass required in LEO for a manned Mars mission by 20 to 75 percent (Ref. 18-19). Although most modern mission

architectures call for aerobraking to a specific target orbit, rather than direct entry to the surface (as was considered in Ref. 14-17), the technique is quite similar, although the guidance requirements are somewhat more stringent for precise orbital insertion. To successfully accomplish an aerocapture maneuver, the spacecraft must dissipate enough energy in its initial pass through the atmosphere to be captured into a planetocentric orbit without overheating or subjecting the crew and structure to excessive deceleration loads. To accomplish this, the vehicle's entry angle must fall within a fairly narrow range known as the entry corridor (Fig. 1). If the angle is too shallow, the vehicle will fail to dissipate enough energy to be captured and will continue in a heliocentric orbit; conversely, if the angle is too steep, the vehicle will either overheat, hit the surface, or subject the crew and structure to an excessive deceleration load. The shallowest allowable entry angle is known as the overshoot boundary and the steepest as the undershoot boundary. For a lifting vehicle, the overshoot angle will be minimized by directing the lift downward throughout the atmospheric passage. To achieve the steepest possible entry angle, the vehicle's lift vector is directed upward during the initial portion of the trajectory and then modulated to place the vehicle into the desired orbit and prevent skipout (Ref. 20). The difference between the overshoot and undershoot boundaries is known as the entry corridor width.

Constraints on Aerocapture Maneuvers

The types of constraints which must be placed on an aerocapture maneuver depend upon the nature of the mission. For example, designers may choose to limit the peak heating rate in order to be able to employ a reusable thermal protection system (TPS) similar to that on the Space Shuttle. The integrated heat load could be constrained to control the amount of insulation required for a reusable TPS or the thickness of an ablative heat shield. To minimize the probability of a terrain impact or indirectly control aerodynamic heating, designers may also choose to limit the minimum altitude which the spacecraft may reach during its atmospheric trajectory. For manned missions, one of the most significant considerations is the limit on vehicle and crew deceleration since this typically determines the undershoot boundary (the vehicle is unable to enter any more steeply without exceeding this constraint). Deceleration limits are typically expressed in Gs where 1 G is the acceleration of gravity on the Earth's surface (9.806 m/s^2). Of course the most important requirement of an aerocapture maneuver is that it dissipate the correct amount of energy and place the vehicle into the desired target orbit.

Corridor Width Determinants and Requirements

Entry corridor width is a function of several factors; the most influential of these are the atmospheric entry velocity, the vehicle's lift to drag ratio (L/D), and the deceleration limit imposed on the trajectory. The entry velocity is the main determinant of the amount

of energy which must be dissipated during the atmospheric passage, and the vehicle's L/D reflects the degree to which the spacecraft can control this process; for example, a vehicle with a high L/D can capture at a relatively shallow angle since it is able to hold itself in the atmosphere more effectively than one with a low L/D. Similarly, by directing its lift upward, the high L/D vehicle is able to enter more steeply without violating the deceleration limit than one with low L/D. On the other hand, corridor width is inversely related to entry velocity and the required energy decrement. In general, as the arrival velocity increases, greater control authority (higher L/D) is required for a successful aerocapture maneuver. Other factors which exert second order effects on corridor width are the vehicle's ballistic coefficient ($m/C_D A$) and the energy of the orbit into which the spacecraft is captured.

The corridor width must be great enough to allow for inaccuracies in the approach navigation system (i. e. differences in the actual entry angle from its intended value), mispredictions of vehicle aerodynamics, and unexpected atmospheric conditions at the time of entry. It has generally been recommended that the the corridor width needed to allow for the navigational uncertainty be doubled to account for the latter two factors (Ref. 21). Each of these three issues is one of considerable complexity. For example, the accuracy of the approach navigation will depend upon the sophistication and expense of the system which is employed; similarly, our knowledge of the state of the Martian atmosphere will be determined by the investment made in precursor missions to study atmospheric

conditions. Large expenditures in these areas could lead to very small corridor width requirements and allow higher atmospheric entry velocities. Potential options for the approach navigation system and their accuracies will be discussed later.

The importance of the value chosen for the deceleration limit and its influence on the required aerobrake L/D is illustrated in Fig. 2. These calculations are for a typical aerocapture at Mars and assume a one degree entry corridor width requirement. This figure makes it apparent that the deceleration limit is a major determinant of the overall aerobrake design - perhaps *the most* influential factor.

The Use of Lift Modulation to Maximize Corridor Width

It has long been recognized that modulation of a vehicle's lift to drag ratio during atmospheric entry can lead to improved trajectory characteristics (Ref. 17,20). Several techniques have been proposed to accomplish this. Perhaps the first of these involved the use of flaps to modulate the drag of a conically shaped body (Ref. 17). It was found that this could decrease the peak G loads encountered during reentry by approximately 30 to 50 percent. More recently investigators have considered the use of angle of attack (Ref. 22) and bank angle (Ref. 23-25) variation to modulate vehicle L/D. (More precisely, changing bank angle does not effect vehicle L/D but only alters the direction of the lift vector; however, for simplicity, this effect will be referred to as a variation in L/D.) Significant increases in entry corridor width have been accomplished by applying bank angle modulation of vehicle L/D during atmospheric entry (Ref.

23). These gains are effected by increases in the undershoot angle rather than alterations in the overshoot boundary. The use of maximum available lift early in the trajectory (prior to perigee) allows steeper entries without exceeding G limitations than are possible with a fixed bank angle trajectory.

Pitch angle modulation has the disadvantage of requiring an additional fuel expenditure to fly at off-trim angles of attack. Moreover, the variation of ballistic coefficient with L/D inherent with pitch modulation complicates the guidance strategy somewhat. When considering this type of L/D modulation, it should be realized that there are two classes of vehicles (Fig. 3). For a winged configuration or a slender cone, the vehicle's longitudinal axis rotates in the opposite direction from the force vector as the vehicle pitches up to generate an upward lift (Fig. 3a); however, for a capsule type configuration, the longitudinal axis and the force vector rotate in the same direction as the vehicle pitches (Fig. 3b). This means that with pitch modulation, the force vector changes its orientation with respect to the vehicle significantly for the configurations such as that in Fig. 3a and only slightly for vehicles similar to that in Fig. 3b. For example, the Space Shuttle flies at an angle of attack of approximately 40 degrees with an L/D near 1.1; in this position, the force vector has rotated about 90 degrees from the vehicle's axis, whereas in the zero lift, zero angle of attack situation, these two axes are coincident. As will be discussed later, since human acceleration tolerance varies significantly with direction, it is desirable to maintain the force vector at a relatively

constant orientation with respect to a manned vehicle that is expected to encounter high G loads.

Target Orbit Selection

Over the last several years, significant efforts have been devoted to the issue of target orbit selection for Mars aerobraking (Ref. 26-28). These studies have examined the problem from an orbital mechanics point of view, considering issues such as orbital precession, spacecraft position for departure, and fuel requirements for the trans-Earth injection burn. From this perspective, the choice of target orbit (also referred to as parking orbit) is a matter of some debate. High, eccentric ($e=0.81$), long-period orbits such as a 1 sol or 24 hour orbit have the advantage of not placing the Earth return vehicle deep in the Martian gravity well; this significantly reduces propellant requirements for the escape delta-V (Ref. 26). However, more complex analysis has shown the advantages of orbits with low to moderate eccentricities (0.25 to 0.5) and shorter periods if high inclinations are desired to increase landing site options (Ref. 26).

Although, the choice of the orbit into which an aerobrake is captured has been extensively studied from an orbital mechanics perspective, little attention has been given to its effect on the aerocapture maneuver. However, recent studies of Earth return aerobraking have shown that the choice of target orbit impacts entry corridor width in certain cases (Ref. 29). This is intuitively apparent, since high, long period target orbits require less energy dissipation than lower orbits, and the resulting brief atmospheric

passes afford less opportunity to exert aerodynamic control. Moreover, in general, vehicle decelerations required to reach high target orbits are less severe than those which result from capture to low orbits; therefore, deceleration limits are more easily met in these cases, and more energetic entries are feasible.

Selected Aerobrake Design Considerations

Numerous issues must be considered in the design of an aerobraking vehicle (Ref. 30-32). Perhaps the most important of these is the amount of on-orbit work which is required to assemble the vehicle. This is particularly critical when it involves astronaut extravehicular activity since this is considered a high-risk activity. Recent proposals for Mars mission aerobrake designs range from winged vehicles similar to the Space Shuttle which could be launched fully assembled (Ref. 7,31) to multi-petal parasol shapes which would be launched in up to ten pieces and require extensive on-orbit assembly.

Potential aerobrake L/Ds range from less than 0.2 to about 2.5 (Ref. 7,18) ; capsule shapes similar to the Viking probe, the Aeroassist Flight Experiment (AFE) vehicle or the Apollo capsule provide low lift to drag ratios, while biconics and bent biconics generate moderate L/Ds (0.5 to 1.5), and winged vehicles have hypersonic L/Ds of 1.5 to 2.5 or 3.0. Ballistic coefficient tends to increase with L/D as is indicated in Fig. 4 (Ref. 30). High L/D vehicles have wider entry corridors and are able to withstand more energetic aerocaptures than low L/D vehicles. Moreover, for the

same entry conditions, a vehicle with a high L/D will experience a more benign deceleration pulse. In some mission scenarios, the same vehicle is used for the aerocapture and surface descent maneuvers. In this case, a high L/D provides good lateral range during the descent. This is desirable since it allows for a wide range of potential landing sites even from a low inclination parking orbit.

Payload packaging considerations are of great importance and tend to favor low L/D vehicles since these have open leesides with good view factors for radiators and antennae (Ref. 33). Moreover, it is easier to place the center of gravity forward of the center of pressure and thereby achieve static stability with low or moderate L/D configurations (Ref. 21,29). However, aeroshells with open leesides expose the payload to potential wake impingement and aerodynamic heating (Ref. 34). Therefore, with these configurations, vehicle angle of attack must be limited to keep the payload safely in the shielded region, and efforts must be made to calculate payload heating and assure that it is not excessive.

The design and type of the thermal protection system is another major consideration in aerobrake systems studies (Ref. 31,35,36). Some authors have considered the application of reusable vehicles which would employ a radiatively cooled TPS similar to that on the Space Shuttle. This type of TPS can withstand peak heating rates of about 50 W/cm^2 . Atmospheric entries which result in peak rates higher than this require the use of ablative heat shields such as that on the Apollo reentry capsule. Unlike radiatively cooled materials, ablative shields impose no upper limit on the peak heating rate.

However, the thickness and weight of the ablator is determined by the integrated heat load over the entire trajectory; similarly, the thickness of the insulating materials which back a radiatively cooled shield are primarily determined by the integrated heat load. Therefore, the peak heating rate imposed on the vehicle will determine the type of heat shield required, and the integrated load will influence its weight. For a given entry scenario, the undershoot trajectory imposes the highest peak heating rate while the overshoot trajectory encounters the most severe integrated heat load. As a result, these two trajectories help to define the design points for the thermal protection system.

Both peak heating rate and integrated heat load increase with ballistic coefficient. For shallow entries with upward lift, peak rate is inversely related to L/D (see the sections on aerodynamic heating in the Analysis chapter). Thus from an aerothermodynamic standpoint, it would be advantageous to have a low $m/C_D A$ and a high lift-to-drag ratio. However, as Figure 4 shows, these are not independent parameters.

Despite the fact that the Martian atmosphere is much thinner than the Earth's, frequent dust storms occur which can cover the entire planet (Ref. 2,37). As a result, possible erosion of the heat shield by atmospheric dust is another issue which must be considered (Ref. 35, 36). However, studies to date have indicated that the additional required TPS thickness is relatively modest and will result in an increase in the overall aerobrake weight of about one percent (Ref. 36).

Atmospheric Structure

One of the most important aspects of an aerobraking analysis is the atmospheric model used. Early descriptions of the Martian atmosphere significantly overpredicted density and lead to erroneous atmospheric trajectory calculations with unrealistically high pull-out altitudes (Ref. 6). Even today, our direct measurements of Mars' atmosphere are primarily limited to data collected by the two Viking probes, both of which landed during the Martian summer at mid-latitudes in 1976. These missions deduced atmospheric density from measurements of vehicle deceleration made onboard during entry (Ref. 38). Surface atmospheric composition, determined using mass spectrometers, was found to be 95.6% CO₂, 2.7% N₂, and 1.6% argon (Ref. 39). Using the relatively scanty data from these probes and theoretical considerations, complex models of the Martian atmosphere have been developed which account for seasonal and diurnal changes as well as variations with latitude (Ref. 37,40). In addition to periodic changes, the Martian atmosphere is subject to sporadic, unpredictable variations just as at Earth. Current estimates suggest that the actual upper altitude density profile at the time of entry could vary by 50 to 300 percent (Ref. 3,37) from its expected value, although the most authoritative sources predict the more modest discrepancies (Ref. 37). In sharp contrast to the situation for Mars, detailed, highly accurate information on the Earth's atmosphere is readily available (Ref. 41), and weather satellites and balloons provide frequent updates on current conditions.

Interplanetary Navigation Schemes

There are several potential methods for providing the approach navigation for a Mars aerobraking mission (Ref. 42). The existing interplanetary navigation system is called the Deep Space Network (DSN) and uses Earth-based radiometric measurements. Its reported accuracy for Martian atmospheric entry is ± 1.8 degrees (Ref. 18, 43). Recent work indicates that with significant improvements in our knowledge of DSN station locations, Martian ephemeris, and other parameters, the accuracy of this system could be improved substantially (Ref. 41), and it could potentially provide adequate navigation for an aerocapture mission. A more sophisticated and accurate scheme would employ either a Mars orbiter or surface probes acting as navigational aides in conjunction with the Deep Space Network (Ref. 44). Other investigators have shown that with the use of onboard optical sightings of the Martian moons, the error in the atmospheric entry angle could be reduced to ± 0.25 degrees without the need for secondary spacecraft to serve as navigational aides (Ref. 45).

As approach navigation accuracy improves, the control authority required during the aerocapture maneuver decreases, and payload packaging becomes simpler with the use of low L/D configurations. The sophistication, cost, and accuracy of the navigation system which is eventually selected must be traded off against these other mission design requirements.

Launch Opportunities and Atmospheric Entry Velocities

Mars and Earth return to the same relative angular alignment approximately once every 26 months. This results from the two planets moving with different angular velocities in their orbits about the Sun. As a result of this periodic alignment, launch opportunities occur with approximately the same frequency. The velocity of a spacecraft with respect to the planetary atmospheres at the times of arrival depends upon which of these launch dates is used. Additional factors which influence atmospheric entry velocity include mission duration and the possible use of a Venus swingby maneuver (Ref. 18). As a result of these three factors, potential entry velocities range from 6 to 10 km/s at Mars and 11.5 to 15 km/s at Earth.

OBJECTIVES

The main objectives of this study are to determine the entry corridor widths and the aerothermal environments over the range of atmospheric entry conditions probable for a manned mission to Mars. In general, vehicles are captured to low circular orbits with altitudes of approximately 500 kilometers. Aerocapture environments at both Earth and Mars are examined. The assumed mission architecture involves the use of a large aerobrake at Mars to decelerate a crew of four to six and all equipment required for the remainder of the mission. In contrast, for Earth return, a small capsule is used to recover only the crew and scientific samples. This scheme forgoes the need for on-orbit assembly of the Earth return vehicle and reduces the radiative heating encountered during the Earth aerocapture by avoiding large vehicle nose radii and thick shock layers.

Another significant objective is to determine the appropriate value for the trajectory deceleration limit. This is critical since in the majority of cases, the undershoot boundary and the corridor width are determined by this constraint. Figure 2 illustrates the impact of the deceleration limit on the required aerobrake L/D for capture at Mars. This emphasizes the importance of setting this constraint at an appropriate level when performing aerocapture systems studies. The deceleration limit is governed by the physiological tolerance of the crew which is altered by prolonged exposure to microgravity. Therefore, efforts will be made to

quantitatively describe existing data regarding the impact of microgravity exposure on acceleration tolerance and to determine the applicability of this data to current Mars mission scenarios.

In addition, all major parameters which influence corridor width and aerodynamic heating must be varied over their potential ranges; these include vehicle lift-to-drag ratio and ballistic coefficient and atmospheric entry velocity. Both the peak heating rate and integrated heat load are determined for the overshoot and undershoot trajectories.

The impact of target orbit selection on the Martian aerocapture maneuver is also examined. Parking orbit period is varied from 110 minutes, corresponding to a 500 km circular orbit, to 1500 minutes, corresponding to the highly elliptical, 1 sol orbit (Fig. 5).

The results of the study are used to make recommendations regarding specific aspects of mission architecture, including the required entry vehicle lift-to-drag ratios and thermal protection system characteristics as well as Martian parking orbit period.

ANALYSIS

The mathematical equations which describe atmospheric flight trajectories, aerodynamic heating, and atmospheric density profiles will be examined in this section. These relations provide the theoretical foundation upon which much of the following work is based. For brevity, full derivations of these equations are not presented in the text, but the original sources are referenced.

ATMOSPHERIC MODELS

One important aspect of an aerobrace systems study is the atmospheric model used. Some advanced models include density variations with season, latitude, and time of day and allow for sporadic, unanticipated fluctuations. In contrast, the simplest schemes vary density as a function of altitude only. In these models, known as exponential atmospheres, density is calculated by a series of expressions of the form:

$$1) \quad \rho = \rho_0 e^{-\beta(h-h_0)}$$

where ρ is the local density, ρ_0 is a reference density, h is the altitude, and h_0 is the altitude at which the reference density is specified. The inverse of the parameter β is known as the atmospheric density scale height. The Martian atmospheric model employed in this investigation is of this type and is based on data

collected by the Viking probes described earlier (Ref. 38). The values used for β and ρ_0 at various altitudes on Mars are listed in Table 1. The model used for Earth's atmosphere is based on a similar curvefit of the 1976 U.S. Standard Atmosphere (Ref. 41). Both atmospheres were assumed to be non-rotating.

At high altitudes, the low Reynolds numbers lead to thick laminar boundary layers which increases the drag coefficient of reentry vehicles (Ref. 46). As a result, there is a high altitude decrement in vehicle L/D. To account for this effect, the maximum L/D of vehicles in this study was decreased with Reynolds number as illustrated in Fig. 6. This curve was based on calculated values for the Space Shuttle, a proposed winged Mars aerobrake, and a bent biconic AOTV (Ref. 47).

Entry is defined to occur at 122 km (400000 ft) at Earth and 125 km at Mars, and the atmospheres are assumed to be insensible above these levels. The altitude specified for the entry interface is important since the measured entry angle is a function of this parameter. Although this is a purely geometric effect (Fig. 7), it must be considered when comparing the results of different studies. The 125 km interface set at Mars corresponds to the altitude used in the guidance studies discussed earlier (Ref. 21,42,45), and the 122 km interface at Earth is the altitude where entry has traditionally been assumed to occur.

EQUATIONS OF MOTION

The motion of a lifting, unpowered vehicle in a spherically symmetric, non-rotating atmosphere is described by a system of three first-order, linear, ordinary differential equations (Ref. 17,48) together with expressions for atmospheric density and the local gravitational constant. The differential equations, derived in Ref. 48, are:

$$2) \quad dV/dt = -(\rho/2) (C_D A/m) V^2 - g \sin \gamma$$

$$3) \quad d\gamma/dt = \rho/2 (C_D A/m) V L/D - (g - V^2/R) \cos \gamma / V$$

$$4) \quad dh/dt = V \sin \gamma$$

$$5) \quad \rho = \rho_0 e^{-\beta(h-h_0)}$$

$$6) \quad g = g_0 / (1 + h/R_0)^2$$

(See the preceding nomenclature section.) At Mars, a planetary radius (R_0) of 3,400,000 m was used, and the gravitational constant (g_0) was set at 3.7 m/s². The corresponding values at Earth were 6,378,135 m and 9.8066 m/s², respectively. The values for the other constants (h_0, β , and ρ_0) are given in Table 1.

For such a vehicle, the G load experienced by the crew is given by (Ref. 49):

$$7) \quad N = F_A / mg = dV/dt [1 + (L/D)^2]^{1/2}.$$

It should be noted that this is *not* equivalent to the total deceleration since it does not include all forces acting on the vehicle; the gravitational force is deliberately omitted. The dV/dt term in Eq. 7 is measured along the flight path and is the change in speed effected by the drag force. Multiplying by the quantity in brackets accounts for the increase in the perceived load due to lift. The reason for omitting the gravitational force from this calculation becomes clear when one considers an object in free fall in a vacuum; the object experiences gravitational force and accelerates but is not subjected to a G load (see Ref. 50).

AERODYNAMIC HEATING

This study encompasses flight regimes in which both radiative and convective heating may be at significant levels. Over the last forty years, many techniques have been developed which can be used to calculate these heating rates; these methods range from full, computational solutions of the equations describing a viscous, hypersonic flowfield to approximate analytic equations which have been shown to provide reasonably accurate answers when applied appropriately. Because of the number of heating calculations which were made in this study, analytic expressions were employed to minimize computational requirements.

Convective Heating

The stagnation-point convective heating rate in Watts/cm² can be determined using an equation first published by Marvin and Deiwert in Reference 51:

$$8) \quad q_c = C1 \ (\rho_1 / r_n)^{1/2} \ V^{C2} \ (1 - h_w/h_T)$$

where C1 and C2 are constants which depend on the atmospheric composition; their values for Earth and Mars are given in Table 2. ρ_1 is the local atmospheric density and r_n is the vehicle nose radius. The total enthalpy, h_T , and wall enthalpy, h_w , are calculated as described in Appendix 1. The equation assumes that the surface of the thermal protection system is fully catalytic to chemical recombination, and that ablation products in the boundary layer do not effect the heat transfer processes. Therefore, it provides a conservative estimate of the heating rate and can be used to study the response of a variety of heat shield materials. Figure 8 illustrates the close agreement between heating rates calculated for a carbon dioxide atmosphere using this equation and experimental measurements made in a ballistic range and shock tube (Ref. 52). Further details regarding this method may be found in reference 51.

The peak stagnation-point convective heating rate for a vehicle with constant upward lift entering an atmosphere at a small flight path angle is proportional to the square root of the ballistic coefficient divided by the lift-to-drag ratio (Ref. 53). Since the vehicles in this study, in general, do not fly constant L/D

trajectories, this relation is not directly applicable. However, increasing the ballistic coefficient causes a vehicle to penetrate more deeply into the atmosphere before it is decelerated to a given fraction of its entry speed. As a result, the peak convective heating grows with ballistic coefficient. For the same type of entry, the total convective heat input to the vehicle is directly proportional to $m/C_D A$ (Ref. 53).

Radiative Heating

The calculation of radiative heating rates is a complex and inexact science; high temperatures in the shock layer cause molecular dissociation and atomic ionization, and radiation results from the subsequent recombinations. Part of this radiant energy goes upstream and preheats gas in the freestream. A complete description of a flowfield which involves radiative heating includes a determination of the concentration of various species in the shock layer, a knowledge of their formation and recombination rates and self-absorption characteristics, and proper coupling of the fluid mechanics and optical phenomena (Ref. 54,55).

Because of the complex nature of complete radiative heating calculations, Tauber and Sutton (Ref. 55) developed a simple correlation expression which is applicable under certain circumstances for entries at Earth and Mars. This equation gives stagnation-point radiative heating as:

$$9) \quad q_r = C_3 (r_n)^a \rho^b f(V)$$

where C_3 is a constant which depends on atmospheric composition, $f(V)$ is a function of vehicle velocity, and a and b in some cases are constants but in other cases vary with density and velocity. Table 3 lists the values of a , b , and C_3 at Earth and Mars, while Table 4 shows the variation of f with velocity for both planets. This equation was developed under the assumptions that the boundary layer is in thermochemical equilibrium and that ablation products do not interact with the transport phenomena. The latter is commonly known as the "cold-wall" assumption.

At Earth, this expression is valid for velocities from 10 to 16 km/s, at altitudes from 54 to 72 km, and for vehicles with nose radii between 0.3 and 3.0 m. The equation applies at Mars for velocities between 6.5 and 9 km/s, at altitudes of 30 to 51 km, and for vehicles with nose radii of 1 to 20 m. Despite the apparent limited range of the equation, it is quite useful since the peak heating rate at both planets occurs well within these bounds (Ref. 7,19,55).

Reference 55 compares the results of this method with those of other computational techniques for determining heating in Martian and terrestrial atmospheres. The discrepancies reportedly ranged from -12 to +30 percent. Uncertainties of this magnitude are quite common in radiative heating computations and are considered acceptable for the purposes of this study.

Using an approach similar to that described for ballistic entries in Reference 56, Tauber has recently shown that the stagnation-point radiative heat load per unit area for shallow entries is proportional to the vehicle's ballistic coefficient (personal communication, Nov.

1991). It should be noted from Equations 8 and 9 that the stagnation-point convective heating rate is inversely related to the square root of nose radius while radiative heating increases approximately with nose radius to the one half power. The convective heating rate is related to velocity gradients in the boundary layer which decrease with larger vehicle dimensions. Conversely, radiative heating grows with nose radius because the incandescent shock layer becomes thicker and there is more hot gas to serve as a source. This implies that when radiative processes are predominant, vehicles with small nose radii have an advantage, while blunter configurations are aerothermodynamically preferable when convective heating is dominant.

PHYSIOLOGICAL ASPECTS OF AEROBRAKING

INTRODUCTION

The use of aerobraking on long-duration manned missions involves subjecting astronauts who have been deconditioned by prolonged weightlessness to the high g loads of atmospheric entry. The importance of applying an appropriate deceleration limit for aerocapture maneuvers has been described previously and is graphically illustrated in Fig. 2. This section will discuss the physiological issues which influence the choice of the deceleration limit.

To examine these issues in a comprehensive manner, background information will first be given on relevant aspects of acceleration physiology and microgravity physiology, and then their interaction will be discussed. Potential countermeasures to both zero-g deconditioning and to high acceleration loads will be described. Although a large physiological database exists from ground-based and spaceflight studies, the applicability of this information to Mars missions must be carefully examined since most current scenarios involve significantly longer duration flights than have heretofore been accomplished. Therefore, studies which examined the timecourse of zero-g induced physiological changes will be reviewed, and attention will be devoted to the success of countermeasures in slowing or arresting deconditioning processes. This type of information provides the basis for understanding the degree to which the results of shorter duration flights can be applied to manned Mars missions.

ACCELERATION PHYSIOLOGY

Normal Response to Acceleration

The physiological response to acceleration has been extensively studied over the last fifty years, predominantly in connection with military aviation. Human response to acceleration depends to a large degree on the direction of the force with respect to the body. The definitions of the force axes are depicted in Fig. 9 (Ref. 57); however, some concrete examples help to clarify the meaning of this figure. A positive G_z is experienced by the passenger when an elevator begins to move upward, while positive G_x is felt when one steps on an automobile accelerator. Human tolerance to acceleration differs markedly depending upon the direction along which the force is applied; tolerance is greatest along the $+G_x$ direction and is least along the $-G_z$ direction.

When standing upright on the Earth's surface, one is constantly exposed to $+1 G_z$. When an individual quickly moves from a supine to an erect position, his cardiovascular system is suddenly subjected to hydrostatic forces due to the acceleration of gravity. These gravitational forces tend to pool blood in the legs, and the body must compensate to maintain blood pressure at the level of the brain and avoid a loss of consciousness. This physiological response is mediated by the baroreceptors which are located in the carotid arteries in the neck and in the great vessels of the thorax. These are sensors which, in response to changes in blood pressure, initiate reflexes that change vascular tone, heart rate, and the strength of the heart's contraction to maintain blood pressure at an acceptable level. In certain pathological conditions (which have analogs in

individuals adapted to zero gravity) the baroreceptor response fails. This notably occurs in conditions of dehydration and in disease states which impair the function of the autonomic nervous system (such as diabetes).

The body is not adapted as well to accommodate application of $-G_z$ since this is a situation which rarely occurs in nature. Under $-G_z$ loading, the baroreceptors induce a slow heart rate which can progress to a complete failure of the heart to contract. This decreases cardiac output (the flow rate through the heart), and the arterial/venous pressure differential (the pressure gradient which drives blood flow) approaches zero, with a resulting deterioration in the level of consciousness. Moreover, the high hydrostatic vascular pressures in the head arouse some concern over the possible risk of hemorrhagic stroke (Ref. 58).

Acceleration along the x axis is better tolerated than along the z axis since force in the x direction does not induce hydrostatic gradients which must be overcome to maintain blood flow to the brain. The main limitation along the x axis involves respiratory mechanics. Normally, blood and air flow are well matched in the lungs to produce proper oxygenation of the red blood cells. However, acceleration in the x direction causes fluid shifts in the lungs (the blood and other fluids tend to pool toward the back for $+G_x$) which result in regional mismatches in the flow rates of blood and air. This compromises the lungs' ability to properly oxygenate the blood (Ref. 59-62). This phenomenon is known as an arterio-venous (or A-V) shunt since some blood effectively bypasses the lungs without

being adequately oxygenated. In addition, the chest wall motion required for breathing (the upward/outward rotation of the ribs and concomitant expansion of the thoracic cavity) becomes increasingly difficult as G_x is applied.

Acceleration Tolerance Limits

The physiological results of overloading the body's compensatory mechanisms depend upon the direction in which the acceleration is applied. Table 5, adapted from Ref. 57, describes the effects of various levels of acceleration in the x and z directions for a normal, healthy, unprotected individual. In examining g tolerance data from various sources, it should be realized that no consistent set of criteria have been used to determine tolerance limits. Some studies have used objective criteria such as reduction in the sensitivity of peripheral vision or decreases in temporal artery blood flow as measured by Doppler; others have applied endpoints such as subject discomfort or loss of consciousness.

The visual changes described for $+G_z$ result from impaired perfusion of the retina (the neural portion of the eye which serves as the light sensor). The peripheral vision deteriorates first since its blood supply is the most distal; this deterioration is manifested as a decreased peripheral visual sensitivity (or an increase in illumination required for perception). Centrifuge studies (Ref. 63,64) have shown that this occurs along with progressive dimming of the vision (grayout) when the systolic blood pressure at head level

drops to 56 mm Hg, while a drop to 39 mm Hg results in complete loss of vision (blackout).

Between 4.5 and 6 G_z, blood pressure at the level of the brain drops below a threshold value, and, after a latent period of 6-7 seconds of inadequate oxygen delivery, confusion and loss of consciousness occur (Ref. 59,65). The fact that visual deterioration occurs prior to cognitive dysfunction is related to a relative reduction in retinal perfusion caused by the intraocular pressure. (The pressure inside the eyeball is about 20 mm Hg above that in the brain. This results in a higher blood pressure being required to perfuse the retina and support vision than is needed to maintain consciousness. Ref. 58,66) The visual changes discussed above and the phenomenon of G-induced loss of consciousness (GLOC) were reported as early as World War I and have resulted in many fatal aircraft accidents. The frequency of these crashes has actually increased as fighter planes have become more agile and capable of sustaining high-g maneuvers for longer periods of time (Ref. 67,68).

As mentioned previously, the limitations of acceleration in the x direction are primarily respiratory, with the onset of chest pain and shortness of breath at about 7 G; as the load increases, these steadily become more severe. Respiratory rate and minute volume (the volume inhaled in one minute) increase with G_x while vital capacity (the maximum amount which can be inhaled), tidal volume (the volume of one breath), and inspiratory reserve (the difference between vital capacity and tidal volume) decrease (Ref.58,69). These decreases in lung capacities are related to an upward displacement

of the posterior portion of the diaphragm and a reduced anterior-posterior diameter of the thorax (Ref.58,70). The shift of the thoracic contents caused by the acceleration load have, in at least one case, been associated with the development of tears in the bronchial tree in a healthy, young man at an acceleration of only 5.5 G_x (Ref.60). However, more typically, healthy subjects can withstand + 12-15 G_x for brief periods without suffering any serious effects. The much higher g tolerance along the x direction than along the z axis accounts for the couch position used in all previous manned space capsule entries and underscores the importance of maintaining the deceleration vector in the proper orientation for manned aerocapture maneuvers. Studies of the effect of body position on acceleration tolerance have found that with the subject seated, bending the torso forward 25 degrees increases tolerance to horizontal acceleration despite the resulting G_z component (Ref.58,71). This enhanced tolerance may result from a downward displacement of the abdominal contents and diaphragm, leading to more efficient respiratory mechanics.

Although the principal effects of acceleration along the x axis are respiratory, high G loads also result in visual disturbances and difficulty in moving. The latter stems directly from the increased effective limb weight resulting from the acceleration. The visual disturbances likely result from several factors. First, it should be noted that since a line from the top of the aorta to the retina lies about 15 degrees anterior to the vertical, positive G_x accelerations introduce a hydrostatic decrease in retinal perfusion pressure

(Ref.58). In addition, it has been suggested that displacement of the lens of the eye and tearing may contribute to visual deterioration (Ref. 58,72,73). Moreover, the pulmonary A-V shunts discussed previously have been shown to drop arterial oxygen saturation (the degree to which the red blood cells are carrying their maximum possible oxygen load) to 75 percent at 8 G_x (Fig. 10 - Ref. 58,74). Similar decreases in oxygen saturation have been associated with visual disturbances in persons at high altitude (Ref. 75).

The maximum g load which can be tolerated strongly depends on the duration of exposure. Figure 11 from Ref. 76 shows the guidelines used in the design of the Apollo entry trajectories. This figure, which was adapted from Ref. 58, was developed using data from numerous sources, and is applicable to healthy, unprotected men.

The effect of g onset rate on tolerance depends on the duration of the acceleration pulse and the level of its peak. A gradual onset rate allows time for appropriate compensatory responses, and therefore results in better tolerance for moderate peak loads; however, if the load is severe enough to result in G-induced loss of consciousness (GLOC), a gradual onset implies a longer total G exposure and this produces a greater insult and a longer period of unconsciousness than occurs with a rapid onset (Ref. 64). Conversely, if the peak load is high enough typically to produce GLOC, but the pulse duration is quite brief, rapid onset and offset rates may allow a subject to reach a very high peak level without experiencing decreased blood flow to the brain long enough to cause unconsciousness.

High G Countermeasures

Numerous techniques have been developed over the last 50 years to enhance g tolerance for military pilots flying high performance aircraft. Perhaps the best known of these is the anti-g suit; these were initially developed in the 1930s in Great Britain, Canada, the United States, and Germany (Ref. 77). One of the best known of these early devices was a water-filled garment known as the Frank's flying suit which covered the lower torso and legs. Current designs employ pneumatic bladders on the legs and abdomen which inflate when the aircraft undergoes a high g maneuver. Both schemes work by preventing pooling of blood in the lower part of the body. Modern suits typically increase tolerance by 1-2 G (Ref. 57).

To further enhance tolerance, pilots use anti-G suits in conjunction with a muscular contraction of the abdomen and legs called the M-1 maneuver. The muscular contractions of the M-1 maneuver are done while bending forward and exhaling slowly through a partially closed airway. This technique has been found to provide about 1.7 Gz additional protection which is directly additive to the increased tolerance resulting from use of an anti-g suit (Ref. 78). The military has also examined the use of a special seat called PALE (pelvis and leg elevation) to take advantage of the greater tolerance to g loads along the x axis. The back of this seat is inclined 75 degrees to the vertical, compared to the usual 15 degree seat back angle. This results in loads being directed primarily along the x axis and thereby enhances tolerance by more than 3 g (Ref.78).

As mentioned previously, exposure to G_x compromises pulmonary function while decreasing lung volumes. Work done over the last thirty years has shown that the use of positive pressure breathing during high G exposure can minimize the decrease in lung volumes and enhance G tolerance considerably (Ref.58,79). Exposure duration at 10 G is increased by 67 percent (Ref. 58). Although positive pressure breathing using air does not increase arterial oxygen saturation (Ref. 58,80), it does decrease respiratory effort (Ref. 81,82) and allow speech at higher G levels than is otherwise possible (Ref. 82). The Air Force is now in the process of installing this technology in its high performance fighter planes for the first time (Ref. 82).

PHYSIOLOGICAL CHANGES INDUCED BY WEIGHTLESSNESS

Exposure of humans to the microgravity of space results in numerous physiological changes which can largely be viewed as appropriate adaptations to the body's new environment. These changes involve the cardiovascular, hormonal, immune, vestibular, hematopoetic (blood forming), and skeletal systems among others. Alterations in the cardiovascular system have the greatest impact on deceleration tolerance, and therefore will be emphasized here.

Cardiovascular/ Fluid Alterations

One of the most apparent initial physiological changes upon arrival in orbit is the headward shift of fluid which results from the lack of

gravitational pooling that one experiences on Earth. This is associated with a decrease of lower leg volume and leads to a feeling and appearance of facial puffiness (Ref. 83). The fluid shift is sensed by the kidneys as an excess of blood volume, and a diuresis (increased urination) results, leading to volume contraction and a concomitant loss of sodium. Although this diuresis has not been measured on American flights (Ref. 83), Soviet data confirms that it occurs during the first three days in orbit (Ref. 84). Skylab studies showed an 8 percent decrease in blood plasma volume following the 28 day flight and a 15 percent decrease after the 84 day mission (Ref. 57).

This decrease in plasma volume is probably at least partially responsible for the postflight orthostatic intolerance (tendency to lose consciousness with standing) which has been observed since the early days of manned spaceflight (Ref. 85). During the Skylab missions, lower body negative pressure (LBNP) was used to pool blood in the legs and pelvis and thereby simulate a 1 G load on the cardiovascular system (Ref. 86). These studies confirmed that orthostatic intolerance is present inflight as well as upon return to Earth. The decreased tolerance was present by the fourth day in orbit and was manifested by an increased pulse rise in response to LBNP as compared to preflight levels. Additional factors which may contribute to postflight orthostatic instability are increased vascular compliance in the lower extremities (Ref. 87) and decreased leg muscle tension (Ref. 85).

Recent studies have suggested that postflight orthostatic intolerance may also be related to decreased baroreceptor sensitivity following exposure to microgravity (Ref. 88). This assertion is supported by the fact that endurance exercise maintains blood volume in bedrest subjects but does not prevent the development of orthostatic intolerance (Ref. 89). Moreover, a reduced baroreceptor response to tilt tests has been measured in subjects exposed to thirty days of bedrest (Ref. 88).

Both U.S. and Soviet studies of cardiac function during long duration missions have shown an increase in resting heart rate while cardiac output and stroke volume responses have been inconsistent (Ref. 84,90,91). Exercise capacity inflight appears to be unchanged from preflight levels, but is substantially decreased postflight in both American and Soviet studies (Ref. 83,84,92). The recovery time for exercise capacity has actually been inversely related to flight duration, probably because of the improved exercise regimes on the longer missions (Ref. 84,90). Missions of 13 to 28 days (Apollo 15, Soyuz 9, and Skylab 2) have resulted in the longest recovery periods (20 to 25 days), while cardiovascular parameters for the crew of the 84 day Skylab 4 returned to baseline in only 4 to 5 days (Ref. 85,93). Soviet studies have also found that readaptation time for missions up to 185 days does not increase with flight duration (Ref. 83,84).

Cardiac arrhythmias (abnormal electrical discharge patterns) have been associated with spaceflight since the Gemini missions, and have ranged from premature ventricular contractions (PVCs) to runs

of bigeminy, episodes of wandering pacemaker, and even a five beat run of ventricular tachycardia. The etiology of these arrhythmias has not been clearly delineated and is likely multifactorial. Although their frequency has been significantly higher in space than for the same individuals on the ground, arrhythmias have generally not been felt to pose a serious threat (Ref. 57,83).

Postflight echocardiography has consistently shown a decrease in end diastolic volume (the volume of the left ventricle at the end of each heart beat), stroke volume (the blood volume pumped in one beat), and ejection fraction (the percent of the blood in the left ventricle ejected in each beat) as compared to preflight levels (Ref. 83,94). However, by plotting Frank-Starling curves (end diastolic volume vs. stroke volume), investigators have shown that myocardial contractility (the strength of the heart's contraction) is essentially unchanged after prolonged space flight. Five to ten days after return to Earth, echocardiographic studies are back to their baseline (Ref. 91,95). Left ventricular muscle mass decreases by about eleven percent on long duration flights but recovers within three weeks of return to Earth; it is believed that the mass decrease may result from intracellular fluid losses (Ref. 90) which are rapidly replaced once back on the ground.

The Bedrest Analog for Microgravity

For many years investigators have used bedrest to simulate the gravitational unloading which is experienced in spaceflight. Bedrest stimulates many of the physiological changes which are induced by

microgravity such as a headward fluid shift, plasma volume loss, orthostatic intolerance, bone calcium loss, cardiovascular deconditioning, lower extremity muscle atrophy, and red cell mass loss (Ref. 96). However, the calcium losses are not as severe as in space flight, and bedrest fails to induce other changes such as the nausea and vomiting which often occurs early in missions. In addition, bedrest generally adds the confounding effects of hypokinesia (decreased movement) to the desired gravitational unloading. Nevertheless, this technique provides a valuable model for the physiological changes which are critical to this investigation.

Numerous American and Soviet bedrest studies have yielded valuable information on the probable effects of space flight on deceleration tolerance (Ref. 96-101). Some of these studies such as those of Miller and Leverett (Ref. 98) and Jacobson et al. (Ref. 99) were designed to simulate the deceleration profiles of specific missions. Bedrest studies have also been used extensively in the development of deconditioning countermeasures such as lower body negative pressure (LBNP), isometric and isotonic exercise protocols, and fluid loading (Ref. 102-104).

COUNTERMEASURES FOR ZERO G DECONDITIONING

Numerous techniques have been developed over the last thirty years to minimize the adverse physiologic effects of space flight. These include rigorous inflight exercise regimes, the application of lower body negative pressure (LBNP) to simulate gravitational

stresses on the cardiovascular system, fluid loading prior to reentry, and the use of anti-G suits for descent.

Inflight exercise programs on long duration missions currently require about two to three hours per day. The majority of this time is devoted to cardiovascular conditioning on a treadmill or bicycle ergometer with brief periods spent using bungee-type devices to exercise the upper body. These programs have been fairly effective in reducing cardiovascular deconditioning (Ref. 88,105) and decreasing postflight recovery time (Ref. 84); the crew of the 84-day Skylab 4 actually increased their average maximum oxygen uptake by 8 percent during the mission from preflight levels (Ref. 88). However, this endurance type exercise has not been altogether effective in preventing postflight orthostatic intolerance. Recent work has suggested that this is because endurance exercise does not affect the deconditioning of the baroreceptor response which was discussed earlier and recommended the addition of brief bouts of maximal intensity exercise to overcome this shortfall (Ref. 88).

Both American and Soviet investigators have used lower body negative pressure (LBNP) on long duration flights to simulate gravitational stresses on the cardiovascular system (Ref. 86,94,105,106). Repeated application of LBNP in the weeks immediately prior to reentry helps to improve vascular tone and decrease cardiovascular deconditioning and orthostatic intolerance (Ref. 94,104,105). The Soviets routinely employ the 'Chibis' vacuum suit which permits cosmonauts to walk and exercise while being subjected to LBNP. American inflight applications of LBNP have

focused more on assessment than prevention of cardiovascular deconditioning (Ref. 86) and have been carried out using a static tank, rather than a mobile system like Chibis.

The 'Penguin' elastic suit is a device which the Soviets use to apply a longitudinal load to the legs and lower body. It is worn on a regular basis throughout waking hours and is believed to help maintain muscle strength and tone (Ref. 104,105).

Post-bedrest orthostatic and acceleration tolerance have been shown to improve considerably with hydration using isotonic oral saline solution (Ref. 102,106). As a result, both U.S. and Soviet crew members routinely ingest increased amounts of water with a proportional number of salt tablets in the last few days before reentry. Postflight tests have confirmed that this technique enhances orthostatic tolerance upon return from space as evidenced by a reduced rise in pulse rate when astronauts move from a seated to a standing position.

During reentry, both Soviet and American crew members wear anti-G suits similar to those described earlier. For all high G entries, crews have been positioned so that the acceleration vector lies along the x axis, although during the relatively benign entries of the Space Shuttle (which has peak loads of only about 1.5 G) the acceleration is in the +z direction. To further enhance G tolerance, it is conceivable that future vehicles could employ positive pressure breathing systems for reentry.

EFFECTS OF MICROGRAVITY ON ACCELERATION TOLERANCE

The previous sections serve as background for an issue of central importance to this study - the deterioration of acceleration tolerance with spaceflight. As previously discussed, this phenomenon enormously impacts manned aerobraking missions by determining the deceleration limit for the aerocapture maneuver. Although no manned missions have yet lasted as long as a future Mars excursion, a significant database exists which can be used to predict crew acceleration tolerance during such a voyage. This database consists of limited American and extensive Soviet flight experience in conjunction with numerous ground-based bedrest studies.

Ground-Based Studies

Many bedrest studies have been conducted over the last thirty years to evaluate the effect of gravitational unloading on acceleration tolerance. While some of these have attempted to simulate actual mission profiles, others have been more generic. The majority have examined degradation in G_z tolerance since this axis is most severely effected (Ref. 97,99-101,106,107), but a few have considered the changes in G_x tolerance which are more directly applicable for the purposes of this investigation (98,108,109).

Studies done by Sandler et al. (Ref. 100,101,107) in support of the Space Shuttle have shown a decrease in $+G_z$ tolerance time of 50 to 60 percent for both men and women after bedrest of 7 to 21 days. The reduced tolerance was apparently established after seven days and did not degrade further after that time. Age did not seem to

adversely effect men's tolerance. However, sex apparently is a critical factor with women's tolerance times being about one third those of men of the same age both before and after bedrest.

In the mid-1960s, Miller and Leverett (Ref. 98) did a four week bedrest study followed by exposure of the subjects to a +G_x profile similar to that expected for the Gemini missions (Fig. 12). This work showed no increase in visual disturbances, subjective physical discomfort or electrocardiographic abnormalities. However, pulse rate at peak G increased by an average of 38 percent.

In the late 1960s, Kotovskaya et al. presented results from Soviet studies of +G_x tolerance after bedrest of up to seventy days (Ref. 108,109). This work suggested that tolerance deteriorates over the first 15 to 30 days and stabilizes thereafter. This same work indicated that the "use of drugs and physical exercise during hypodynamia" eliminated the degradation of G tolerance, but did not specify what drugs or types of exercises were used (Ref. 109). More recently, there have been references in Soviet papers to a 370 day bedrest study (Ref. 110); however, no details have been published regarding the findings of this work.

Flight Data

To date, American experience with long-duration space flight has been limited to the 28, 59, and 84 day Skylab missions. In each of these cases, the astronauts returned to Earth in an Apollo-type capsule and experienced deceleration pulses similar to that shown in Fig. 13 (Ref. 111). However, Soviet cosmonauts have been subjected

to much more severe deceleration pulses after flights up to eight months in duration (Ref. 112 and personal communication with Soviet cosmonaut-physicians Valeri Polyakov and Oleg Atkov, Nov. 1990 and May 1991). Peak reentry loads between 5 and 6 G_x have been encountered on at least two such occasions (Soyuz T10B and Soyuz TM-6). Figure 14 shows a calculated approximation of this deceleration pulse. Although the precise shape of the curve depends on several factors which were estimated for the calculation (capsule L/D and ballistic coefficient and de-orbit delta V), the peak deceleration closely matches the reported 5-6 G level. Cosmonauts Atkov and Polyakov both felt that this deceleration level was not excessive and would not interfere with necessary piloting tasks (Personal communication, Nov., 1990 and May, 1991). It should be emphasized that on both missions the cosmonauts maintained strict exercise programs, sometimes in excess of 2 1/2 hours a day.

Kotovskaya and Vil'-Vill'yams recently published a review of cosmonauts' tolerance to reentry G pulses on missions varying from 8 to 326 days in duration (Ref. 113). This study compared individuals on long-duration (two months or more) missions who used anti-G suits on reentry and engaged in adequate inflight exercise programs with those who did not. A continued deterioration of G tolerance occurred in those who did not employ adequate countermeasures, with an increasing frequency of visual disturbances, vertigo (a sensation of spinning), palpitations (a sensation of rapid or irregular heartbeat), and shortness of breath with increasing flight duration. Elevation in pulse rate upon reentry leveled off after the first two

months of exposure to zero G. However, when adequate countermeasures were used, there was no increase in subjective complaints, visual disturbances, or pulse rate for long-duration flights as compared with those of only 8 to 12 days. Apparently, the countermeasures which have been developed are sufficient to maintain tolerance for flights up to 11 months long.

Unfortunately, despite such reports, a complete set of data relating G tolerance to flight duration is still lacking. For example, the paper by Kotovskaya and Vil'-Vill'yams (Ref. 113) does not tell how the peak G loads related to mission duration, but only gives a range of peak loads for the entire series of flights. Few measurements of physiological responses during reentry have been made other than pulse rate, respiratory rate, and EKG. Moreover, the number of individuals who have been subjected to high-G reentries following prolonged flight is known only to the Soviets and must be quite low. The proposed Space Station Freedom will give international investigators the opportunity to significantly expand upon this limited database.

CONCLUSIONS AND RECOMMENDATIONS

The most directly applicable information we have for determining appropriate deceleration limits for manned aerocapture missions comes from long-duration Soviet flights. These flights have shown that a deceleration pulse similar to that illustrated in Fig. 14 is well tolerated after eight months in space, if an adequate inflight exercise regimen is maintained. The majority of current Mars

mission scenarios call for an outbound transfer time of eight months or less. Therefore, a 5 G limit seems to be strongly supported for the Mars arrival aerocapture. Although it is possible that higher loads could be tolerated, it seems prudent not to exceed well established limits since human intervention may be necessary during the aerocapture maneuver.

The question remains, of course, as to whether this level of deceleration tolerance can be maintained until the time of Earth return. The bedrest studies of Sandler et al (Ref. 100,101,107) and Kotovskaya et al (Ref. 108,109) have indicated that deceleration tolerance tends to deteriorate over a fairly short timecourse (1 to 3 weeks) and then levels off. The recent publication by Kotovskaya and Vil'-Vill'yams (Ref. 113) reports a similar stabilization of reentry deceleration tolerance in Soviet cosmonauts if adequate inflight exercise is performed. Therefore a 5 G peak deceleration limit will be used in this study for Earth return as well as Mars arrival. For sprint or opposition class missions, this is a reasonable extrapolation of the existing physiological data. However, for missions with round-trip durations in excess of 15 months, there is no convincing data for recommending an appropriate deceleration constraint. Establishing a limit for such missions must await results from longer duration manned Earth orbital flights.

METHODOLOGY

TRAJECTORY CALCULATIONS AND REQUIREMENTS

Aerocapture trajectories were calculated at Mars and Earth for all combinations of the entry conditions indicated in Table 6. For each entry scenario (consisting of vehicle L/D, ballistic coefficient, and atmospheric entry velocity), the corridor width for capture into a 500 kilometer circular orbit was determined using the 5 G load limit discussed above. A low circular parking orbit was chosen for Earth return because it facilitates rendezvous with the space station and avoids the hazards of repeatedly crossing the van Allen radiation belts. At Mars, the use of a low circular orbit enhances entry corridor width in some situations (as will be discussed later) and makes the surface descent maneuver more benign.

Based on information in References 21 and 45 and the assumed use of optical sightings for approach navigation, a required entry corridor width of 1 degree is used at Mars. The presence of a superior navigational infrastructure allows the Earth return corridor width requirement to be slightly less stringent at 0.7 degrees (Ref. 114).

The trajectory calculations were accomplished by numerically integrating the equations of motion (Eq. 2-5) which were described earlier. These calculations were performed primarily on the Cray YMP at NASA Ames Research Center and were done using the subroutine IVPRK from the International Math and Science Library to solve the system of differential equations. For each time step, an initial value problem was solved to find the subsequent velocity,

flight path angle, and altitude. A time increment of ten seconds was applied for these computations throughout the trajectory. The subroutine employs the Runge-Kutta fifth and sixth-order methods to solve the differential equations.

The overshoot boundary for a given entry scenario was determined by applying maximum lift downward (toward the planet's surface) and increasing the atmospheric entry angle by 0.01 to 0.1 degrees in successive trajectory simulations until the vehicle was captured. This method actually steps slightly *beyond* the overshoot boundary by an amount dependent on the increment in entry angle. The finer increments were used when entry corridors were narrow (less than 1 degree) and a step size of 0.1 degree would have significantly decreased apparent corridor width. Since the algorithm actually finds an entry angle slightly steeper than the overshoot boundary, it is necessary to roll the vehicle upright late in the atmospheric pass to reach the desired target orbit. The timing of this roll maneuver is adjusted in consecutive trajectory simulations until the vehicle exits the atmosphere with the correct energy.

The undershoot boundary is determined by flying the vehicle upright and incrementing the atmospheric entry angle in successive simulations until either the 5 G limit is exceeded, the trajectory passes below 30 kilometers (55 km at Earth), or the vehicle is unable to reach its target orbit because of excessive energy dissipation. Once any one of these constraints is slightly exceeded, the undershoot angle is established. Then the trajectory simulation is run again, and the vehicle's bank angle is varied just prior to and

after the time of peak deceleration. Adjustments are made in this mid- and late-phase bank angle until the aerocapture dissipates the desired amount of energy and the vehicle exits the atmosphere into its target orbit. Full lift up is applied early in the atmospheric passage to allow the steepest possible entry without violating the deceleration limit. Then it is usually necessary for the vehicle to roll into a lift-down position at about the time of its closest approach to the surface to prevent atmospheric skipout. Once sufficient energy has been dissipated, the vehicle rolls back into a lift-up position and exits the atmosphere. Figure 15, adapted from Reference 20, illustrates these phases. The computer code adjusts the timing of the roll reversals to place the vehicle in the desired target orbit. Vehicle roll rates are not directly limited, but impulsive type maneuvers are not allowed, and peak rates are usually less than 12 degrees per second. This is realistic for a large vehicle and is close to the peak rate experienced by the Space Shuttle upon reentry. The control scheme used in this study does not execute the roll reversals which some more sophisticated algorithms employ to prevent undesired vehicle turns and shifts in the inclination of the final parking orbit (Ref. 115). A more detailed description of the algorithm used to vary the bank angle and adjust the orbital period is given in Appendix 2.

Four separate computer programs are used for trajectory calculations in this investigation. One finds the overshoot boundary for the Mars aerocapture maneuver; a second program determines the undershoot trajectory at Mars. The other two codes perform these

same tasks for the Earth return. Except for differences in the atmospheric models, the planetary radii, and the gravitational constants, the two overshoot codes and the two undershoot codes are identical. Appendix 2 discusses the general approach used to determine the undershoot boundaries in addition to describing the algorithm employed to vary the vehicle bank angle. Listings of the computer programs are given in Appendix 3.

In this study, trajectories are not constrained by peak heating rate or integrated heat load. However, the 30 and 55 kilometer minimum allowable altitudes mentioned above indirectly limit peak heating and provide a margin of safety against terrain impact (Olympus Mons, the highest mountain on Mars, has its peak approximately 23 kilometers above the mean surface.)

For the Martian aerocapture maneuver, an extension of the study examines the effect of varying the target from the baseline 500 kilometer circular orbit to a highly elliptical 1 sol orbit. Direct entries to the surface were also considered despite the possibility of a global dust storm. An analogous study has recently examined the use of various target orbits for the Earth return aerocapture (Ref. 29).

HEATING CALCULATIONS

Once an overshoot or undershoot trajectory is determined as described above for a given entry scenario, equations 8 and 9 are used to calculate the stagnation-point convective and radiative heating rates at each time step in the atmospheric pass. Since

vehicles with relatively high lift-to-drag ratios tend to have smaller nose radii than those with a low L/D, the nose radii used for the Mars aerocapture heating calculations are varied as indicated in Table 7. For Earth return, specific entry capsule designs were considered; as was mentioned earlier, these capsules were sized to return only the crew and scientific samples. The capsule configurations and their respective nose radii are shown in Figure 16 (adapted from Ref. 19.) For the vehicle at the left of the figure, an effective nose radius was used since it has an elliptical cross section. The stagnation-point heating rate was integrated over the entire atmospheric trajectory to yield the total heat load for each aerocapture maneuver.

RESULTS

MARS ARRIVAL AEROCAPTURE

Figure 17 shows the overshoot and undershoot trajectories for typical Mars arrival conditions. As can be seen, the energy dissipation occurs at a nearly constant altitude between 35 and 45 kilometers. The corresponding deceleration pulses are shown in Fig. 18. For comparison, the calculated Soyuz entry deceleration pulse described earlier is also shown. The aerocapture G-load profiles are more benign than that of the Soyuz capsule, both in terms of peak load and pulse duration.

Stagnation-point total and radiative heating rate profiles for these overshoot and undershoot trajectories are shown in Fig. 19 (for this case the vehicle's nose radius was 16 m); comparison with Figure 17 shows that the aerodynamic heating pulse occurs well within the range of applicability of the expression used for radiative heating calculations (Eq. 9). These trajectories illustrate the typical pattern of peak heating occurring shortly before peak deceleration.

The bank angle profile employed by the undershoot trajectory for this entry scenario is shown in Fig. 20. It exhibits the characteristic features described in Fig. 15. An early phase of full lift up is followed by a rollover to hold the vehicle in the atmosphere until the proper amount of energy has been dissipated. A second roll causes the vehicle to exit the atmosphere and enter its parking orbit. The peak vehicle roll rate occurs about 80 to 90 seconds after atmospheric entry and is approximately 10 degrees per second.

Entry Corridors

Figure 21 illustrates the relative insensitivity of entry corridor width to the aerobrake ballistic coefficient. The only vehicles for which the ballistic coefficient significantly influences corridor width are those with a high lift-to-drag ratio which enter the atmosphere at a relatively low velocity.

In contrast to the weak effect of ballistic coefficient, vehicle L/D profoundly impacts entry corridor width. This effect is shown in Figure 22 and is marked at all entry speeds considered. Figure 23 illustrates that entry velocity is the second major determinant of corridor width. The curves for high L/D vehicles are qualitatively different from those for the low L/D cases. This results from different constraints determining the undershoot boundary in different entry scenarios. The 5 G deceleration limit sets the undershoot boundary for all entries to the right of the dashed line; cases to the left are constrained by the energy requirements of the parking orbit (i.e. the vehicle cannot enter more steeply without dissipating too much energy to reach its target orbit). This effect is most pronounced for low energy entries (corresponding to low entry velocities) and is exacerbated by the deeper atmospheric penetration experienced by vehicles with high ballistic coefficients. The latter effect is reflected by a shift of the dashed line to the right as $m/C_D A$ increases. This constraint on the entry corridor implies that the choice of parking orbit impacts corridor width. This effect will be examined in detail later.

If the one degree corridor width requirement discussed previously is applied here, Figure 23 indicates that an aerobrake with an L/D of 0.3 would be adequate for entry velocities up to 9 km/s. An L/D of 0.4 to 0.5 would be needed if 10 km/s entries are to be performed. These suggestions are based on the most severe cases examined, and vehicles with lower control authority would be sufficient for the less demanding entry scenarios.

Aerodynamic Heating

The peak stagnation-point heating rate experienced during the undershoot trajectory is plotted in Figure 24 as a function of entry velocity for each ballistic coefficient and vehicle L/D. It should be recalled that these calculations neglected the effects on aerodynamic heating of ablation products in the boundary layer and reduced surface catalyticity. Therefore, these plots represent conservative estimates of the peak heating and actual rates would be somewhat lower.

As discussed previously, for any given entry condition, the undershoot trajectory encounters the most severe peak heating rates. Therefore, the plots in Figure 24 are useful for determining the type of TPS required for different entry scenarios. Because of constraints on the surface temperature, radiatively cooled thermal protection materials are presently limited to peak heating rates as calculated here of 50 to 100 W/cm². Systems such as the Space Shuttle which are intended to endure multiple entries must be limited to even lower peak rates to prevent degradation of the heat shield. If the

peak heating rate exceeds 100 W/cm^2 , current materials technology would require the use of an ablative TPS. Radiatively cooled materials are preferable to ablators because they are lighter. Examination of Figure 24 reveals that for many potential Martian entry scenarios it may be possible to employ a radiatively cooled thermal protection system. The crossover of the curves for vehicles with an $m/C_D A$ of 500 kg/m^2 reflects the growing importance of radiative heating (especially on blunt bodies) as entry velocity increases. The most severe heating rates calculated in this series are comparable to the highest peak rates encountered by an Apollo reentry capsule - 500 W/cm^2 (Ref. 116).

The stagnation-point integrated heat load for the overshoot trajectory is plotted in Figure 25 as a function of entry velocity for each potential aerobrake design. As was discussed earlier, the overshoot trajectory encounters the highest heat load possible for a given set of entry conditions. Therefore, these curves are useful in determining the thickness required for an ablating heatshield or the amount of backside insulation needed if a radiatively cooled system is used. As a point of reference, the Space Shuttle stagnation-point typically experiences an integrated heat load of 40 kJ/cm^2 - a value which is in excess of all but the most severe cases examined here.

These plots illustrate the advantages of using a vehicle with a low $m/C_D A$. If the ballistic coefficient can be kept at or below 100 kg/m^2 , radiatively cooled surfaces may be feasible for entry velocities of 9 km/s or more, and the overall aerothermal

environment can be made more benign than that of either the Space Shuttle or the Apollo reentry capsules.

Impact of Martian Parking Orbit Selection

It was briefly mentioned above that for certain entry scenarios the undershoot boundary could be determined by the energy requirements of the target orbit rather than trajectory deceleration constraints. This issue will now be examined in more detail.

Figure 26 shows the variation of entry corridor width with the period of the parking orbit for vehicles with a ballistic coefficient of 300 kg/m^2 and a range of lift-to-drag ratios. It is apparent that this effect is much more significant for low velocity entries. This is an expected finding, since low velocity entries have to burn off only a small amount of energy to be captured into a high orbit. As a result, their undershoot trajectories are constrained by energy requirements of the target orbit rather than deceleration limits. Conversely, high velocity entries must dissipate enough energy that the G constraint can be reached without excessive energy loss even for capture to long period orbits. As a result, in these cases, the selected orbital period does not influence the undershoot boundary or the entry corridor width.

The same data shown in Figure 26 are plotted from a different perspective in Figure 27. Here corridor width is shown as a function of entry velocity for the various target orbits. The hump-shaped curves are constrained at the low entry velocities by energy requirements, while the deceleration limit determines the

undershoot boundary at all entry velocities when the curves have an exponential shape.

It can generally be viewed that a vehicle with high control authority (either from high L/D, low $m/C_D A$, or a combination) is more able to enter the atmosphere steeply enough to reach the deceleration limit and then successfully pull itself up to the target orbit than one with low control authority. As a result, the impact of orbital period on corridor width is more pronounced for vehicles with low lift-to-drag ratios and high ballistic coefficients. The influence of L/D on corridor width sensitivity to target orbit choice can be appreciated by examining Figure 26. There is a significant variation of corridor width with orbital period for a 7 km/s entry in a vehicle with an L/D of 0.2; however, if the L/D is increased to 0.5, this variation is almost totally eliminated. The impact of ballistic coefficient is apparent when Figures 27c and 28 are compared. The undershoot boundary for capture to a low Mars orbit (period of 110 min) is consistently constrained by the deceleration limit for the case with a ballistic coefficient of 300 kg/m^2 ; as a result, the curve has the exponential shape previously mentioned. If the ballistic coefficient is increased to 500 kg/m^2 , the low velocity undershoot boundaries are limited by energy requirements, and the shape of the curve is changed.

The choice of parking orbit impacts the required aerobrake L/D only for entries at or below 7 km/s. Capture to a high, elliptical orbit at Mars would narrow the corridor width for these low velocity entries and could increase the lift-to-drag ratio required

for these particular cases. Since these scenarios have relatively wide entry corridors for capture to the baseline 500 km circular orbit, an L/D of 0.4 to 0.5 would still be sufficient. However, vehicles with lift-to-drag ratios of 0.2, which might be appropriate for capture to a low circular orbit for entry velocities under 8 km/s, would no longer be adequate (see Fig. 26a).

Table 8 shows the peak stagnation-point heating rate at each entry velocity considered for capture to the various target orbits. The data presented are for a vehicle with an L/D of 0.3. The choice of target orbit impacts the peak heating rates only for the low velocity entries where heating is relatively benign. A similar pattern is seen in Table 9 which shows integrated heat loads.

EARTH RETURN AEROCAPTURE

Figure 29 shows the overshoot and undershoot trajectories for typical Earth return conditions. The corresponding deceleration pulses are compared with that calculated for the Soyuz entry capsule in Figure 30. Again, the Mars aerocapture G profiles are more benign than that of the Soviet vehicle. The bank angle history used during the aerocapture undershoot trajectory is shown in Figure 31. It exhibits the typical features described earlier for undershoot trajectories and requires a peak vehicle roll rate of approximately 8 degrees per second. The overshoot and undershoot heating pulses are shown in Figure 32 (for these calculations, a nose radius of 3.7 m was used); comparison with the altitude vs time plot (Fig. 29)

reveals that vehicle heating occurs well within the range of applicability of the radiative heating expression.

Entry corridor width varied insignificantly with $m/C_D A$. Therefore, results are presented only for the mid-range ballistic coefficient of 300 kg/m^2 . Corridor width is shown as a function of entry velocity in Figure 33. As was described earlier, all captures were to a 500 km circular orbit. For this scenario, the undershoot boundary was determined by the deceleration limit for all entries. This is in sharp contrast to the situation at Mars, where the energy requirements of a 500 km target orbit constrained the undershoot boundary for many low velocity entries. A companion study to this work (Ref. 29) has recently shown that if the Earth return aerobrake is required to capture to a 24 hour parking orbit, rather than a low circular orbit, energy constraints impact the corridor widths for this maneuver as well. This effect is illustrated in Figure 34 from Reference 29. Corridor width is plotted against L/D for the various entry speeds in Figure 35. For the 14 and 15 km/s entries, vehicles with an L/D below those indicated failed to successfully capture.

As was discussed previously, a minimum entry corridor width of 0.7 degrees has been recommended for Earth return aerocapture (Ref. 114). If this criterion is applied here, an aerobrake with an L/D of 0.4 to 0.5 is found to be adequate for entry velocities up to 14.5 km/s.

The peak stagnation-point heating rate for the undershoot trajectory is shown as a function of entry velocity in Figure 36. These rates agree quite well with those calculated in Reference 19

for direct entries to the surface. Again, it should be recalled that the results presented here do not account for the moderating effects of ablation products in the boundary layer. The peak rates shown here vary enormously with ballistic coefficient and entry velocity and weakly with vehicle L/D. However, all entries considered are severe enough to require the use of ablative heat shields. As points of reference, the highest heating rate encountered by any of the Apollo capsules was approximately 500 W/cm^2 , while the predicted peak rates for the Pioneer Venus probes exceeded 5 kW/cm^2 (Ref.117). Therefore, the Earth return aerocapture heating rates will be more severe than those encountered on previous manned missions but well within the experience of unmanned vehicles.

The relative importance of radiative and convective heating vary widely with entry conditions and vehicle characteristics. Radiation accounts for a higher fraction of the total peak heating rate as ballistic coefficient and entry velocity increase. These effects are illustrated in Figure 37. The influence of $m/C_D A$ on undershoot peak heating rate and overshoot integrated heat load is illustrated for an entry velocity of 13 km/s in Figures 38 and 39. For comparison, the original Apollo entry capsule had a ballistic coefficient of approximately 350 kg/m^2 .

The overshoot integrated heat load is shown in Figure 40 as a function of entry velocity. The calculated values range from about 25 to 600 percent of the 43 kJ/cm^2 heat load experienced by the Apollo 6 command module. However, all entries considered are much more benign than the 800 kJ/cm^2 heat load expected for the Galileo

probe (Ref. 118). It should be noted that vehicles with a high lift-to-drag ratio have a larger integrated heat load for their overshoot trajectories than vehicles with a lower L/D. This effect is most pronounced when high lift-to-drag is combined with a low ballistic coefficient to produce a vehicle with substantial control authority. In this situation, a very shallow entry is able to result in a successful aerocapture. Such a maneuver produces a very long duration, fairly low intensity heating pulse which yields a high integrated heat load.

When examining the heating curves presented here, it should be recalled that they are for the overshoot and undershoot trajectories. Therefore, these plots represent the design points for the vehicle's thermal protection system if the full entry corridor is to be useful. However, if the vehicle enters the atmosphere near the middle of its corridor, the heating environment actually encountered will be somewhat less severe than those described above.

CONCLUSIONS AND RECOMMENDATIONS

An examination of the results of previous spaceflight and ground-based studies has suggested that manned aerocapture maneuvers for Mars missions be constrained by a 5 G peak deceleration limit. This is supported by Soviet missions which subjected long-duration flight crews to loads of 5 to 6 Gs upon reentry into the Earth's atmosphere. The recommendation is applicable to both the Mars arrival and Earth return phases for sprint and opposition class missions. Existing data are inadequate to determine an appropriate limit for the Earth return maneuver for a conjunction class mission.

Application of this deceleration limit to aerocapture maneuvers for manned Mars missions allows the calculation of entry corridor widths for Mars arrival and Earth return. If a 1 degree corridor is required at Mars and the vehicle is inserted into a 500 km circular orbit, an aerobrake L/D of 0.3 is adequate for entry velocities up to 9 km/s. If entry speeds are to reach 10 km/s, an L/D of 0.4 to 0.5 is necessary. Requiring the spacecraft to capture to a higher, more elliptical target, such as a 1 sol orbit, does not substantially alter these conclusions. Moreover, as an independent parameter, the vehicle's ballistic coefficient has little impact on corridor width or L/D requirements.

For Earth return aerocapture, a corridor width requirement of 0.7 degrees is applied and the vehicle is inserted into a 500 km circular orbit. With these constraints and a 5 G peak load limit, a lift-to-

drag ratio of 0.4 to 0.5 is sufficient for entry velocities up to 14.5 km/s.

Stagnation-point aerodynamic heating for Martian aerocapture will be great enough to require the use of ablative heat shields in most entry scenarios. However, a radiatively cooled thermal protection system may be possible if the vehicle's ballistic coefficient can be kept near 100 kg/m^2 . This would be advantageous, since the TPS would be lighter than if an ablative shield were required. The integrated heat load will be comparable to or more benign than the 43 kJ/cm^2 encountered by the Apollo 6 entry capsule.

Potential Earth return stagnation-point peak heating rates range from 150 to 3000 W/cm^2 with an integrated heat load of 10 to 250 kJ/cm^2 . Although this entry will probably be more severe than that encountered by any of the Apollo missions, it is well within the range of experience for unmanned vehicles.

This study confirms that aerocapture can be effectively used over a very wide range of potential Mars mission scenarios. However, it is still uncertain if the crew will be able to function safely and effectively on missions substantially longer than previous one year Soviet flights. Extrapolation of the limited data from earlier missions to Mars voyages lasting up to three years could lead to erroneous conclusions. In the opinion of the author, the limiting factors on mission duration will probably involve both physiological and, perhaps more importantly, psychological factors. Unfortunately, strong, objective information on these issues is not currently available. Substantial efforts must be devoted to

resolving these questions before multi-year missions can be planned with confidence. To a large extent, this will require prolonged flights in low Earth orbit; however, ground based studies will also be useful, particularly with regard to the psychological issues.

REFERENCES

- 1) von Braun, Wernher, *The Mars Project*, The University of Illinois Press, Urbana, 1962.
- 2) *Pioneering the Space Frontier; The Report of the National Commission on Space*, Bantam Books, New York, 1986.
- 3) *America at the Threshold; America's Space Exploration Initiative*, the report of the Synthesis Group on America's Space Exploration Initiative, May 1991.
- 4) *Report of the Advisory Committee on the Future of the U.S. Space Program*, December 1990.
- 5) Ride, S.K., *Leadership and America's Future in Space*, report to the NASA Administrator, August 1987.
- 6) Walberg, G.D., "A Review of Aerobraking for Mars Missions," IAF paper 88-196, Oct. 1988.
- 7) Tauber, M.E., Bowles, J.V., and Yang, L., "The Use of Atmospheric Braking During Mars Missions," AIAA Paper 89-1730, June 1989.
- 8) McKay, C.P. and Meyer, T.R., "Architectures for the Scientific Exploration of Mars," AIAA Paper 91-0327, Jan. 1991.
- 9) Zubrin, R. and Baker, D., "Humans to Mars in 1999," *Aerospace America*, Vol. 28, No. 8, August 1990, p. 30.
- 10) Syvertson, C.A. and Dennis, D.H., "Trends in High-Speed Atmospheric Flight," NASA TM X-54062, June 1964.
- 11) Sohn, R.L., ed. "Manned Mars Landing and Return Mission," NASA Ames Research Center, Contract NAS 2-1409, TRW Space Technology Laboratories, Rep. 8572-6011-RV-000, March 1964.
- 12) Braun, R.D. and Blersch, D.J., "Propulsive Options for a Manned Mars Transportation System," AIAA Paper 89-2950, July 1989.

- 13) Strogonova, L.B. and Leonid, G., "Manned Expedition to Mars: Concepts and Problems," *Acta Astronautica*, Vol. 23, pp. 279-287, 1991.
- 14) Chapman, D.R., "An Approximate Analytical Method for Studying Entry into Planetary Atmospheres," NASA TR R-11, 1959.
- 15) Chapman, D.R., "An Analysis of the Corridor and Guidance Requirements for Supercircular Entry into Planetary Atmospheres," NASA TR R-55, 1959.
- 16) Lees, L., Hartwig, F.W., and Cohen, C.B., "Use of Aerodynamic Lift During Entry into the Earth's Atmosphere," *American Rocket Society Journal*, Sept. 1959, pp. 633-641.
- 17) Phillips, R.L. and Cohen, C.B., "Use of Drag Modulation to Reduce Deceleration Loads During Atmospheric Entry," *American Rocket Society Journal*, June 1959, pp. 414-422.
- 18) Braun, R.D., Powell, R.W., and Hartung, L.C., "Effect of Interplanetary Trajectory Options on a Manned Mars Aerobrake Configuration," NASA TP-3019, August 1990.
- 19) Tauber, M.E., Palmer, G.E., and Yang, L., "Earth Atmospheric Entry Studies for Manned Mars Missions," AIAA paper 90-1699, June 1990.
- 20) Hillje, E.R., "Report of a Study of a Low Lift-To-Drag Ratio, Hypervelocity Entry into the Earth's Atmosphere Using a Constant Altitude Braking Maneuver," NASA General Working Paper no. 10031, Johnson Space Center, July 1964.
- 21) Gamble, J.D., "JSC Pre-Phase A Study: Mars Rover Sample Return Mission Aerocapture, Entry, and Landing Element," JSC-23230, May 1989.
- 22) Goodrick, T.F., "Methodology and Critical Performance Characteristics of Aerobrake Maneuvers for Earth Return," IAF paper 91-177, Oct. 1991.
- 23) Braun, R.D. and Powell, R.W., "Aerodynamic Requirements of a Manned Mars Aerobraking Transfer Vehicle," AIAA paper 90-2817, August 1990.

- 24) Lyne, J.E., Tauber, M.E., and Braun, R.D., "Earth Return Aerocapture for Manned Mars Missions," AIAA paper 91-2874, August 1991.
- 25) Lyne, J.E., Anagnost, A.E., and Tauber, M.E., "A Parametric Study of Manned Aerocapture at Mars," AIAA paper 91-2871, August 1991.
- 26) Baab, G.R. and Stump, W.R., "Mars Orbit Selection," NASA TM 89320, June 1986, pp. 78-86.
- 27) Desai, P.N., "Aspects of Parking Orbit Selection in a Manned Mars Mission," Master's degree thesis, George Washington University, August 1990.
- 28) Desai, P.N. and Braun, R.D., "Mars Parking Orbit Selection," *The Journal of Astronautical Sciences*, Vol. 39, No. 4, Oct.- Dec. 1991.
- 29) Braun, R.D., Powell, R.W., and Lyne, J.E., "Earth Aerobraking Strategies for Manned Return from Mars," AIAA paper 91-2873, August 1991.
- 30) Cruz, M.I., "The Aerocapture Vehicle Mission Design Concept -- Aerodynamically Controlled Capture of Payload Into Mars Orbit," AIAA Paper 79-0893, May 1979.
- 31) Tauber, M.E., Chargin, M., Henline, W., Chiu, A., Yang, L., Hamm, K.R., and Miura, H., "Aerobrake Design Studies for Manned Mars Missions," AIAA paper 91-1344, June 1991.
- 32) Freeman, D.C., Powell, R.W., and Braun, R.D., "Manned Mars Aerobrake Vehicle Design Issues," IAF paper 90-197, Oct. 1990.
- 33) Wilcockson, W.H., "L/D Requirements for Mars Aerocapture Missions," AIAA paper 90-2937, August 1990.
- 34) Gnoffo, P.A., Price, J.M., and Braun, R.D., "On the Computation of Near Wake, Aerobrake Flowfields," AIAA paper 91-1371, June 1991.
- 35) Papadopoulos, P., Tauber, M.E., and Chang, I.D., "Aerobraking in a Dusty Martian Atmosphere," AIAA paper 90-1700, June 1990.
- 36) Papadopoulos, P., Tauber, M.E., and Chang, I.D., "Heat Shield Erosion in a Dusty Martian Atmosphere," AIAA paper 92-0855, Jan. 1992.

- 37) *SEI Engineering Requirements on Robotic Missions: Report of the Mars Atmospheric Knowledge Requirements Working Group*, Bourke, R.D. (ed.), JPL D-8465, May 1991.
- 38) Seiff, A. and Kirk, D.B., "Structure of the Atmosphere of Mars in Summer at Mid-Latitudes," *Journal of Geophysical Research*, Vol. 82, No. 28, Sept. 1977, pp. 4364-4378.
- 39) Owen, T., Biemann, K., Rushneck, D.R., Biller, J.E., Howarth, D.W., and LaFleur, A.L., "The Composition of the Atmosphere at the Surface of Mars," *Journal of Geophysical Research*, Vol. 82, No. 8, 1977, pp. 4633-4639.
- 40) Justus, C.G., "A Mars Global Reference Atmospheric Model (MarsGRAM) for Mission Planning and Analysis," AIAA paper 90-0004, Jan. 1990.
- 41) U.S. Standard Atmosphere, 1976, NOAA - S/T 76-1562.
- 42) Konopliv, A. and Wood, L.J., "High-Accuracy Mars Approach Navigation with Radio Metric and Optical Data," AIAA paper 90-2907, August 1990.
- 43) Wood, L. "MRSR Navigation Studies Performed During FY88," JPL, OAST PATHFINDER High Energy Aerobraking Workshop Proceedings, Feb. 1989.
- 44) Edwards, C.D., Folkner, W.M., Border, J.S., and Wood, L.J., "Spacecraft-Spacecraft Interferometry for Planetary Approach Navigation," AAS paper 91-181, Feb. 1991.
- 45) Brand, T.J., Fuhry, D.P., and Shepperd, S.W., "An Onboard Navigation System Which Fulfills Mars Aerocapture Guidance Requirements," AIAA paper 89-0629, Jan. 1989.
- 46) Potter, J.L. and Peterson, S.W., "Local and Overall Aerodynamic Coefficients for Bodies in Hypersonic, Rarefied Flow," AIAA paper 91-0336, Jan. 1991.
- 47) Tauber, M.E., Bowles, J.V., and Yang, L., "Atmospheric Environment During Maneuvering Descent from Martian Orbit," *Journal of Spacecraft and Rockets*, Vol. 26, No. 5, pp. 330-337.

- 48) Ferri, A., Feldman, L., and Daskin, W., "The Use of Lift for Re-Entry From Satellite Trajectories," *Jet Propulsion*, Vol. 27, Nov. 1957, pp. 1184-1191.
- 49) Tauber, M.E. and Yang, L. "Performance Comparisons of Maneuvering Vehicles Returning from Orbit," *Journal of Spacecraft and Rockets*, Vol. 25, No. 4, July-August 1988, pp.263-270.
- 50) Perry, D.J., Aircraft Structures, McGraw-Hill, New York, 1950.
- 51) Marvin, J.G. and Deiwert, G.S., "Convective Heat Transfer in Planetary Gases," NASA TR R-224, July 1965.
- 52) Yee, L., Bailey, H.E., and Woodward, H.T., "Ballistic Range Measurements of Stagnation-Point Heat Transfer in Air and in Carbon Dioxide at Velocities Up to 18,000 Feet per Second," NASA TN D-777, March 1961.
- 53) Loh, W.H.T., Entry Thermodynamics, in Re-entry and Planetary Entry / I, ed. Loh, W.H.T., Springer-Verlag, New York, 1968.
- 54) Anderson, J.D., Hypersonic and High Temperature Gas Dynamics, McGraw-Hill, New York, 1989.
- 55) Tauber, M.E. and Sutton, K., "Stagnation-Point Radiative Heating Relations for Earth and Mars Entries," *Journal of Spacecraft and Rockets*, Vol. 28, No. 1, Jan.-Feb. 1991, pp. 40-42.
- 56) Tauber, M.E., "Some Simple Scaling Relations for Heating of Ballistic Entry Bodies," *Journal of Spacecraft and Rockets*, Vol. 7, No. 7, July 1970, pp. 885-886.
- 57) Berry, C.A. and Berry, M.A., "Aerospace Medicine: The Vertical Frontier," in Management of Wilderness and Environmental Emergencies," ed. Auerbach, P.S., and Geehr, E.C., New York, Macmillan, 1983, pp. 522-555.
- 58) Fraser, T.M. "Human Response to Sustained Acceleration," NASA SP-103, 1966.
- 59) Wood, E.H., "Maximum Protection Anti-G Suits and Their Limitations," *SAFE Journal*, Vol. 18, No.3, 1988, pp.30-40.

- 60) Wood, E.H., "Some Effects of the Force Environment on the Heart, Lungs and Circulation," *Clinical and Investigative Medicine*, Vol. 10 , No. 5, 1987, pp. 401-427.
- 61) Barr, P.O., "Hypoxemia in Man Produced by Prolonged Acceleration," *Acta Physiol. Scand.* Vol. 54, 1962, pp. 128-137.
- 62) Vandenberg, R.A., Nolan, A.C., Reed, J.H. Jr., and Wood, E.H., "Regional Pulmonary Arterial-Venous Shunting Caused by Gravitational and Inertial Forces," *J. Applied Physiol.*, Vol. 25, 1968, pp.516-527.
- 63) Wood, E.H., Lambert, E.H., and Strum, R.E., "Systolic Blood Pressure in Man During Exposure to High Accelerations on the Centrifuge," NRC, CMR Committee on Aviation Medicine, Report No. 338, August 1944.
- 64) Johanson, D.C., "Cephalic Blood Flow Velocity and Tissue Oxygen Desaturation During Exposure to +G_z Acceleration Profiles," doctoral thesis, Drexel University, 1990.
- 65) Rossen, R., Kabat, H., and Anderson, J.P., "Acute Arrest of Cerebral Circulation in Man," *Archiv. Neurol. and Psychiat.*, Vol. 50, 1943, pp.510-528.
- 66) Andina, F., "Schwarzsehen" als Ausdruck von Blutdruckschwankungen bei Sturzflügen. *Schweiz. Med. Wehnschr.*, Vol. 67, 1937, pp. 753-756.
- 67) Wood, E.H., "Development of Methods for Prevention of Acceleration Induced Blackout and Unconsciousness in World War II Fighter Pilots. Limitations: Present and Future," *The Physiologist*, Vol. 30, No. 1 1987, S27-S30.
- 68) Wood, E.H, "G-Induced Loss of Consciousness and Its Prevention," USAFSAM-TR-87-41, Sept. 1988.
- 69) Cherniack, N.S., Hyde, A.S., Watson, J.F., and Zechman, F.W., "Some Aspects of Respiratory Physiology During Forward Acceleration," *Aerospace Medicine*, Vol. 23, 1961, pp. 113-120.

- 70) Hershgold, E.J. "Roentgenographic Study of Humans During Transverse Accelerations," *Aerospace Medicine*, Vol. 31, 1960, p. 213.
- 71) Bondurant, S., Clarke, N.P., Blanchard, W.G., Miller, H., Hessberg, R.R., Hiatt, E.P., "Human Tolerance to Some of the Accelerations Anticipated in Space Flight," WADC TR 58-156.
- 72) White, W.J. and Jorve, W.R., "The Effects of Gravitational Stress Upon Visual Acuity," WADC-TR-56-247, 1956.
- 73) Smedal, H.A., Rogers, T.A., Duane, T.D. Holden, G.R., and Smith, J.R., "The Physiological Limitations of Performance During Acceleration," *Aerospace Medicine*, Vol. 34, 1963, p. 48.
- 74) Steiner, S.H., Mueller, G.C.E., "Pulmonary Arterial Shunting in Man During Forward Acceleration," *J. Applied Physiol.*, Vol. 16, 1961, p.1081.
- 75) Hultgren, H.N., "High-Altitude Illness," in Management of Wilderness and Environmental Emergencies," ed. Auerbach, P.S., and Geehr, E.C., New York, Macmillian, 1983, pp.1-26.
- 76) "Guidance and Navigation for Entry Vehicles," NASA SP-8015, November 1968.
- 77) Wood, E.H., "Development of Anti-G Suits and Their Limitations," *Aviation , Space, and Environmental Medicine*, Vol. 58, July 1987, pp.699-706.
- 78) Cohen, M.M., "Combining Techniques to Enhance Protection Against High Sustained Accelerative Forces," *Aviation, Space, and Environmental Medicine*, April 1983, pp. 338-342.
- 79) Watson, J.F. and Cherniack, N.S., "Effect of Positive Pressure Breathing on the Respiratory Mechanics and Tolerance to Forward Acceleration," *Aerospace Medicine*, Vol. 33, 1962, p. 583.
- 80) Reed, J.H., Jr., Burgess, B.F., and Sandler, H., "Effects on Arterial Oxygen Saturation of Positive Pressure Breathing During Acceleration," *Aerospace Medicine* Vol. 35, 1964, p.238.

- 81) Wood, E.H., "The Acceleration-Induced Loss of Consciousness Problem, Its Discovery During World War I, Elucidation During World War II, Three Decades of 'Middle Ages', Followed By Its Renaissance in the 1980s," in Evolution of Anti-G Suits and Their Limitations, and Alternative Methods for Avoidance of G-Induced Loss of Consciousness, ed. Wood, E.H., report to the Strategic Technology Office, Defense Advanced Research Projects Agency under contract no. N66001-87-C-0079, May 1990.
- 82) Henderson, B.W., "USAF Pilots Begin Operational Testing of System to Increase High-G Tolerance," *Aviation Week and Space Technology*, March 4, 1991.
- 83) Bungo, M.W., "The Cardiopulmonary System," in Space Physiology and Medicine, ed. Nicogossian, A.E., Huntoon, C.L., and Pool, S.L., Philadelphia, Lea and Febiger, 1989, pp. 179-201.
- 84) Gizenko, O.G., Genin, A.M., and Egorov, A.D., "Summary of Medical Investigations in the U.S.S.R. Manned Space Missions," *Acta Astronautica*, Vol. 8, No. 9-10, Jan. 1981, pp. 907-917.
- 85) Berry, C.A., "Medical Legacy of Skylab as of May 9, 1974: The Manned Skylab Missions," *Aviation, Space, and Environmental Medicine*, Vol. 47, No. 4, April 1976, pp. 418-424.
- 86) Johnson, R.L., Nicogossian, A.E., Bergman, S.A., Jr., and Hoffler, G.W., "Lower Body Negative Pressure: The Second Manned Skylab Mission," *Aviation, Space, and Environmental Medicine*, Vol. 47, No. 4, April 1976, pp. 347-353.
- 87) Thornton, W.E. and Hoffler, G.W., "Hemodynamic Studies of the Legs Under Weightlessness," in Biomedical Results From Skylab, NASA SP-377, ed. Johnston, R.S. and Dietlein, L.F., 1977, pp. 324-329.
- 88) Convertino, V.A., "Exercise Training: Blood Pressure Responses in Subjects Adapted to Microgravity," SAE Paper 911458, presented at the 21st International Conference on Environmental Systems, San Francisco, Ca July 1991.
- 89) Greenleaf, J.E., Wade, C.E., and Leftheriotis, G., "Orthostatic Responses Following 30-Day Bed Rest Deconditioning with Isotonic and Isokinetic Exercise Training," *Aviation, Space, and Environmental Medicine*, Vol. 60, 1989, pp. 537-542.

- 90) Nicogossian, A.E., "Overall Physiological Response to Space Flight," in Space Physiology and Medicine, ed. Nicogossian, A.E., Huntoon, C.L., and Pool, S.L., Philadelphia, Lea and Febiger, 1989, pp.139-153.
- 91) Vorobyov, E.I., Gazenko, O.G., Genin, A.M., and Egorov, A.D., "Medical Results of Salyut-6 Manned Space Flights," *Aviation, Space, And Environmental Medicine*, Supplement 1, Vol. 54, No. 12, Dec. 1983, pp. S31-S40.
- 92) Buderer, M., Rummel, J.A., Michel, E.L., Mauldin, D.G., and Sawin, C.F., "Exercise Cardiac Output Following Skylab Missions: The Second Manned Skylab Mission," *Aviation, Space, and Environmental Medicine*, Vol. 47, No. 4, April 1976, pp. 365-372.
- 93) Michel, E.L., Rummel, J.A., Sawin, C.F., Buderer, M.C., and Lem, J.D., "Results of Skylab Medical Experiment M171- Metabolic Activity," in Biomedical Results From Skylab, NASA SP-377, ed. Johnston, R.S. and Dietlein, L.F., 1977, pp. 324-329.
- 94) Yegorov, A.D., "Results of Medical Research During the 175 Day Flight of the Third Main Crew on the Salyut-6-Soyuz Orbital Complex, NASA TM-76450, Jan. 1981.
- 95) Grigoriev, A.I., Bugrov, S.A., Bogomolov, V.V., Egorov, A.D., Kozlovskaya, I.B., Pestov, I.D., Polyakov, V.V., and Tarasov, I.K., "Preliminary Medical Results of the Mir Year-Long Mission," *Acta Astronautica*, Vol. 23, 1991, pp.1-8.
- 96) Nicogossian, A.E. and Dietlein, L.F., "Microgravity: Simulations and Analogs," in Space Physiology and Medicine, ed. Nicogossian, A.E., Huntoon, C.L., and Pool, S.L., Philadelphia, Lea and Febiger, 1989, pp. 240-248.
- 97) Newsom, B.D., Goldenrath, W.L., Winter, W.R., and Sandler, H., "Tolerance of Females to +Gz Centrifugation Before and After Bedrest," *Aviation, Space, and Environmental Medicine*, Vol. 48, No. 4, April 1977, pp. 327-331.
- 98) Miller, P.B. and Leverett, S.D., "Tolerance to Transverse (+G_x) and Headward (+G_z) Acceleration After Prolonged Bed Rest," *Aerospace Medicine*, Vol. 36, No. 1, January 1965, pp. 13-15.

- 99) Jacobson, L.B., Hyatt, K.H., and Sandler, H., "Effects of Simulated Weightlessness on Responses of Untrained Men to +G_z Acceleration," *Journal of Applied Physiology*, Vol. 36, No. 6, June 1974, pp. 745-752.
- 100) Sandler, H., Goldwater, D.J., and Rositano, S.A., "Physiologic Responses of Female Subjects During Bed Rest Shuttle Flight Simulation," preprints of the Annual Scientific Meeting, Aerospace Medical Association, New Orleans, LA, 1978.
- 101) Sandler, H., Goldwater, D.J., Rositano, S.A., Sawin, C.F. and Booher, C.R., "Physiologic Responses of Male Subjects Ages 46-55 Years to Shuttle Flight Simulation," preprints of the Annual Scientific Meeting, Aerospace Medical Association, Washington, D.C., 1979.
- 102) Bungo, M.W., Charles, J.B., and Johnson, P.C., "Cardiovascular Deconditioning During Space Flight and the Use of Saline as a Countermeasure to Orthostatic Intolerance," *Aviation, Space, and Environmental Medicine*, Vol. 56, No. 10, Oct. 1985, pp. 985-990.
- 103) Suvorov, P.M., "Influence of Thirty-Day Hypokinesia in Combination with Exposure to LBNP on Tolerance to Accelerations [+G_z]," *Kosmicheskaya Biologiya i Avialosmicheskaya Meditsina*, Vol. 8, No. 1, Jan.- Feb. 1974, pp. 65-68.
- 104) Nicogossian, A.E., "Countermeasures to Space Deconditioning," *Space Physiology and Medicine*, ed. Nicogossian, A.E., Huntoon, C.L., and Pool, S.L., Philadelphia, Lea and Febiger, 1989, pp. 294-314.
- 105) Garshnek, V., "Soviet Space Flight: The Human Element," *Aviation, Space, and Environmental Medicine*, Vol. 60, No. 7, July 1989, pp. 695-705.
- 106) Greenleaf, J.E., van Beaumont, W., Bernauer, E.M., Haines, R.F., Sandler, H., Staley, R.W., Young, H.L., and Yusken, J.W., "Effects of Rehydration on +G_z Tolerance After 14-Days' Bed Rest," *Aviation, Space, and Environmental Medicine*, Vol. 44, No. 7, July 1973, pp. 715-722.
- 107) Goldwater, D.J., Convertino, V.A., and Sandler, H., "Acceleration Tolerance in 55 to 65 Year Old Men After Shuttle Flight Simulation,"

preprints of the Annual Scientific Meeting, Aerospace Medical Association, 1981.

108) Kotovskaya, A.R., Vartbaronov, R.A., and Simpura, S.F., "Changes in the Capacity of Man to Withstand Transverse Stresses After Hypodynamia of Varying Duration," *Problemy Kosmicheskoy Biologii*, Vol. 16, 1971, pp. 46-54.

109) Kotovskaya, A.R., Vartbaronov, R.A., and Simpura, S.F., "Change in Load-Factor Tolerance After 70 Days of Hypodynamia," *Problemy Kosmicheskoy Biologii*, Vol. 13, 1969, pp. 241-247.

110) Polyakov, V.V., "The Physician-Cosmonaut Tasks in Stabilizing the Crew Members Health and Increasing an Effectiveness of Their Preparation for Returning to Earth," *Acta Astronautica*, Vol. 23, Jan. 1991, pp. 149-151.

111) Johnston, R.S., Dietlein, L.F., and Berry, C.A., (ed.), Biomedical Results of Apollo, NASA SP-368, 1975.

112) Turnhill, R. (ed.), Jane's Spaceflight Directory, Jane's Yearbooks, London, 1987.

113) Kotovskaya, A.R. and Vil'-Vill'yams, I.F., "+G_x Tolerance in the Final Stage of Space Flights of Various Durations," *Acta Astronautica*, Vol. 23, No. 1, January 1991, pp. 157-161.

114) "Orbital Transfer Vehicle Concept Definition and System Analysis Study," Martin Marietta Report MCR 86-2601 under NASA grant NAS8-36108.

115) Braun, R.D. and Powell, R.W., "A Predictor-Corrector Guidance Algorithm for Use in High Energy Aerobraking Systems Studies," AIAA Paper 91-0058, January 1991.

116) Curry, D.M. and Stephens, E.W., "Apollo Ablator Thermal Performance at Superorbital Entry Velocities," NASA TN D-5969, September 1970.

117) Moss, J.N., Zoby, E.V., Sutton, K., and Anderson, E.C., "Aerothermal Environment for the Pioneer Venus Multiprobe Mission," in Aerodynamic Heating and Thermal Protection Systems, Vol. 59 of Progress in Astronautics and Astronautics, 1978.

- 118) Moss, J.N., "A Study of the Aerothermal Entry Environment for the Galileo Probe," AIAA Paper 79-1081, June 1979.

TABLE 1
MARTIAN ATMOSPHERIC DENSITY PROFILE CONSTANTS

Altitude Range, km	ρ_0 , kg/m ³	β , m ⁻¹
>115	2.103 (10 ⁻⁸)	1.154 (10 ⁻⁴)
60 to 115	3.29 (10 ⁻⁵)	1.337 (10 ⁻⁴)
36 to 60	0.039322	1.181 (10 ⁻⁴)
9 to 36	0.019099	9.804 (10 ⁻⁵)
< 9	0.1500	7.124 (10 ⁻⁵)

TABLE 2
CONSTANTS FOR CONVECTIVE HEATING EQUATION

	C1	C2
MARS	1.35 (10 ⁻⁸)	3.04
EARTH	1.83 (10 ⁻⁸)	3.00

TABLE 3
CONSTANTS FOR RADIATIVE HEATING EQUATION

EARTH

$$C_3 = 4.736 \times 10^4$$

$$a = 1.072 \times 10^6 V^{-1.88} \rho^{-0.325}$$

$$\text{if } 1 < r_n < 2, \quad a < 0.6$$

$$\text{if } 2 < r_n < 3, \quad a < 0.5$$

$$b = 1.22$$

MARS

$$C_3 = 2.35 (10^4)$$

$$a = 0.526$$

$$b = 1.19$$

TABLE 4
RADIATIVE HEATING VELOCITY FUNCTIONS
FOR EARTH AND MARS

V, m/sec	$f_E(V)$	V, m/sec	$f_M(V)$
9000	1.5	6000	0.2
9250	4.3	6150	1.0
9500	9.7	6300	1.95
9750	19.5	6500	3.42
10000	35	6700	5.1
10250	55	6900	7.1
10500	81	7000	8.1
10750	115	7200	10.2
11000	151	7400	12.5
11500	238	7600	14.8
12000	359	7800	17.1
12500	495	8000	19.2
13000	660	8200	21.4
13500	850	8400	24.1
14000	1065	8600	26.0
14500	1313	8800	28.9
15000	1550	9000	32.8
15500	1780		
16000	2040		

TABLE 5
PHYSIOLOGICAL EFFECTS OF G LOADS

	<i>Positive Acceleration: Plus G_x Effects</i>		<i>Transverse Acceleration: Plus G_x Effects</i>
+1 G _x	Equal to upright or seated posture on Earth	+2-3 G _x	Feeling of increased weight and abdominal pressure; progressive slight difficulty in focusing vision; tolerance to +2 G _x -24 hours, +4 G _x -60 minutes, +5 G _x -5 minutes
+2 G _x	Weight doubled; pressure on buttocks; drooping of face and soft body tissues	+3-6 G _x	Progressive tightness of chest; difficulty in speaking, or focusing; breathing, blurred vision
+2½ G _x	Difficult to move body	+6-9 G _x	Chest pain; shallow breathing; more blurred vision with occasional tunnel vision; inability to lift body or limbs at +8 G or head at +9 G
+3-4 G _x	Impossible to raise oneself; difficult to raise arms or legs; progressive dimming of vision after 3-4 seconds, which progresses to tunnel vision	+9-12 G _x	Severe difficulty breathing; increased chest pain; loss of peripheral vision
+4½-6 G _x	Decreased vision progresses to blackout after 5 seconds; hearing and then consciousness lost if continued; mild to severe convulsions in 50% of persons with unconsciousness; loss of orientation to time and place for 15 seconds after acceleration	+15 G _x	Vicelike chest pain; extreme difficulty in breathing and speaking; complete loss of vision
	<i>Negative Acceleration: Minus G_x Effects</i>		<i>Note: G_x effects are similar, with variance due only to direction (27)</i>
-1 G _x	Unpleasant facial congestion		
-2-3 G _x	Severe facial congestion; throbbing headache; progressive blurring, gray-ing, or reddening of vision after 5 seconds		

TABLE 6RANGE OF PARAMETERS FOR AEROCAPTURE STUDY

MARS ARRIVAL	
BALLISTIC COEFFICIENT	100, 300, and 500 kg/m ²
VEHICLE LIFT-TO-DRAG	0.1, 0.2, 0.3, 0.5, 0.7, and 1.0
ENTRY VELOCITY	6, 7, 8, 9, and 10 km/s

EARTH RETURN	
BALLISTIC COEFFICIENT	50, 100, 300, and 500 kg/m ²
VEHICLE LIFT-TO-DRAG	0.2, 0.3, and 0.5
ENTRY VELOCITY	11.5, 12.0, 13.0, 14.0, and 15 km/s

TABLE 7VARIATION OF NOSE RADIUS WITH L/D FOR MARS AEROBRAKES

<u>L/D</u>	<u>NOSE RADIUS</u>
0.3	16.0 m
0.5	11.7 m
1.0	1.0 m

TABLE 8
MARS AEROCAPTURE
UNDERSHOOT TRAJECTORY PEAK STAGNATION-POINT HEATING
RATE FOR VARIOUS TARGET ORBITS (W/CM²)

ORBITAL PERIOD (MIN)	ENTRY VELOCITY			
	6000 M/S	7000M/S	8000 M/S	9000 M/S
DIRECT ENTRY	19.0	73.1	182.7	246.0
110	17.4	72.7	173.9	244.6
500	14.4	66.5	173.9	244.6
1000	13.6	64.7	173.9	244.6
1500	13.1	64.1	173.9	244.5

TABLE 9
MARS AEROCAPTURE
OVERSHOOT TRAJECTORY INTEGRATED STAGNATION-POINT
HEAT LOAD FOR VARIOUS TARGET ORBITS (J/CM²)

ORBITAL PERIOD (MIN)	ENTRY VELOCITY			
	6000 M/S	7000 M/S	8000 M/S	9000 M/S
DIRECT ENTRY	2557	4308	8380	14536
110	2442	4582	8379	14034
500	1935	3958	8060	13812
1000	1835	3849	7907	13671
1500	1803	3781	7852	13621

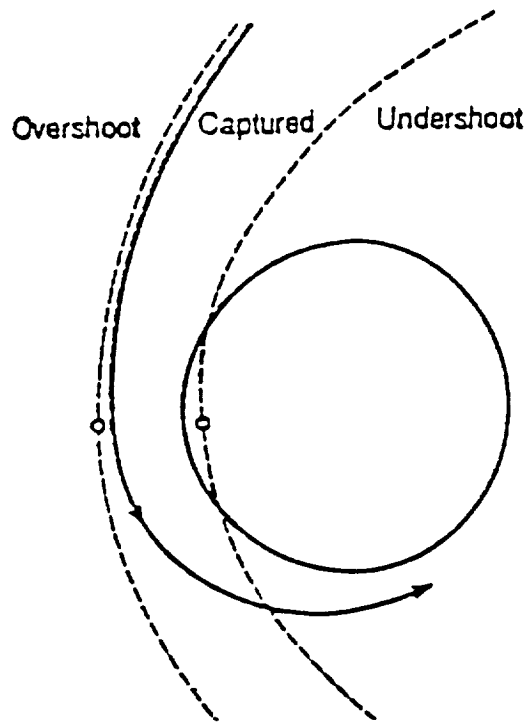


FIGURE 1. AEROCAPTURE

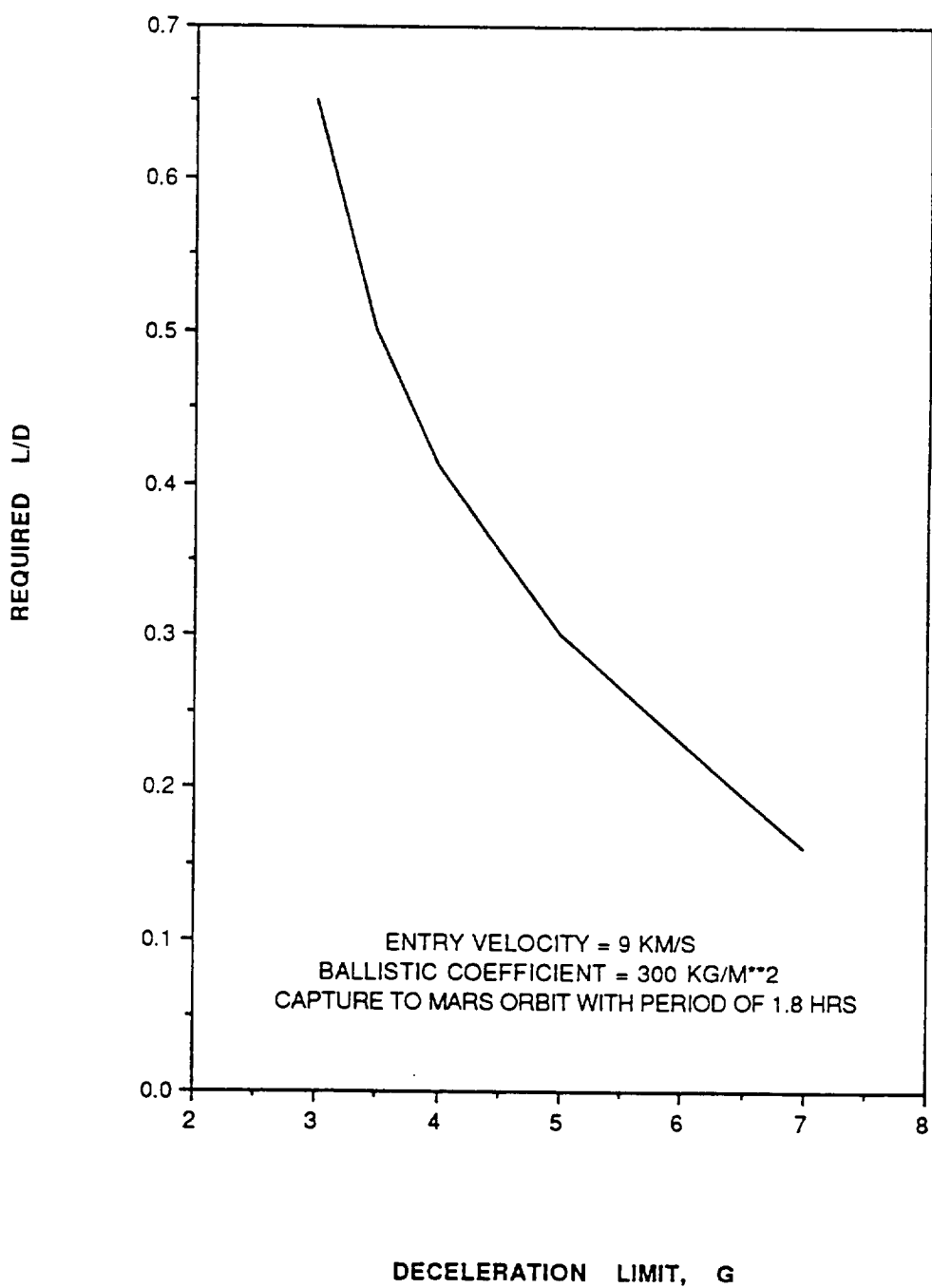
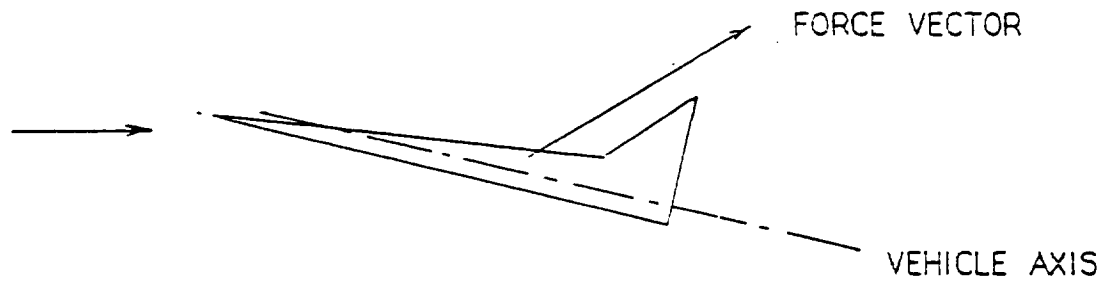
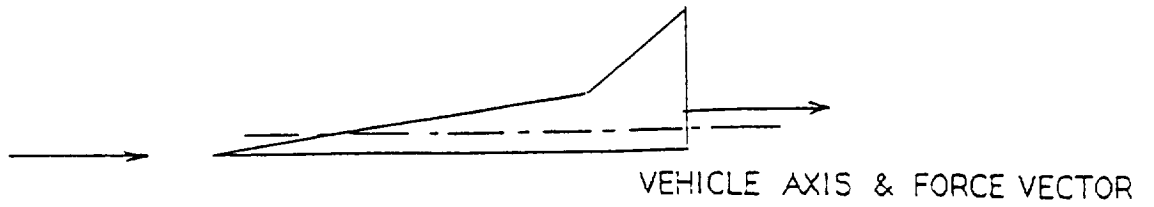
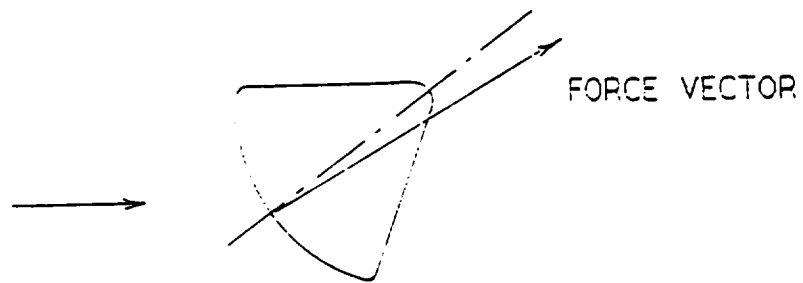
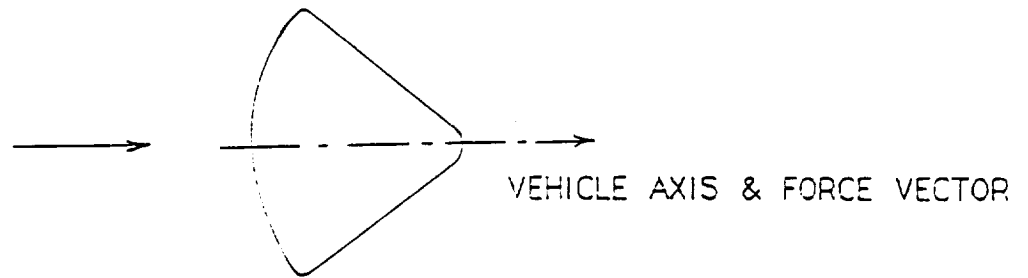


FIG. 2. REQUIRED MARS AEROBRAKE
L/D VS DECELERATION LIMIT

C-2



A) WINGED CONFIGURATIONS



B) CAPSULE CONFIGURATIONS

FIGURE 3. VEHICLE CLASSES FOR PITCH CONTROL

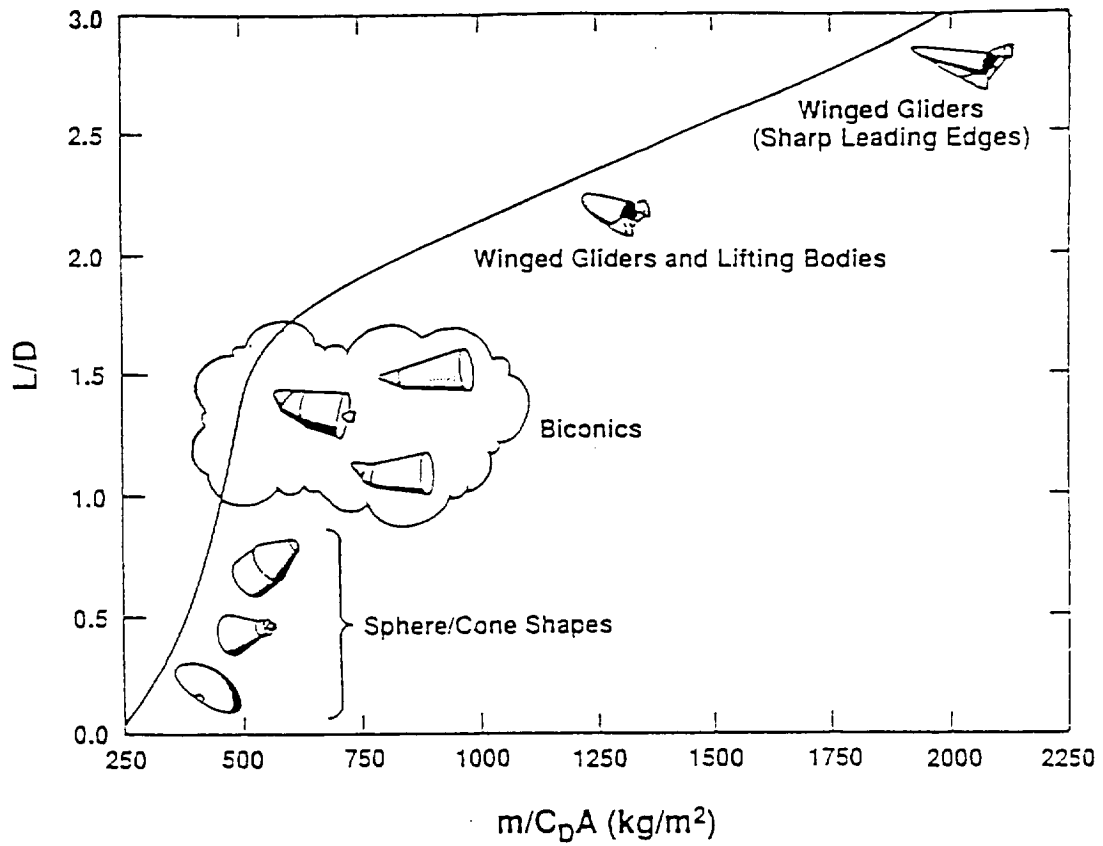


FIGURE 4. L/D VS BALLISTIC COEFFICIENT (REF. 30)

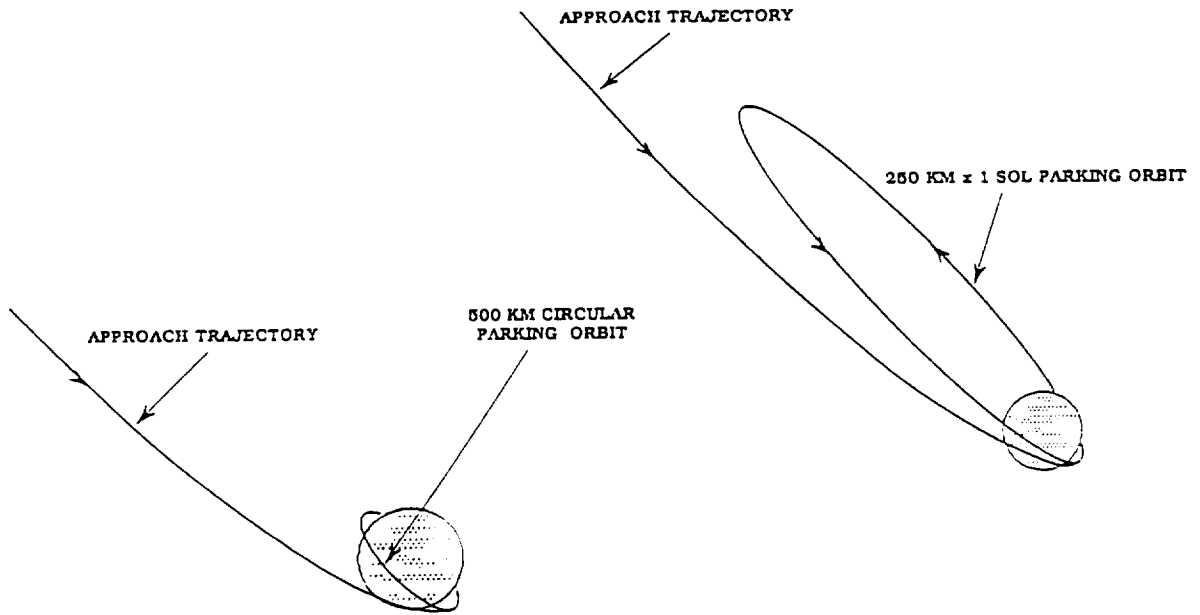


FIGURE 5. POTENTIAL MARTIAN AEROCAPTURE ORBITS

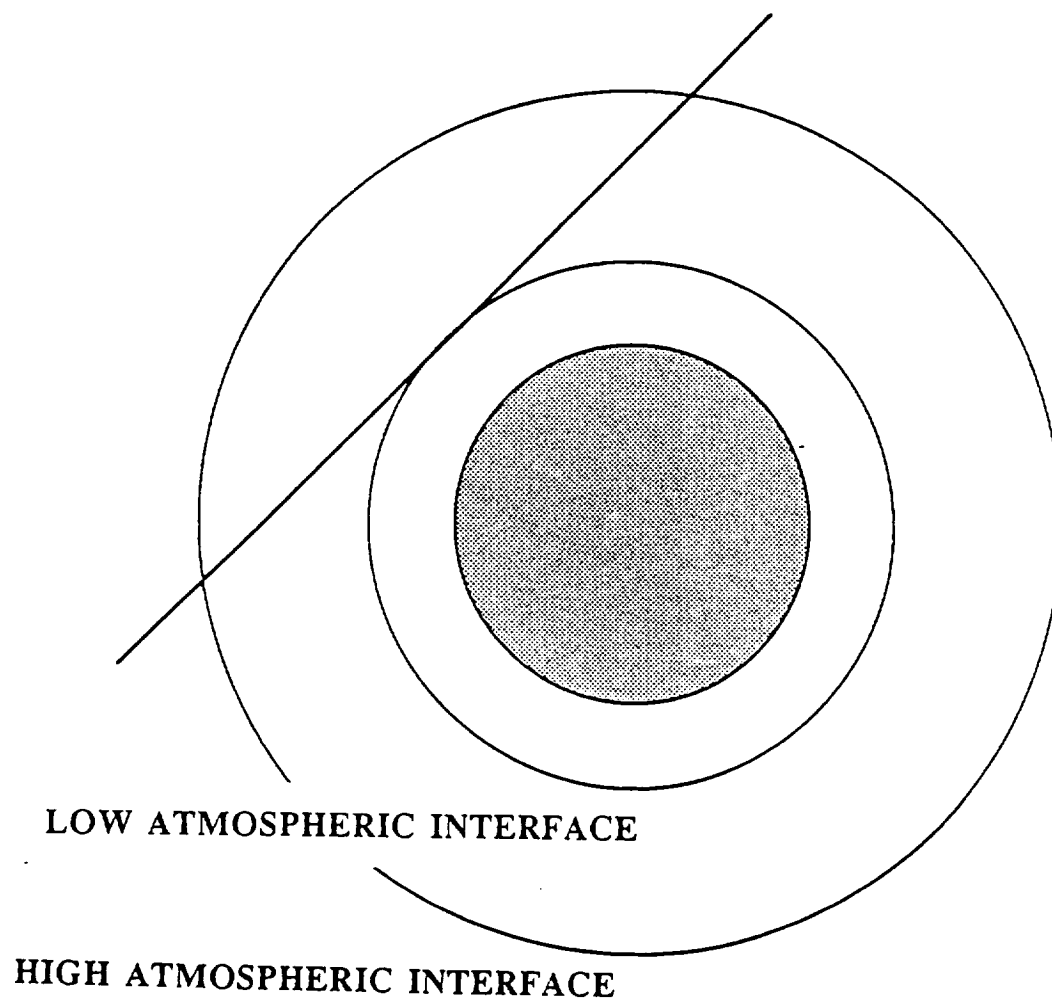


FIGURE 6. EFFECT OF ENTRY ALTITUDE ON ENTRY ANGLE

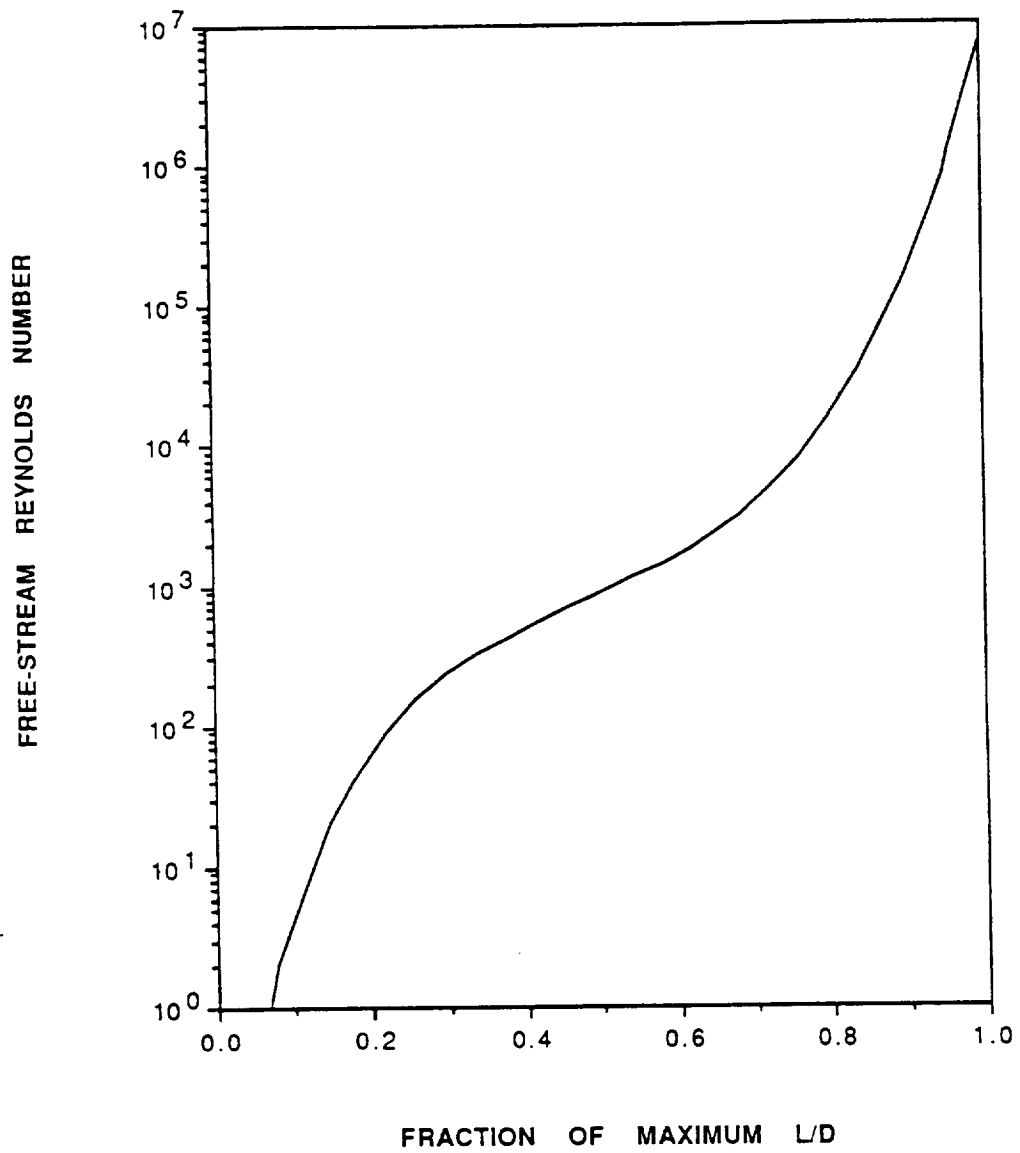


FIGURE 7. VARIATION OF VEHICLE L/D WITH REYNOLDS NUMBER

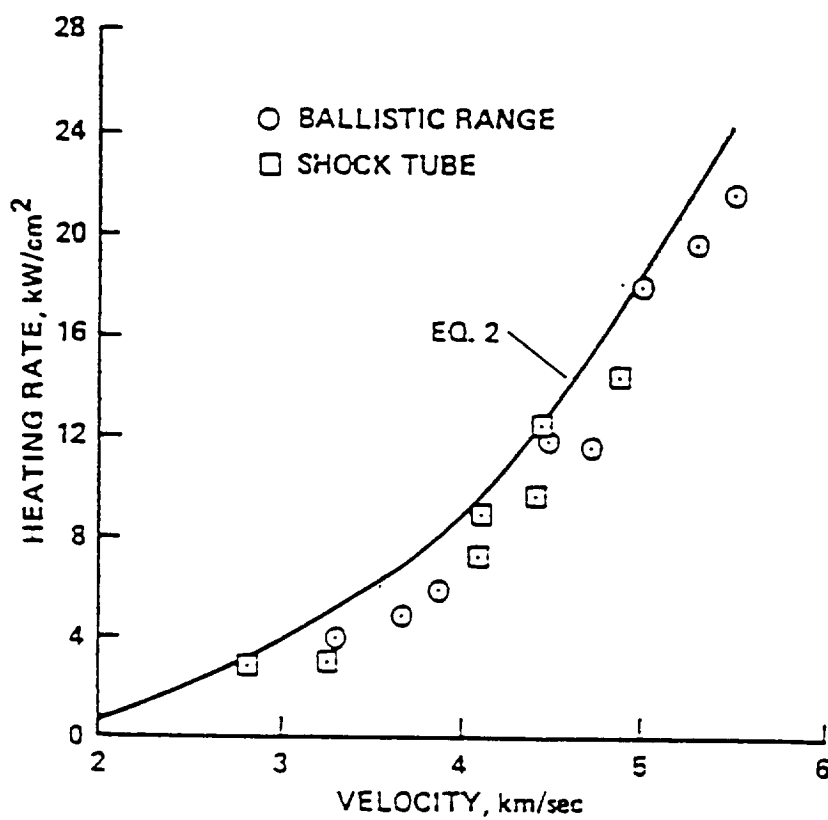


FIGURE 8. HEMISPHERICAL STAGNATION-POINT HEATING RATES IN CARBON DIOXIDE (REF. 52)

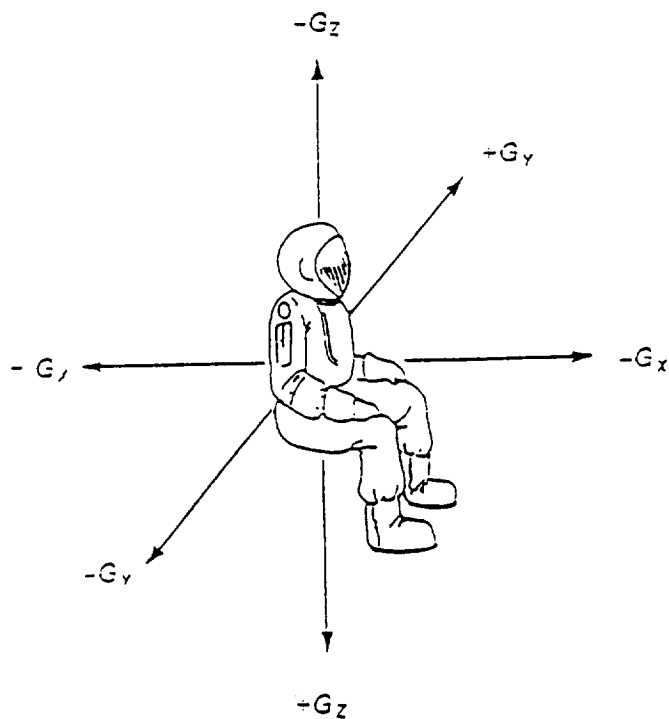


FIGURE 9. PHYSIOLOGICAL FORCE AXES (REF. 57)

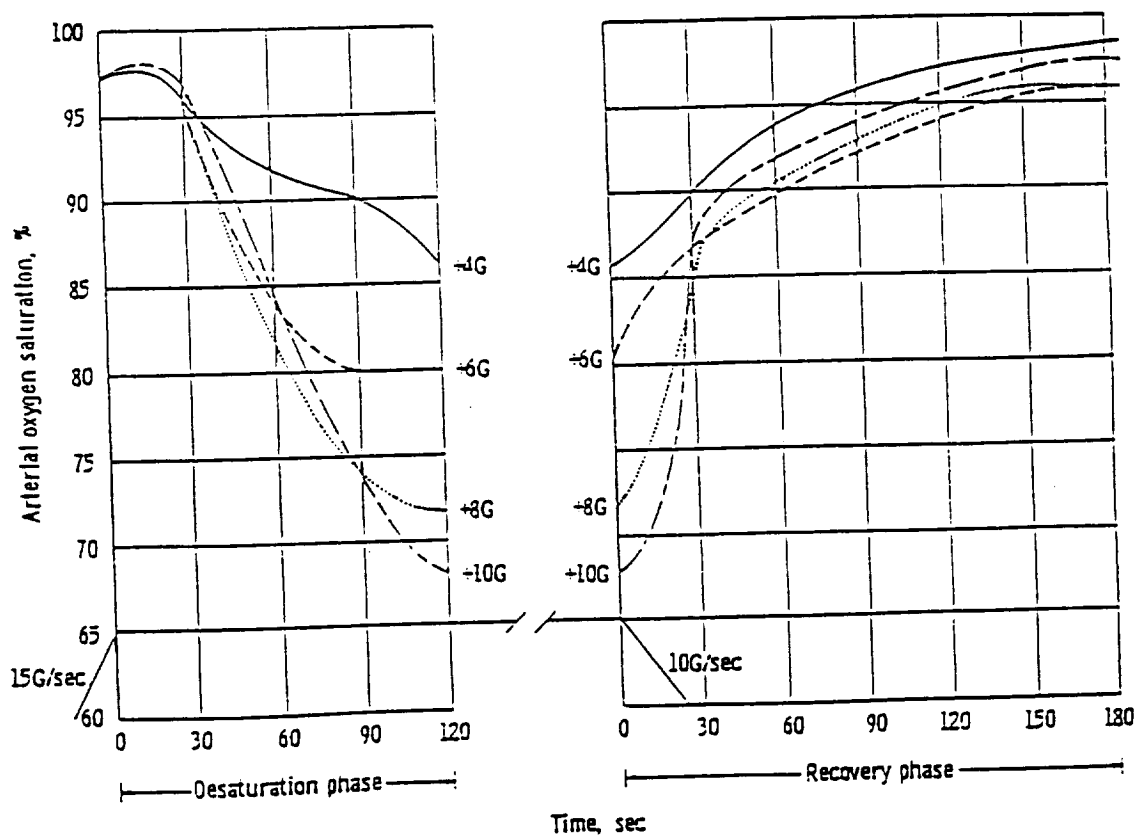


FIGURE 10. ARTERIAL OXYGEN SATURATION (REF. 58,74)

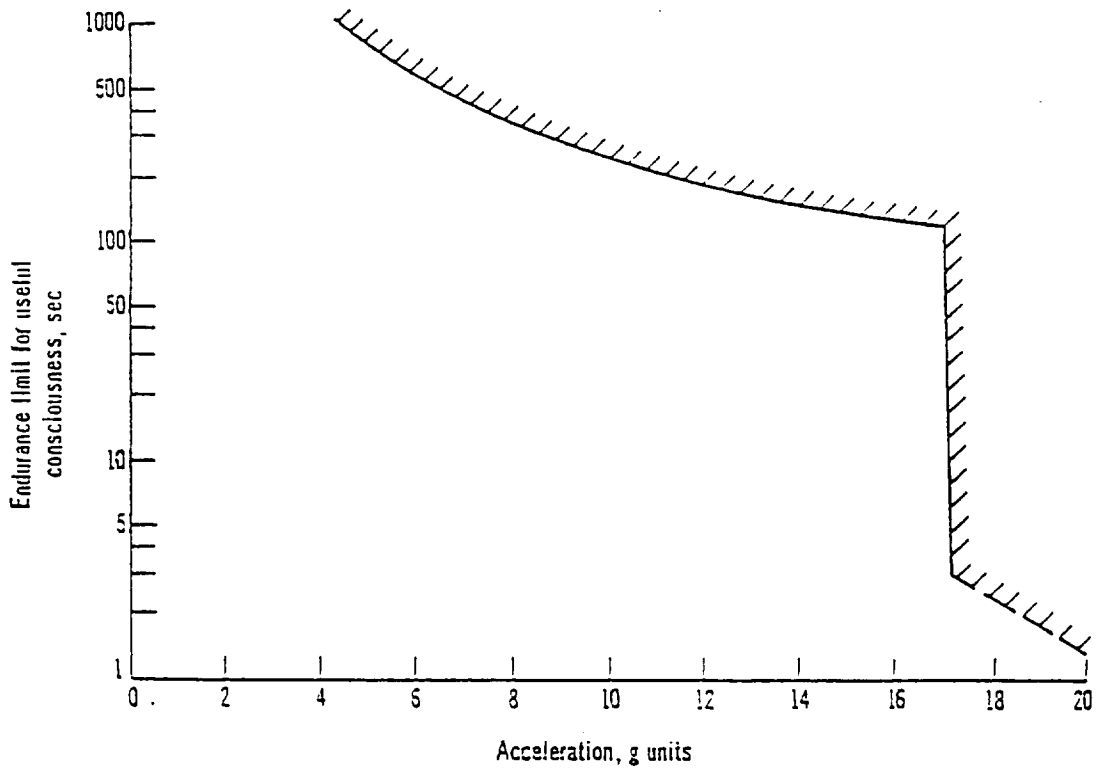


FIGURE 11. APOLLO G LOAD DESIGN LIMITATIONS (REF. 76)

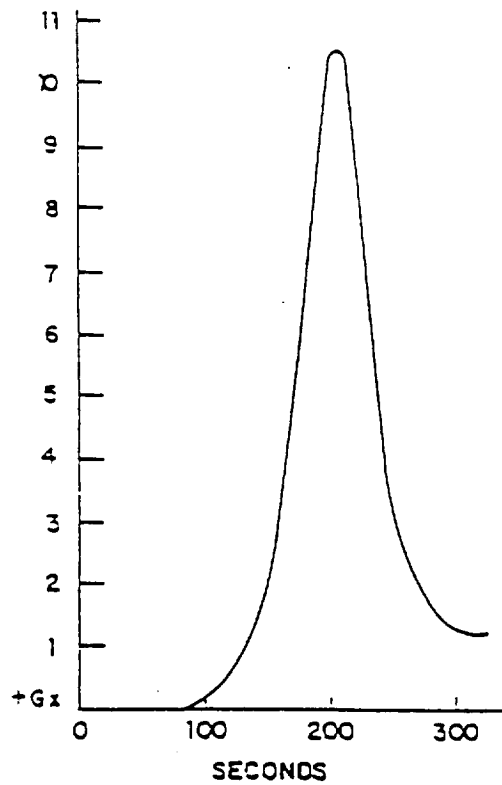


FIGURE 12. EXPECTED GEMINI G LOAD PROFILE (REF. 107)

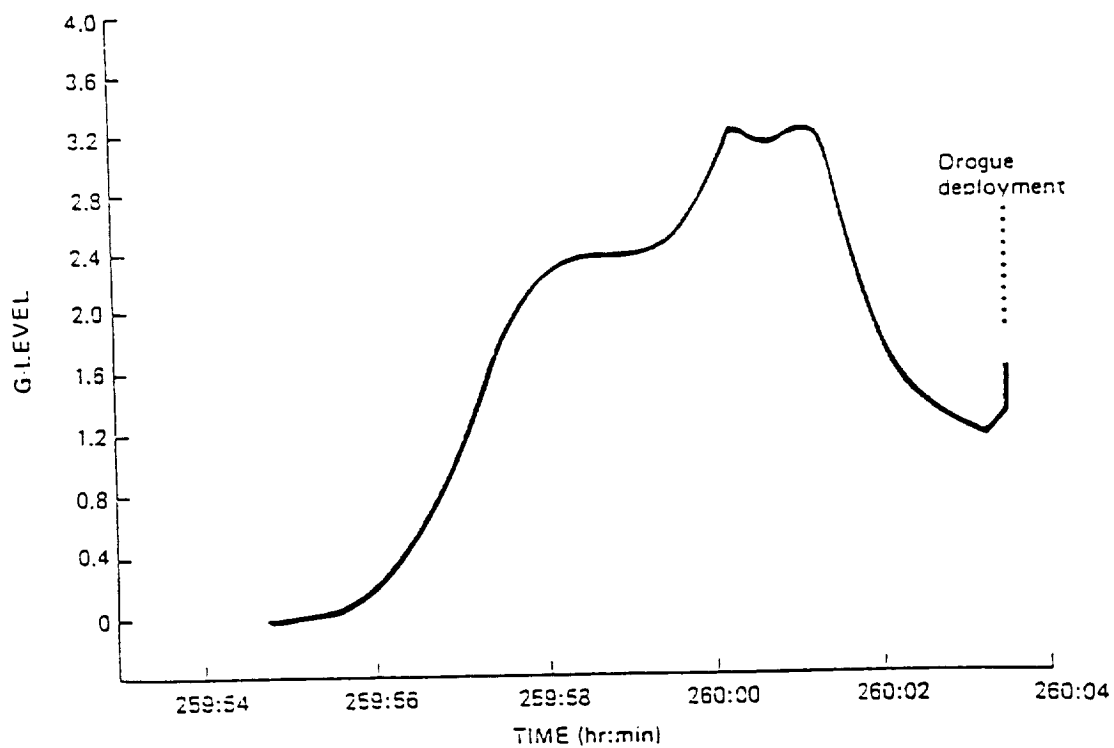


FIGURE 13. APOLLO EARTH ORBITAL REENTRY G PROFILE (REF. 111)

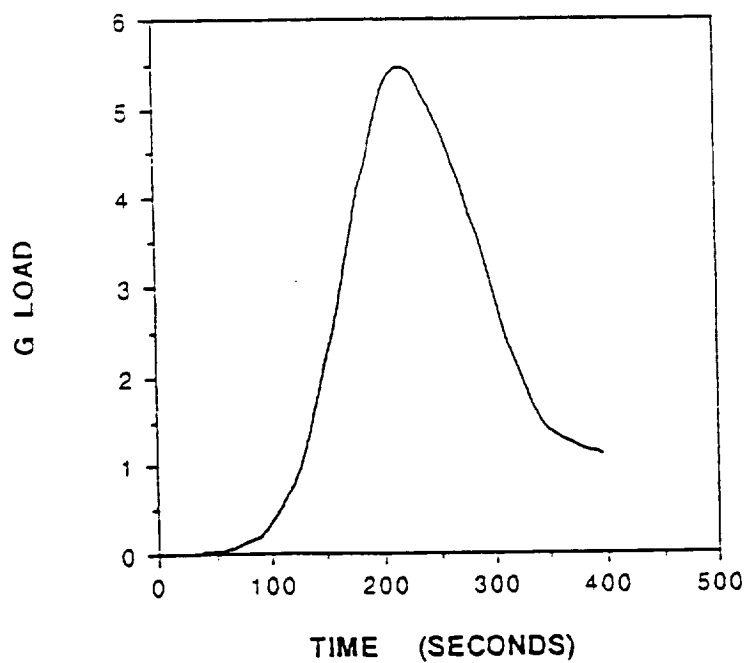


FIGURE 14. CALCULATED SOYUZ T10-B REENTRY G PROFILE

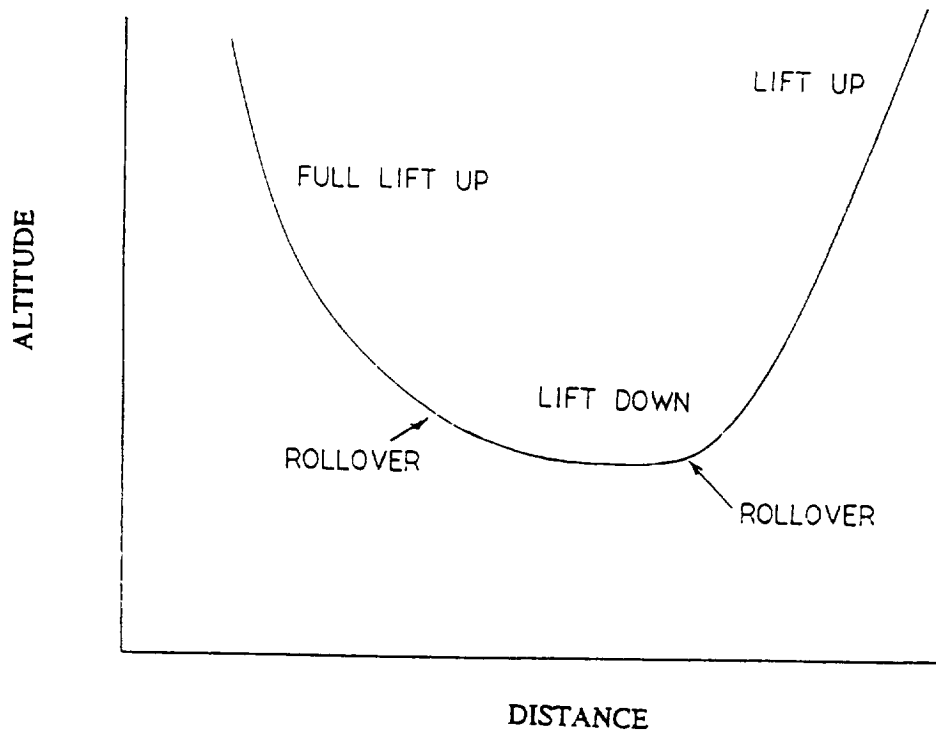


FIGURE 15. UNDERSHOOT TRAJECTORY LIFT MODULATION

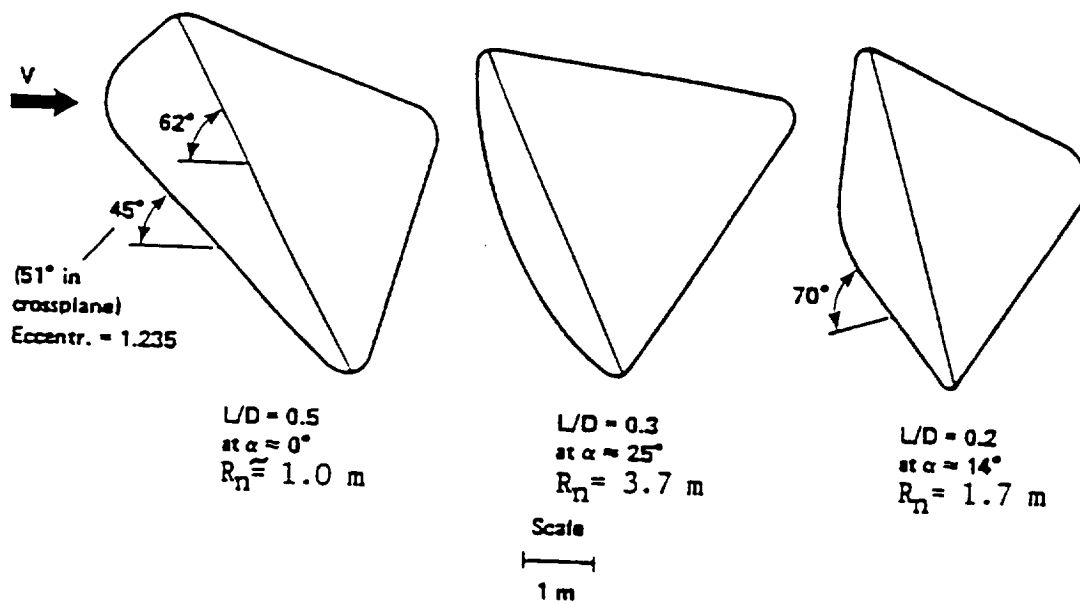


FIGURE 16. EARTH RETURN ENTRY CAPSULES (REF. 19)

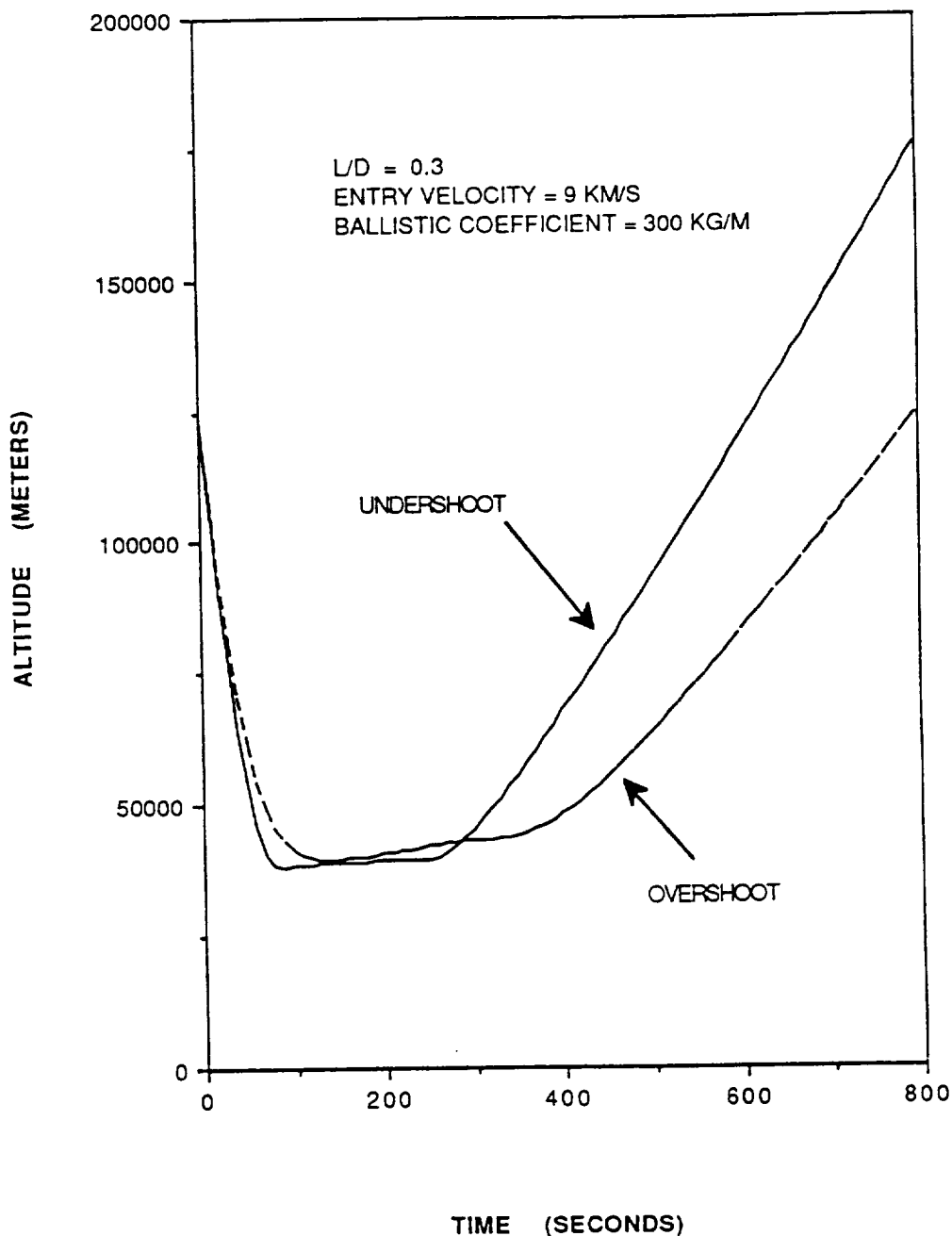


FIGURE 17. TYPICAL MARS AEROCAPTURE TRAJECTORIES

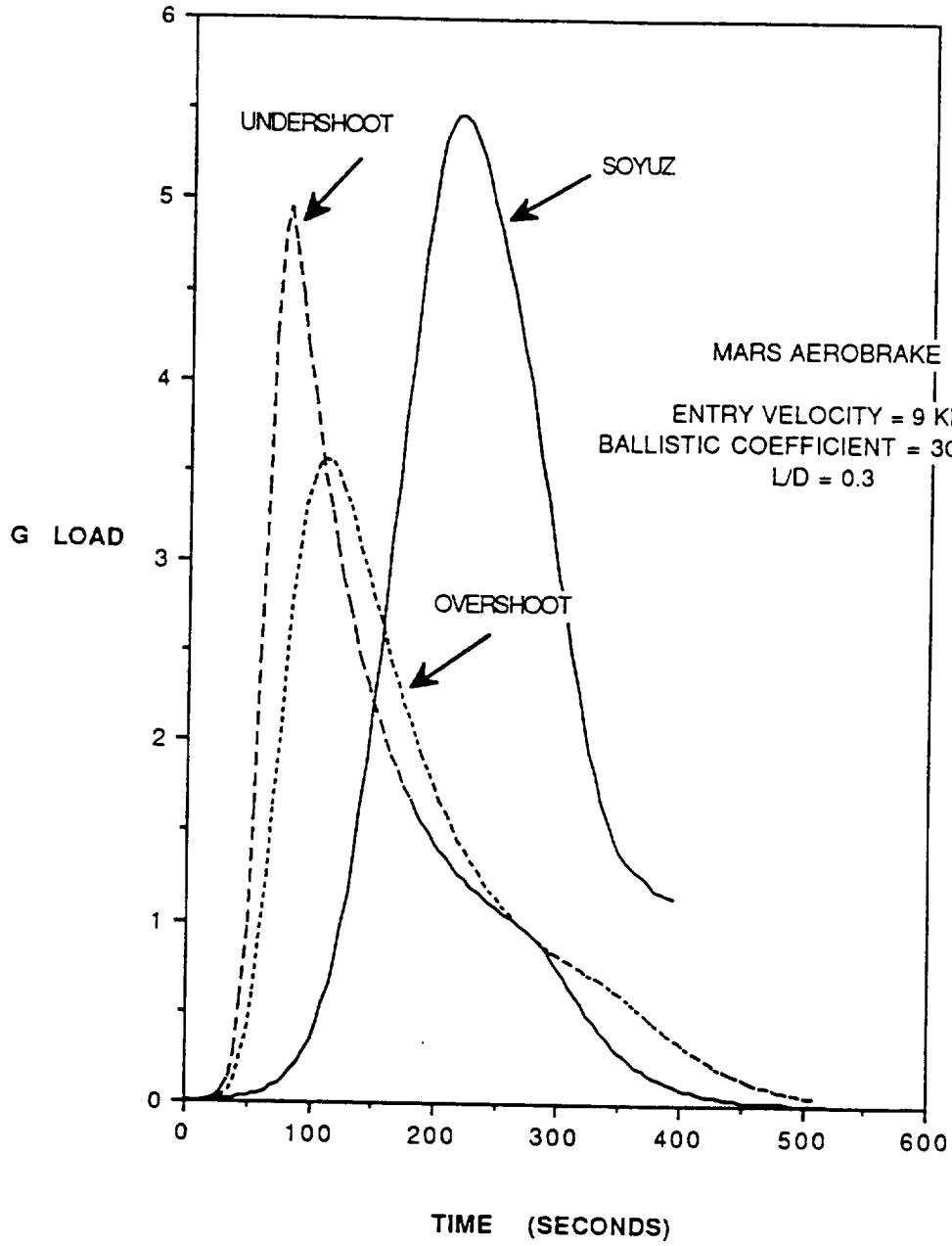


FIGURE 18. MARS AEROCAPTURE AND SOYUZ REENTRY G PROFILES

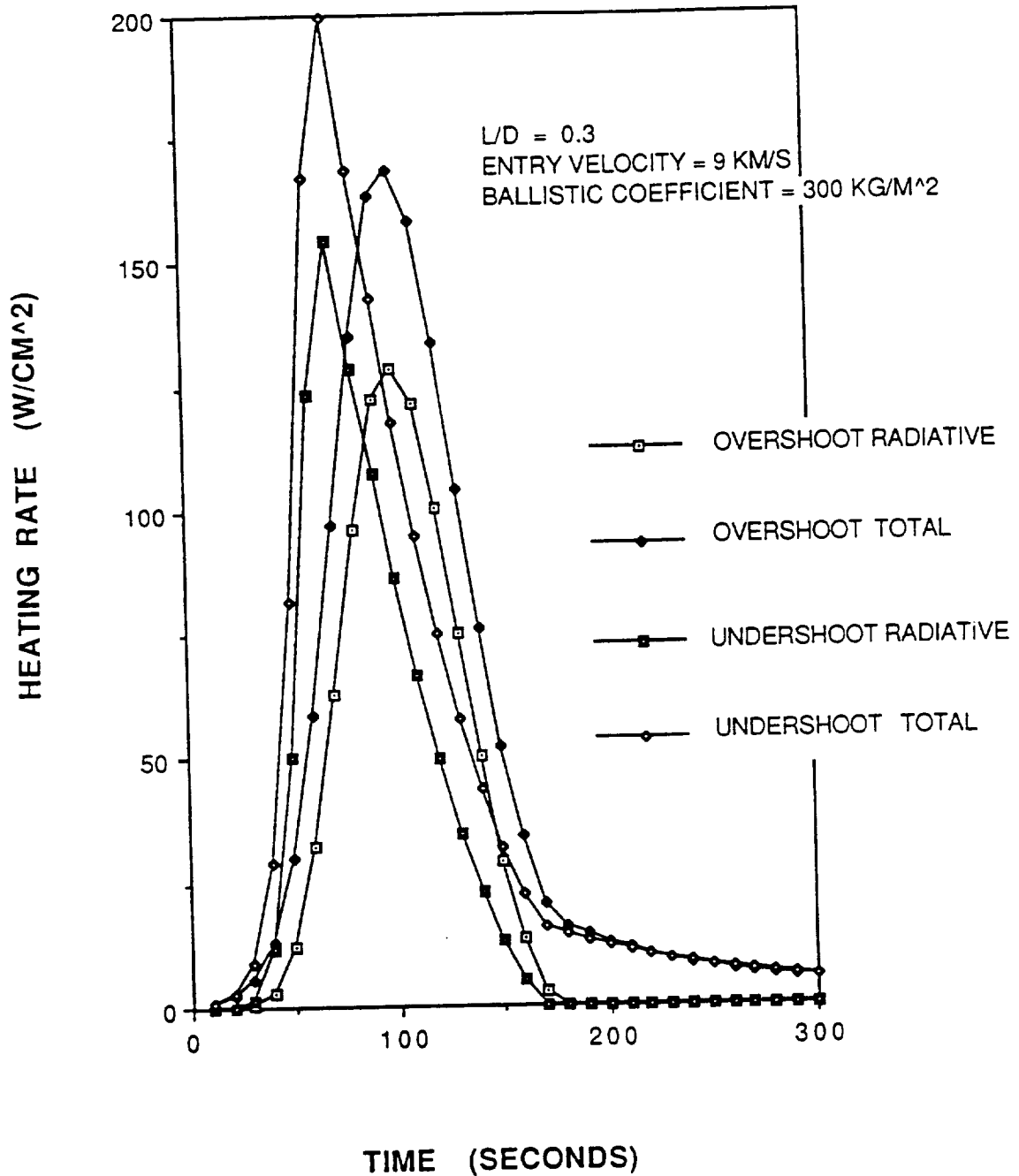


FIGURE 19. MARS AEROCAPTURE HEATING PULSES

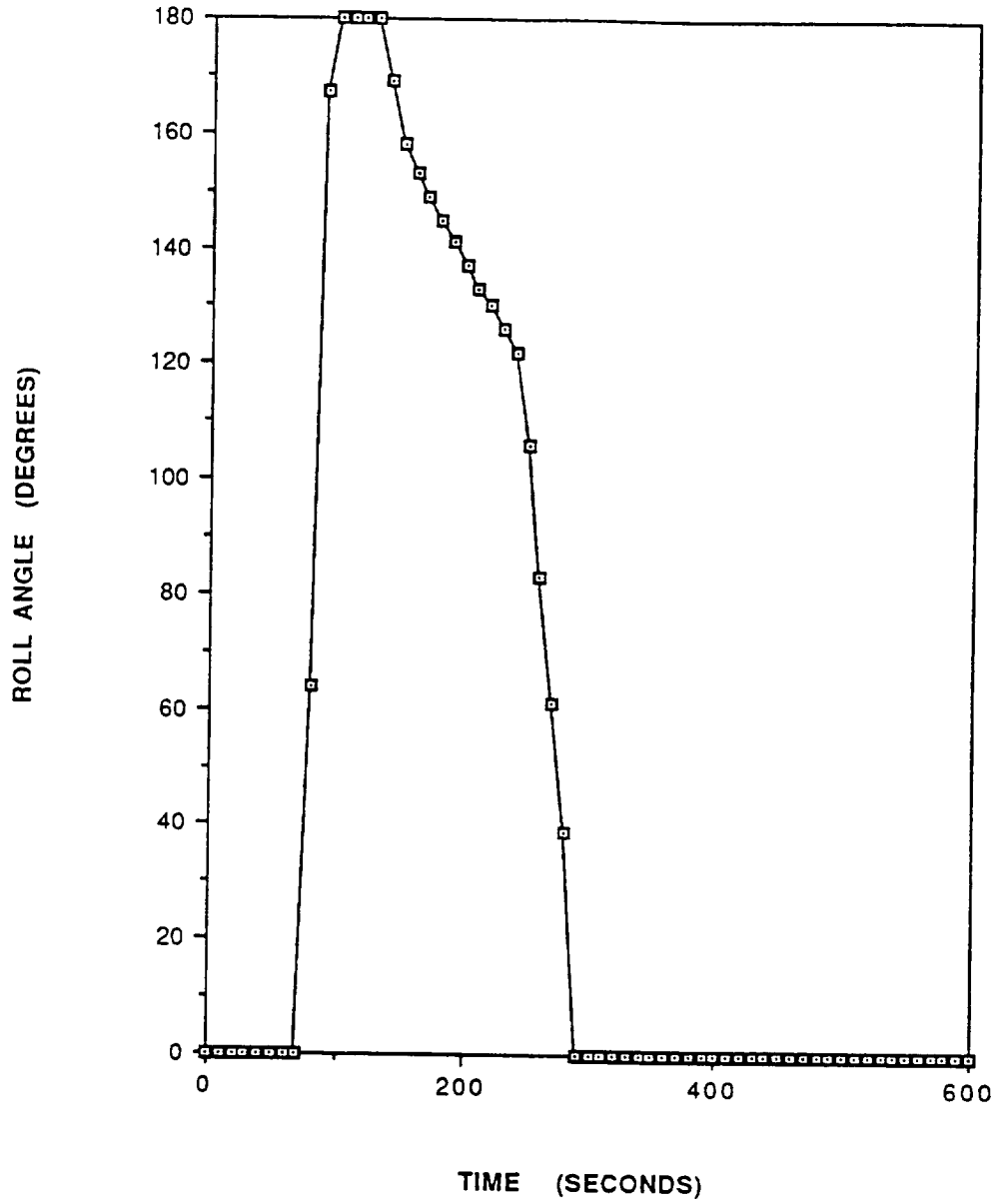


FIGURE 20. MARS AEROCAPTURE UNDERSHOOT TRAJECTORY ROLL ANGLE HISTORY

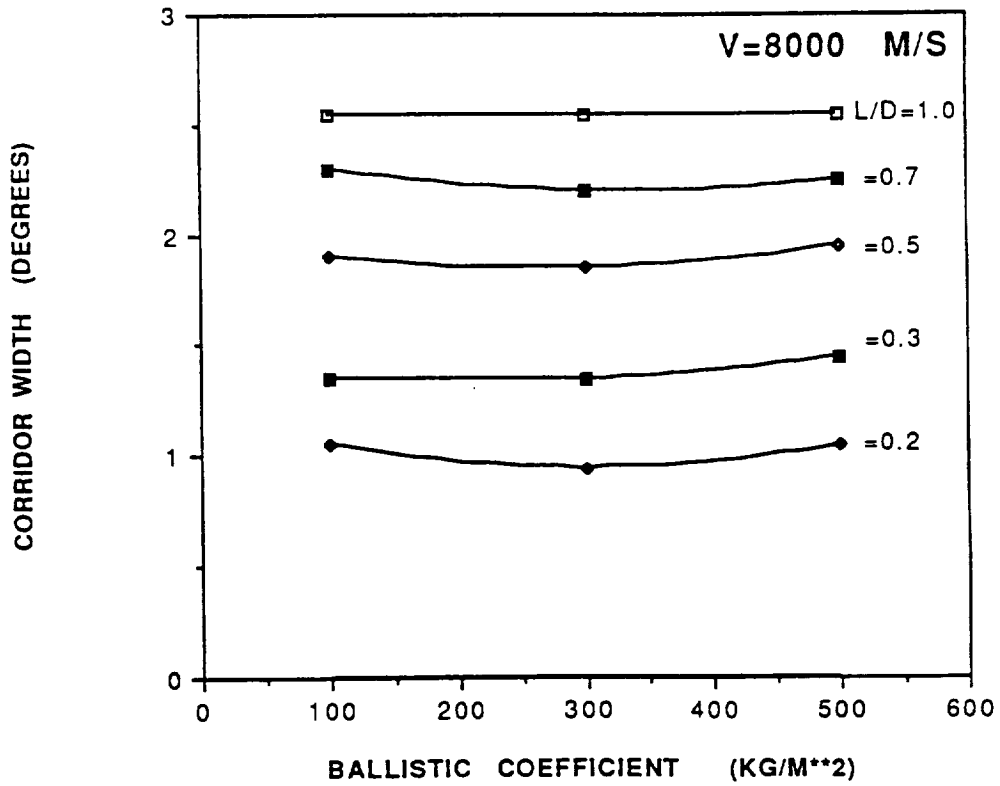
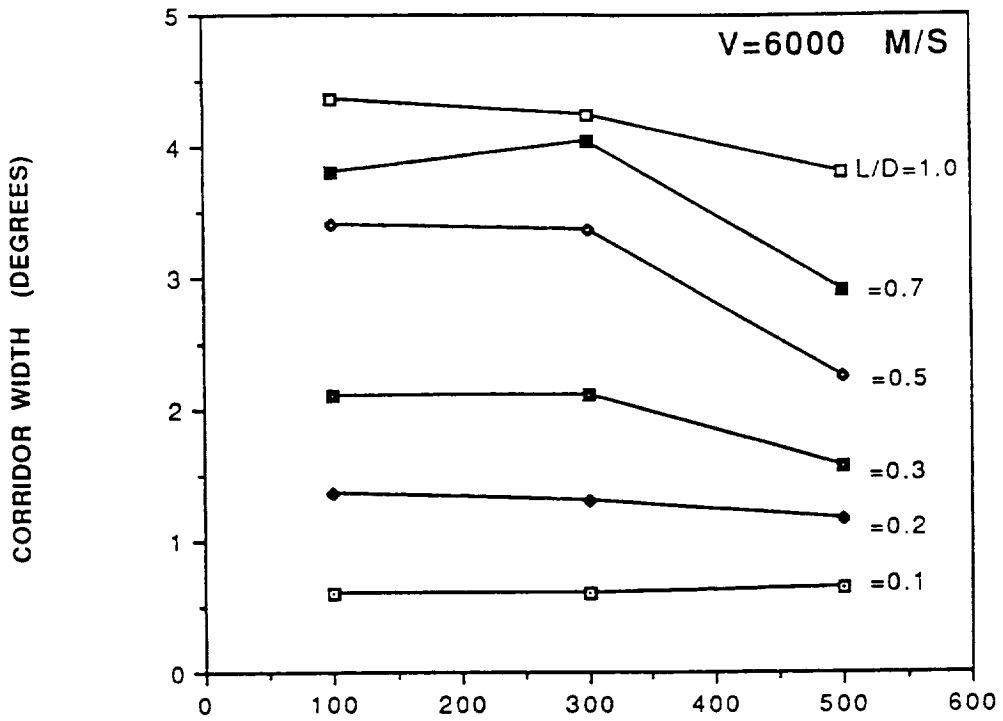
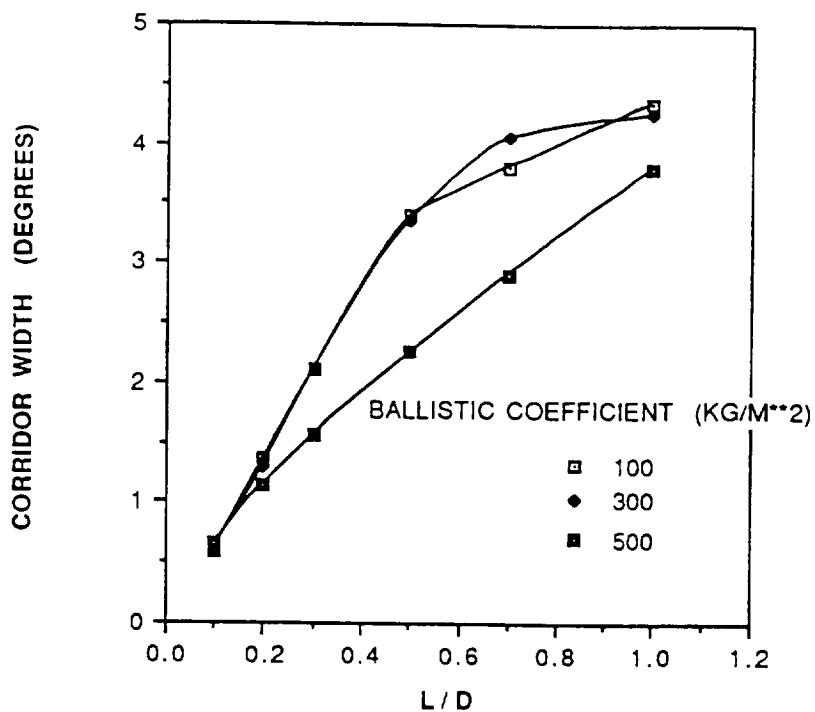
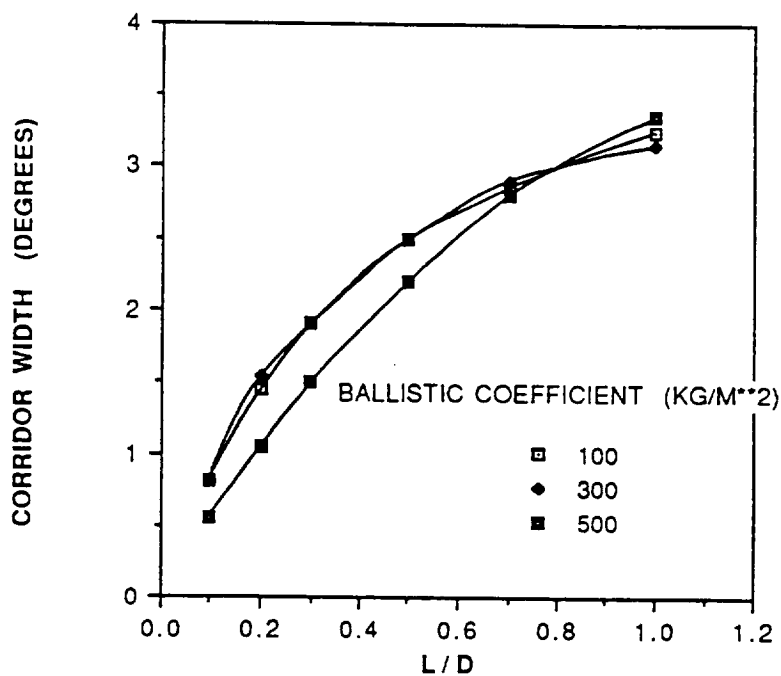


FIGURE 21. MARS AEROCAPTURE CORRIDOR WIDTH VS BALLISTIC COEFFICIENT

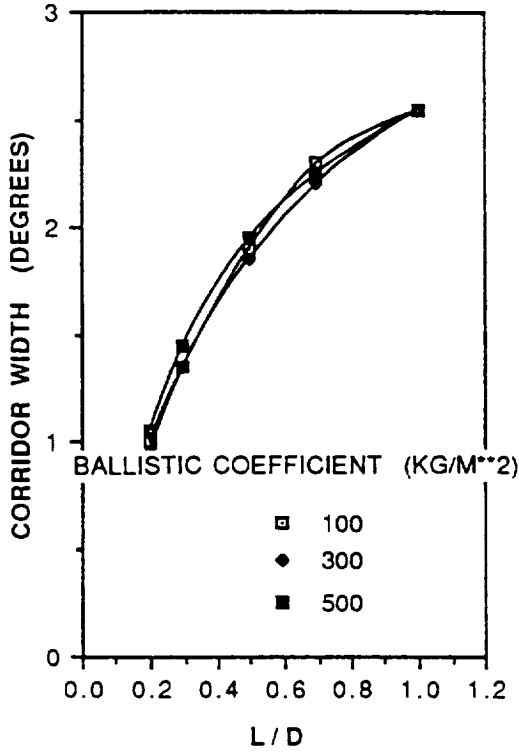


a) ENTRY VELOCITY = 6000 M/S

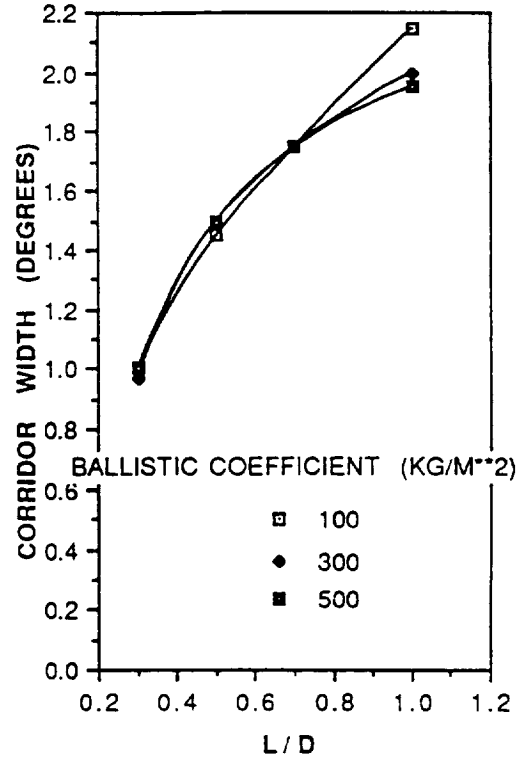


b) ENTRY VELOCITY = 7000 M/S

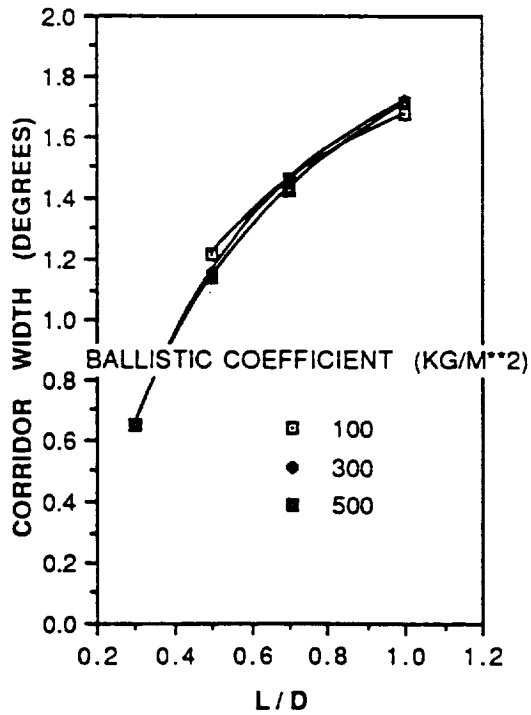
FIGURE 22. CORRIDOR WIDTH VS L/D FOR AEROCAPTURE AT MARS



c) ENTRY VELOCITY = 8000 M/S

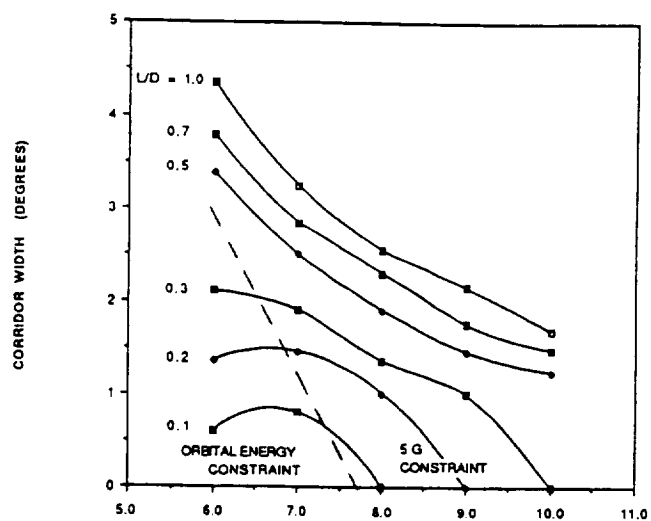


d) ENTRY VELOCITY = 9000 M/S

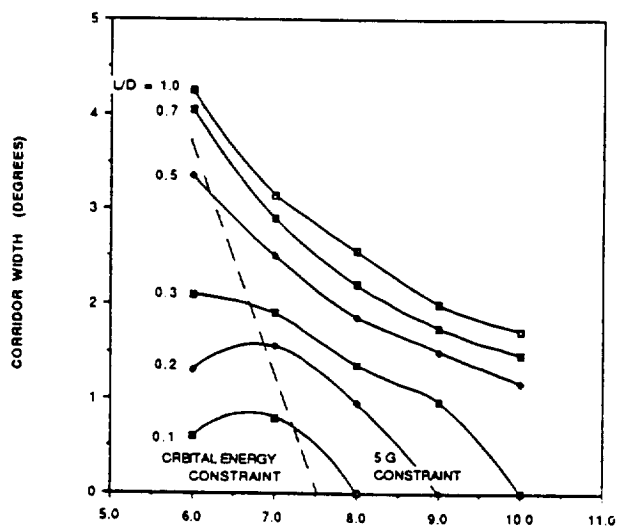


e) ENTRY VELOCITY = 10000 M/S

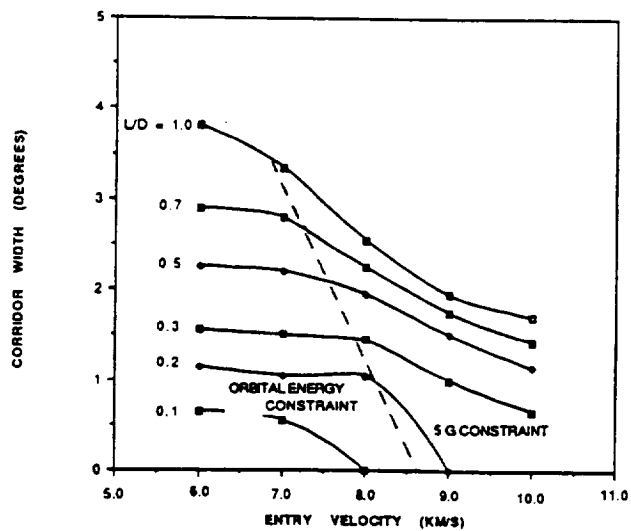
FIGURE 22. (CONTINUED)



a) BALLISTIC COEFFICIENT = 100 KG/M**2

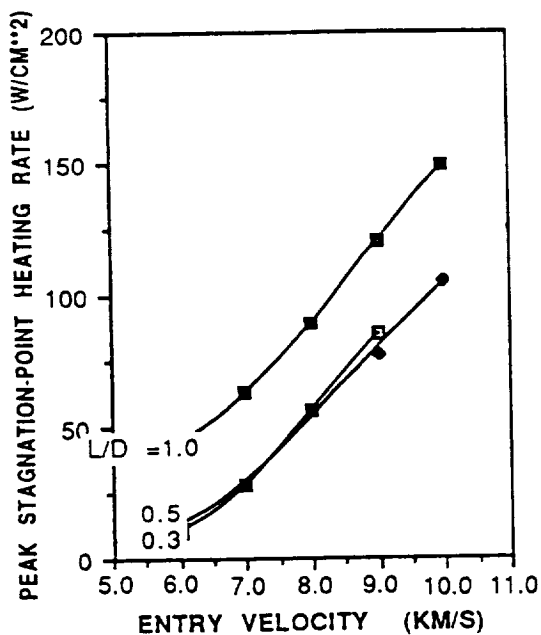


b) BALLISTIC COEFFICIENT = 300 KG/M**2

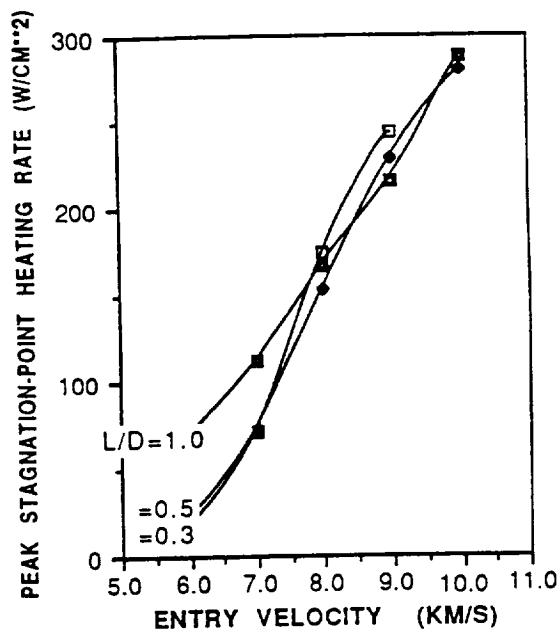


c) BALLISTIC COEFFICIENT = 500 KG/M**2

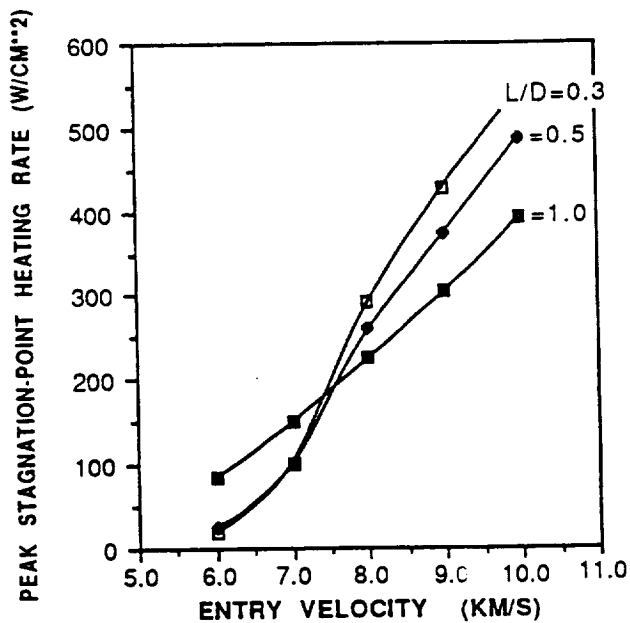
FIGURE 23. CORRIDOR WIDTH VS ENTRY VELOCITY FOR AEROCAPTURE AT MARS



a) BALLISTIC COEFFICIENT = 100 KG/M**2

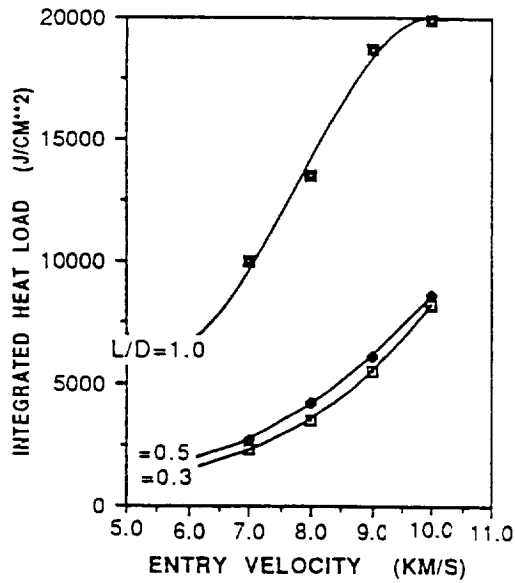


b) BALLISTIC COEFFICIENT = 300 KG/M**2

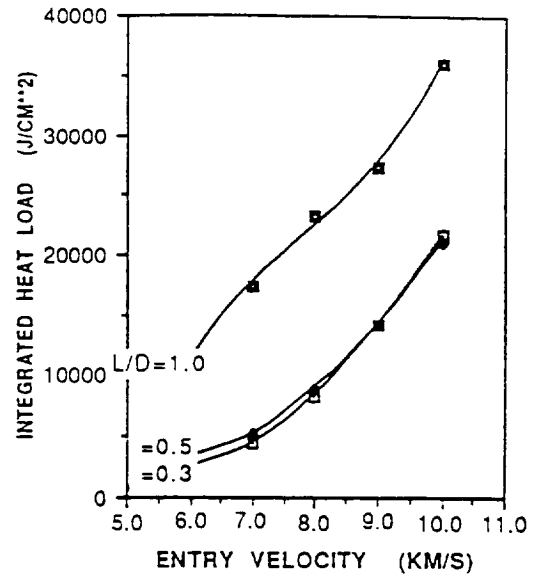


c) BALLISTIC COEFFICIENT = 500 KG/M**2

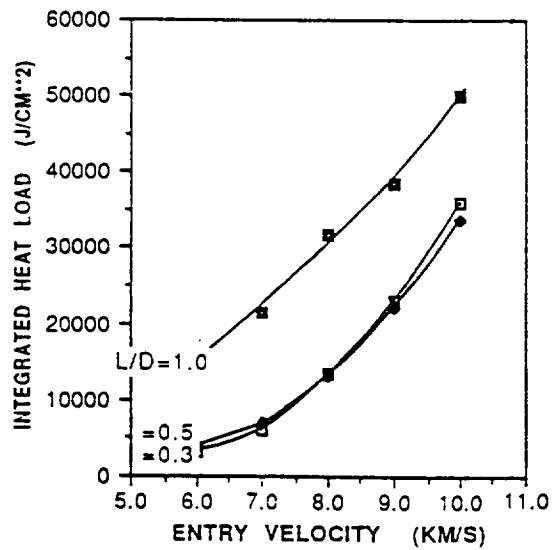
FIGURE 24. MARS AEROCAPTURE UNDERSHOOT TRAJECTORY PEAK STAGNATION-POINT HEATING RATE



a) BALLISTIC COEFFICIENT = 100 KG/M**2

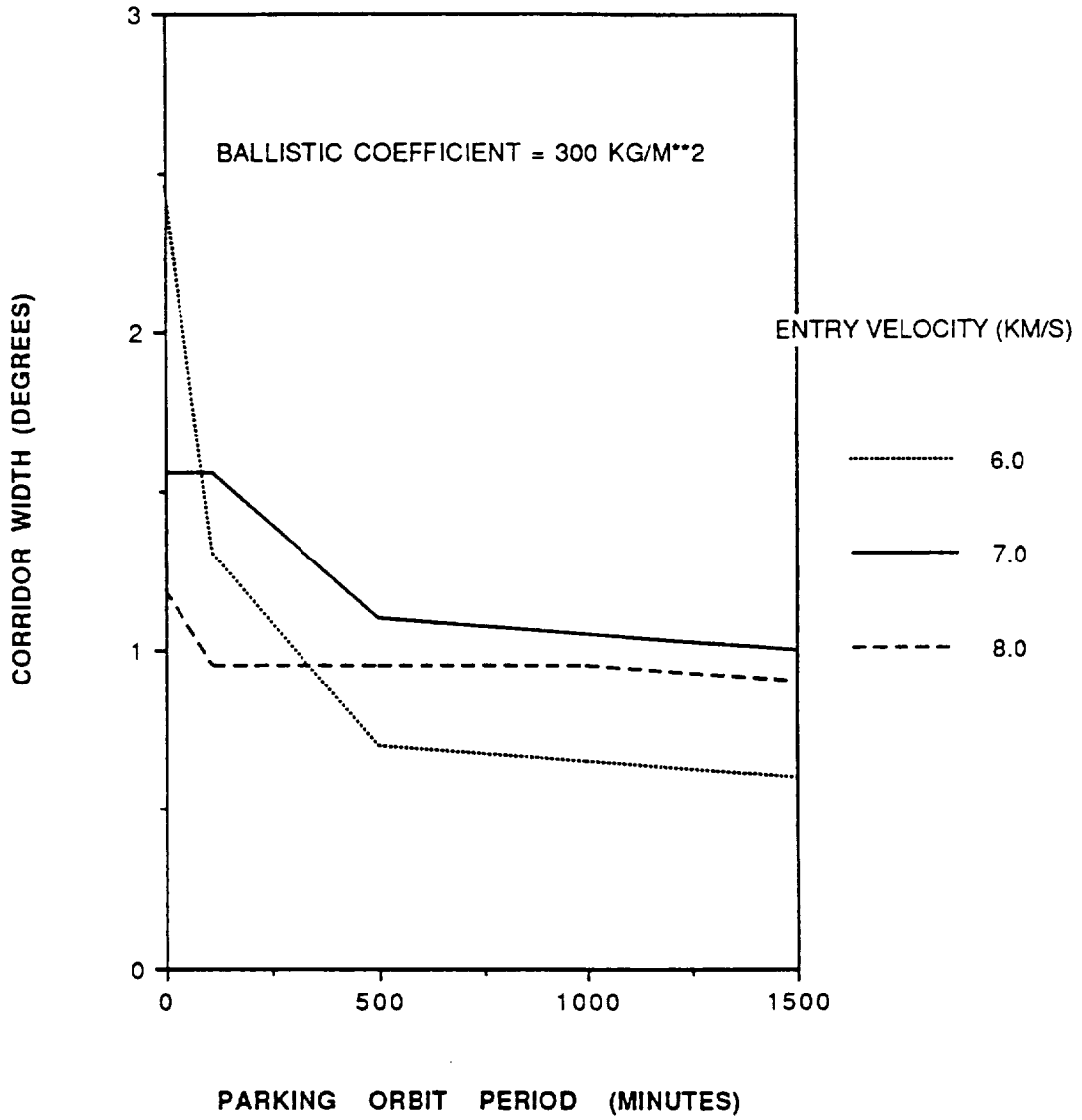


b) BALLISTIC COEFFICIENT = 300 KG/M**2



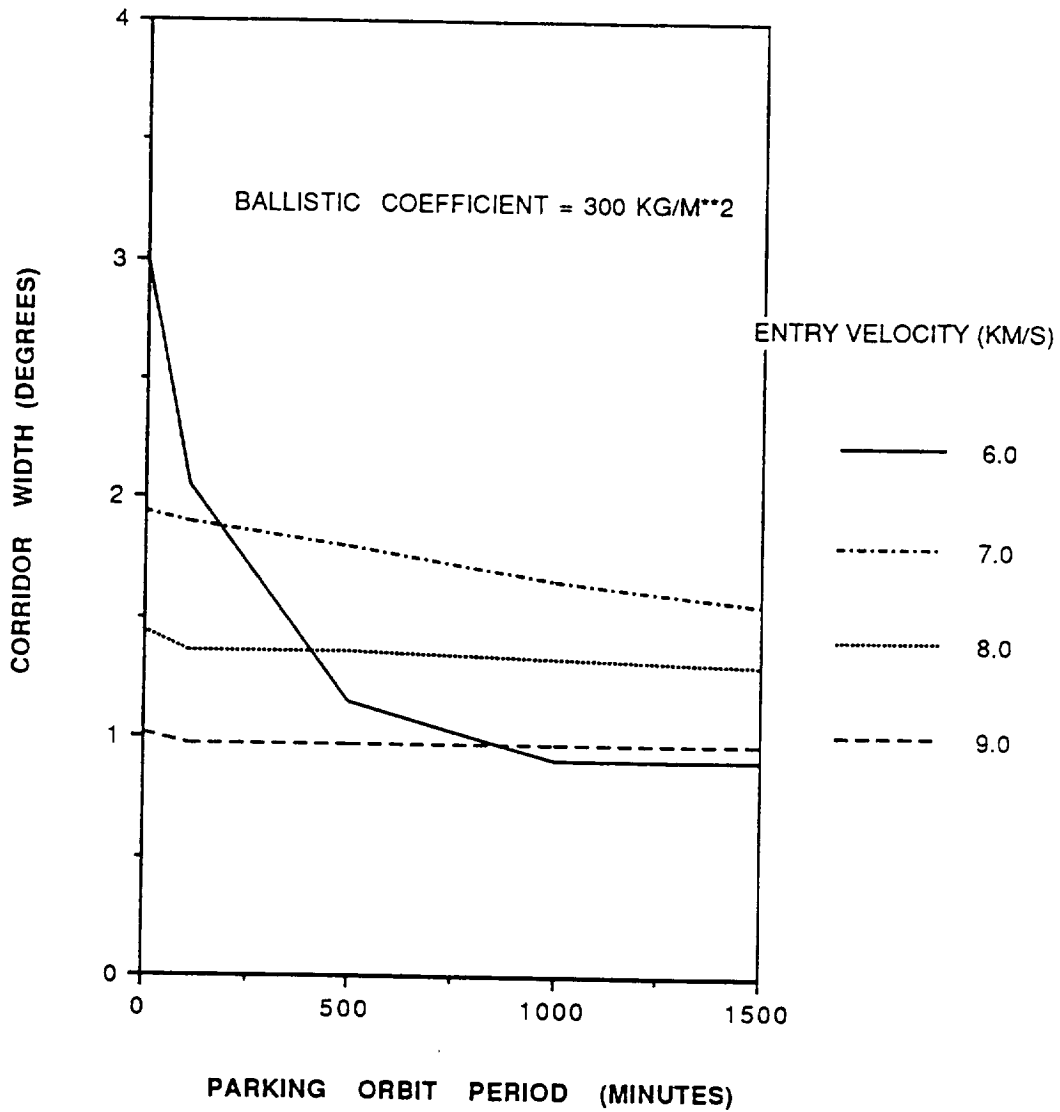
c) BALLISTIC COEFFICIENT = 500 KG/M**2

FIGURE 25. MARS AEROCAPTURE OVERTHOOT TRAJECTORY STAGNATION-POINT HEAT LOAD



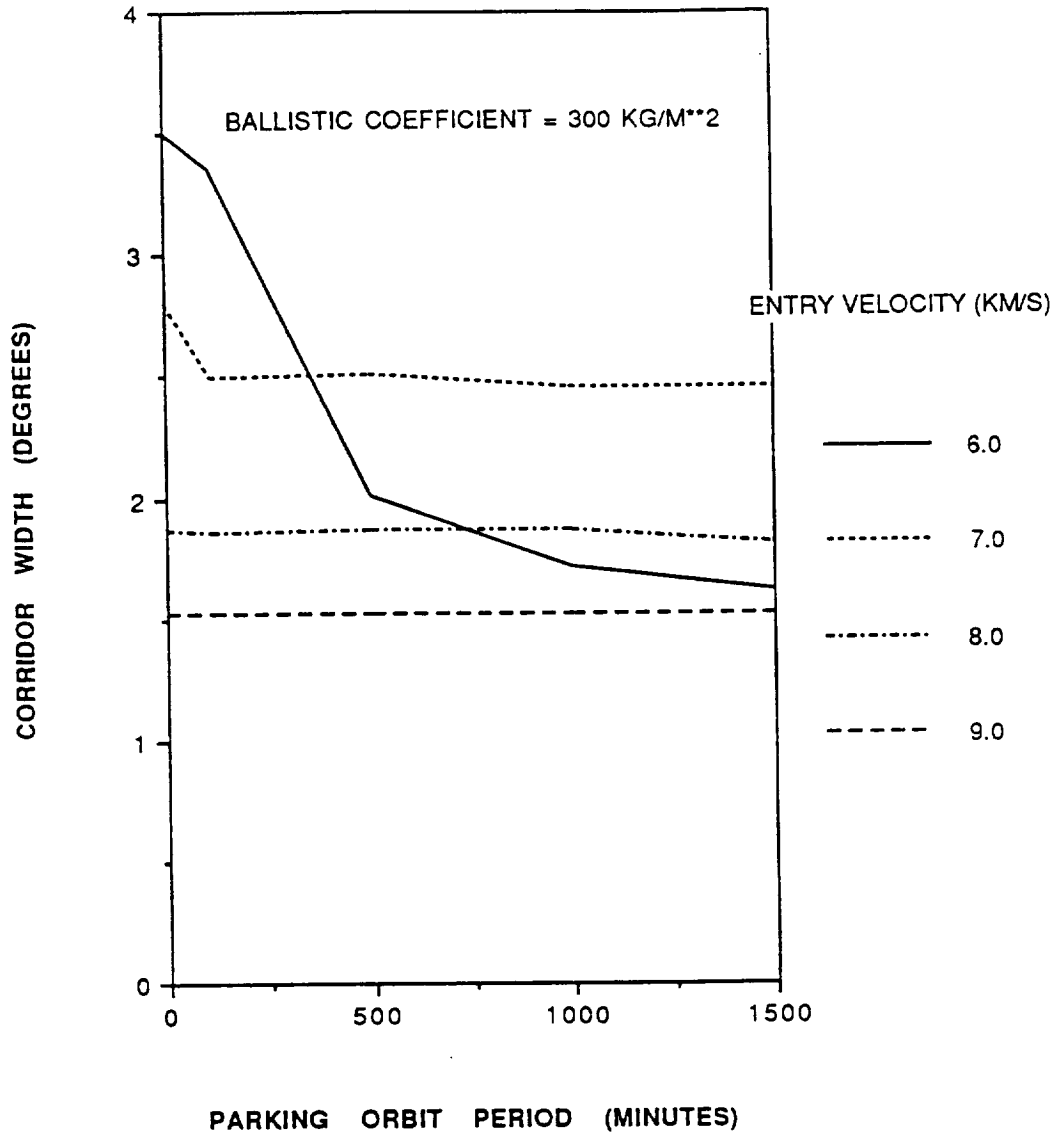
A) L/D = 0.2

FIGURE 26. MARS AEROCAPTURE CORRIDOR WIDTH VS PARKING ORBIT PERIOD



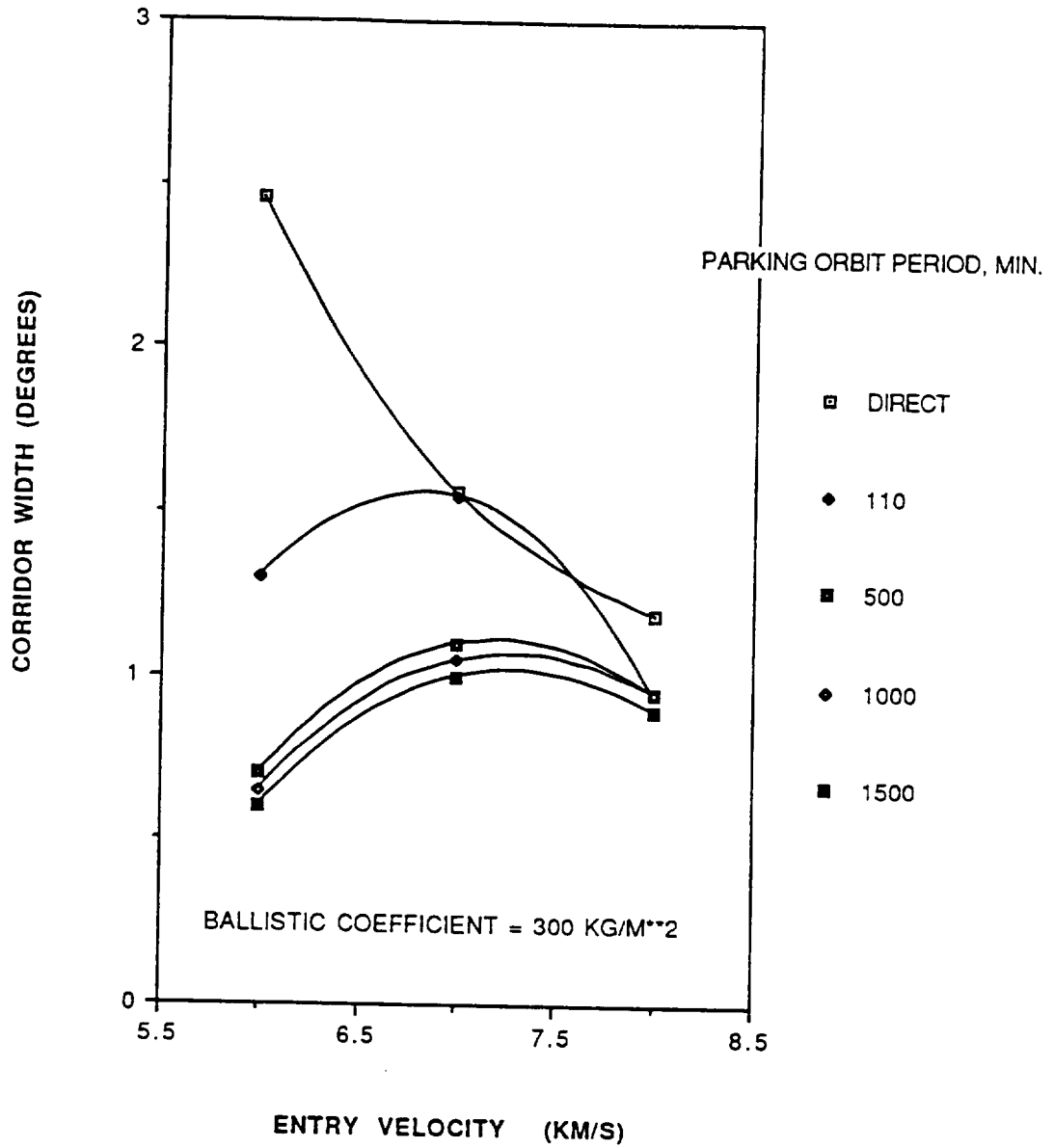
B) L/D = 0.3

FIGURE 26. (CONTINUED)

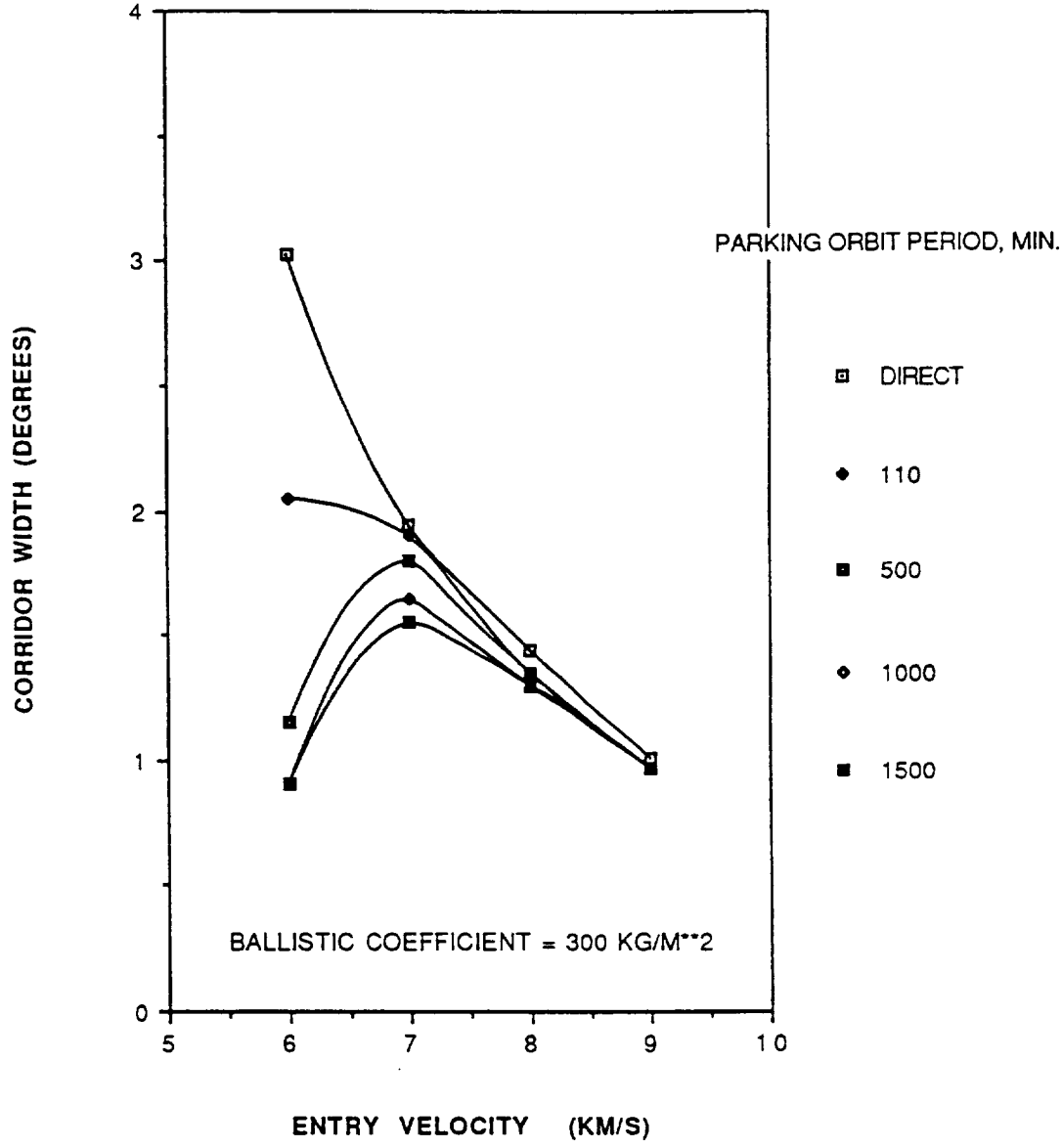


C) L/D = 0.5

FIGURE 26. (CONCLUDED)

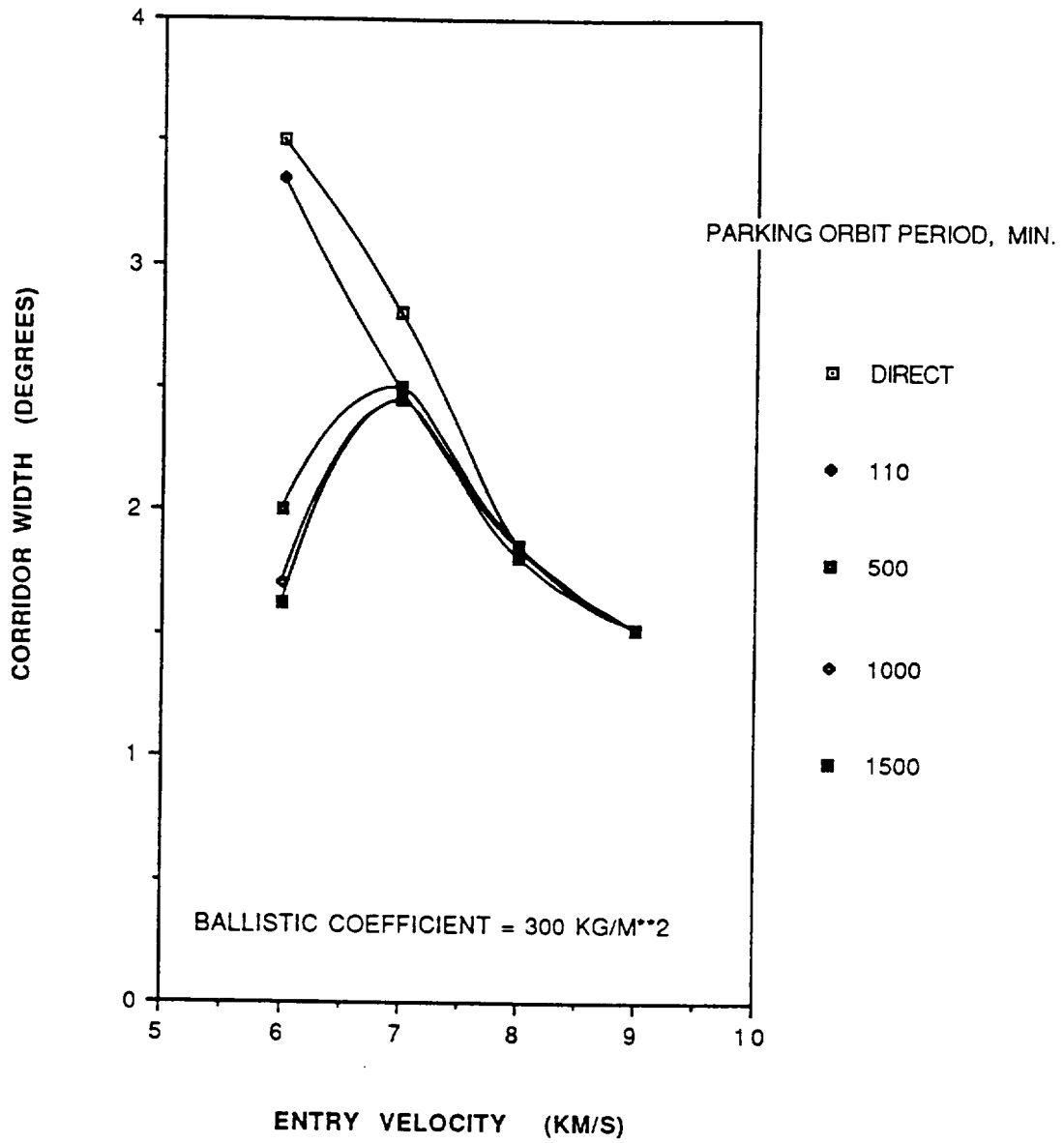


A) L/D = 0.2
 FIGURE 27. MARS AEROCAPTURE CORRIDOR WIDTH VS ENTRY VELOCITY



B) L/D = 0.3

FIGURE 27. (CONTINUED)



C) L/D = 0.5

FIGURE 27. (CONCLUDED)

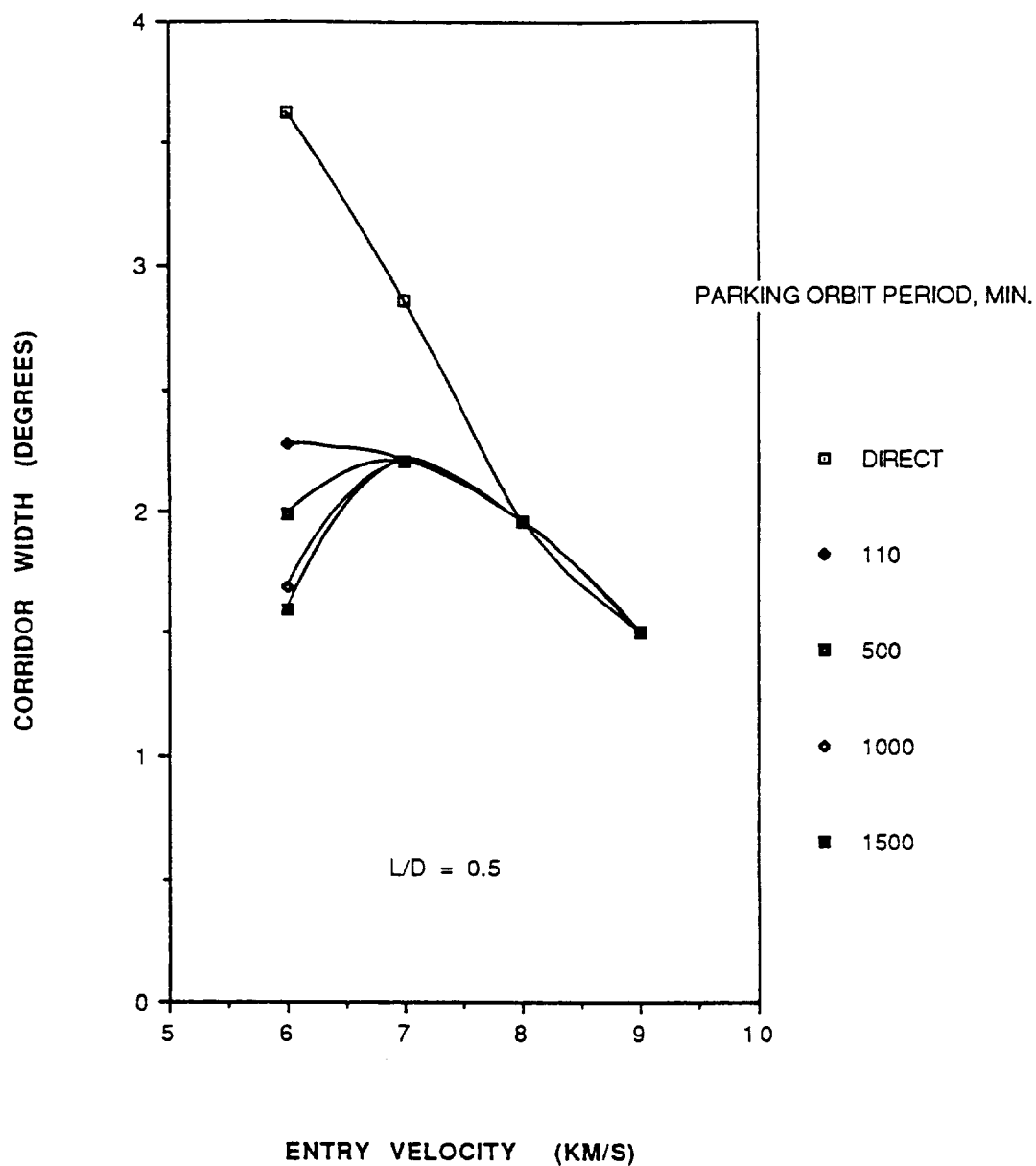


FIGURE 28. CORRIDOR WIDTH VS ENTRY VELOCITY
 BALLISTIC COEFFICIENT = 500 KG/M**2

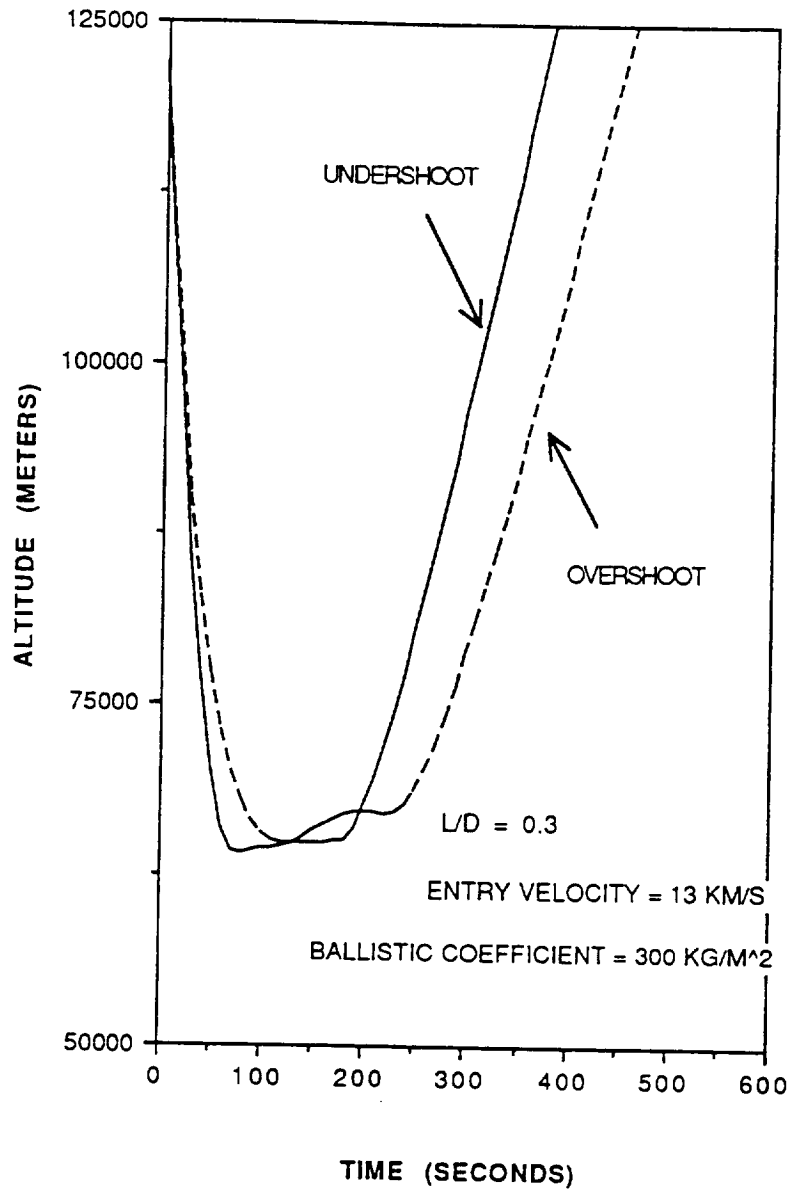


FIGURE 29. TYPICAL EARTH RETURN AEROCAPTURE TRAJECTORIES

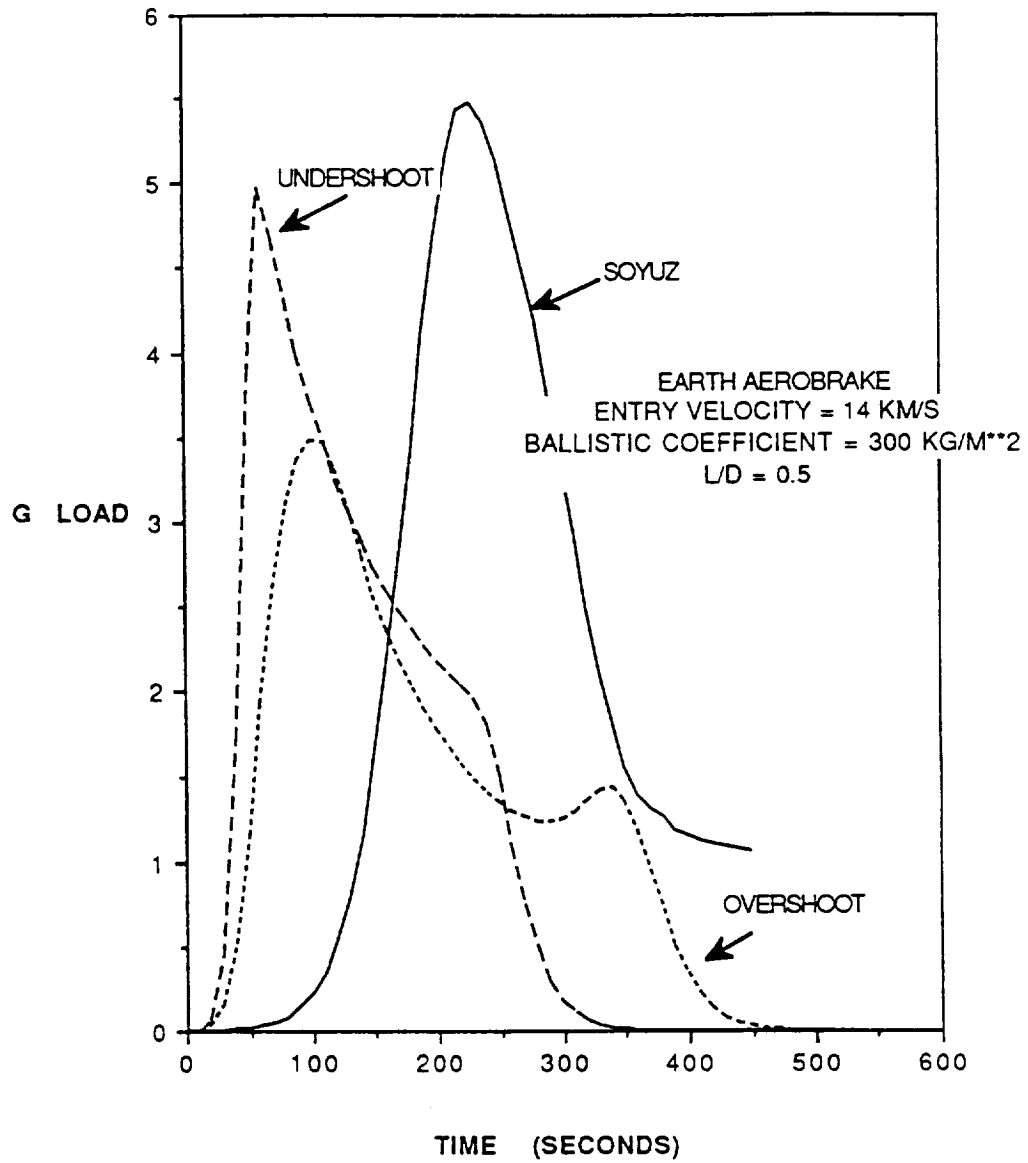


FIGURE 30. G LOADS FOR EARTH RETURN AEROCAPTURE AND SOYUZ REENTRY

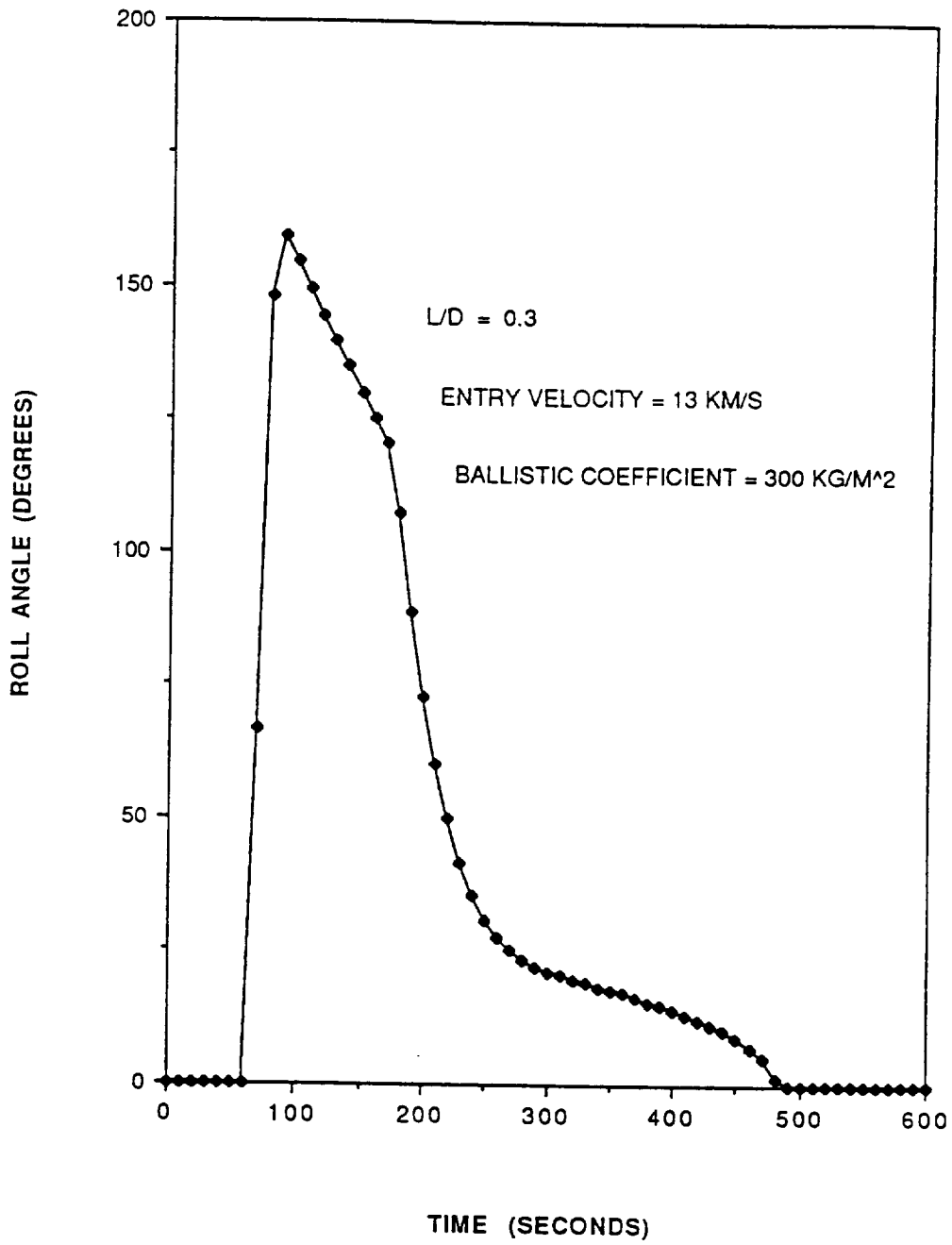


FIGURE 31. EARTH RETURN UNDERSHOOT TRAJECTORY BANK ANGLE PROFILE

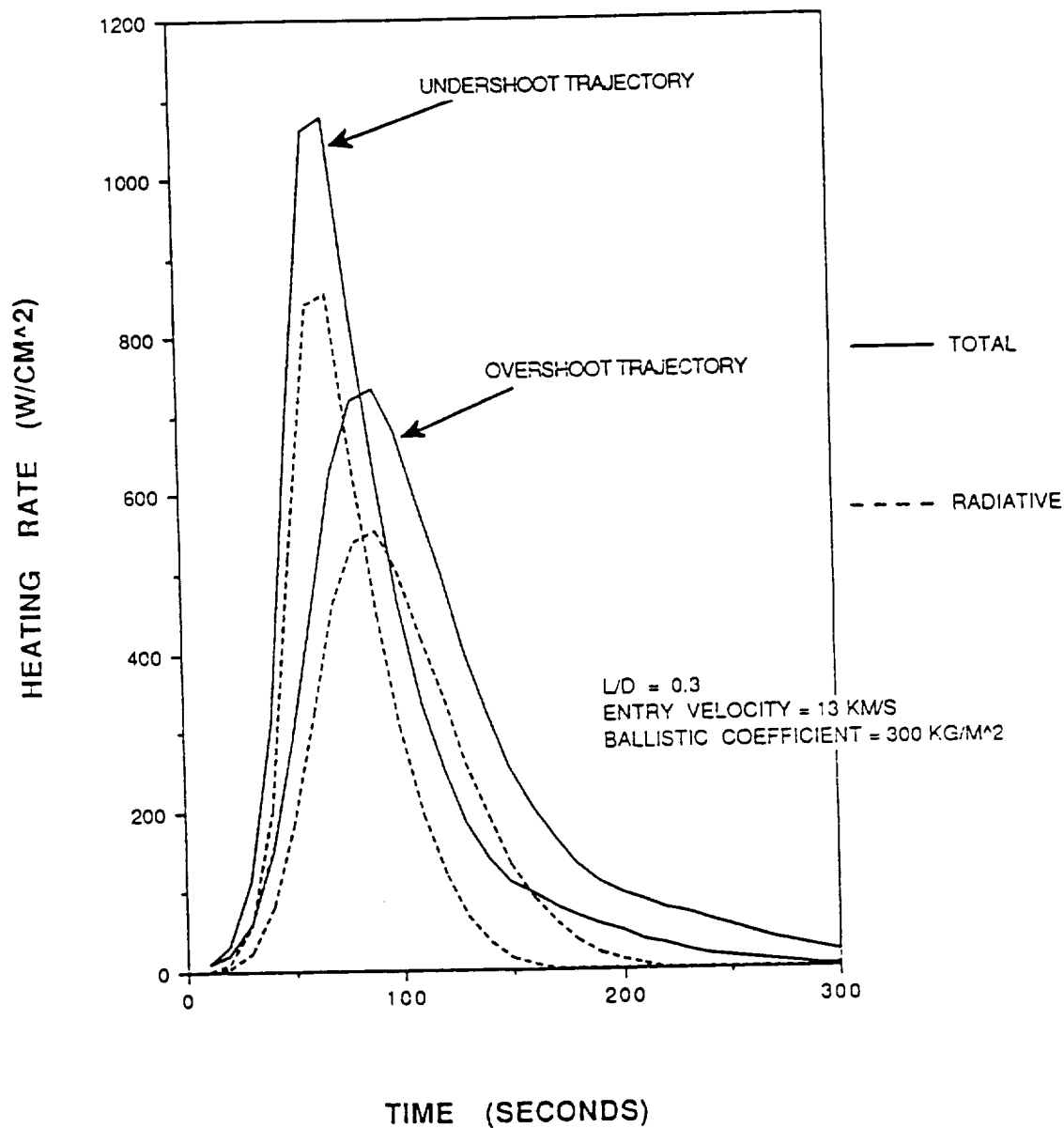


FIGURE 32. EARTH AEROCAPTURE HEATING PULSES

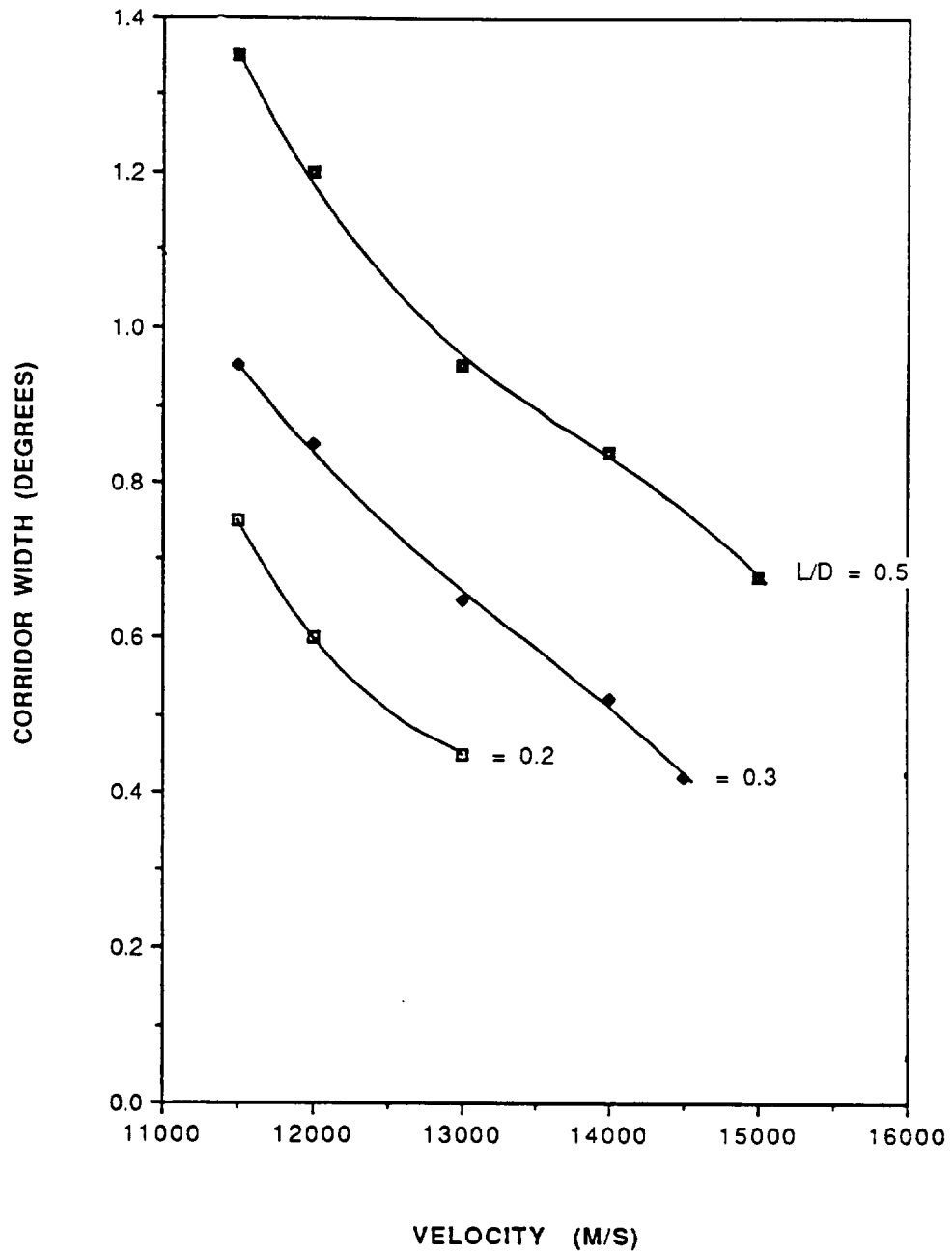


FIGURE 33. CORRIDOR WIDTH VS ENTRY VELOCITY FOR EARTH RETURN AEROCAPTURE

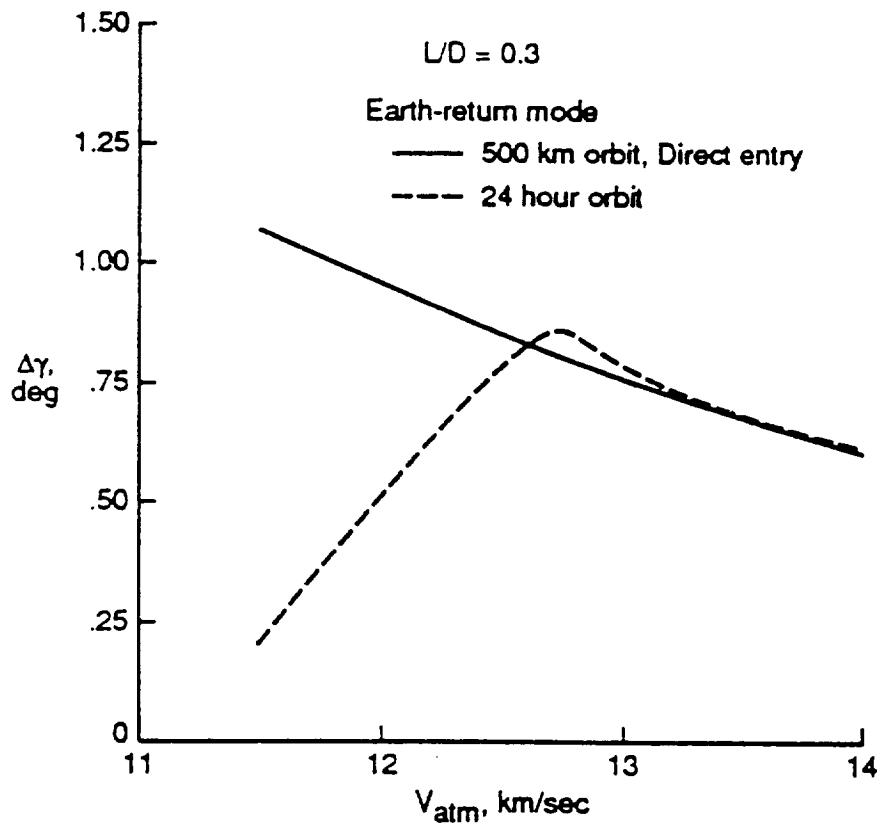


FIGURE 34. EARTH RETURN CORRIDOR WIDTH FOR VARIOUS CAPTURE ORBITS

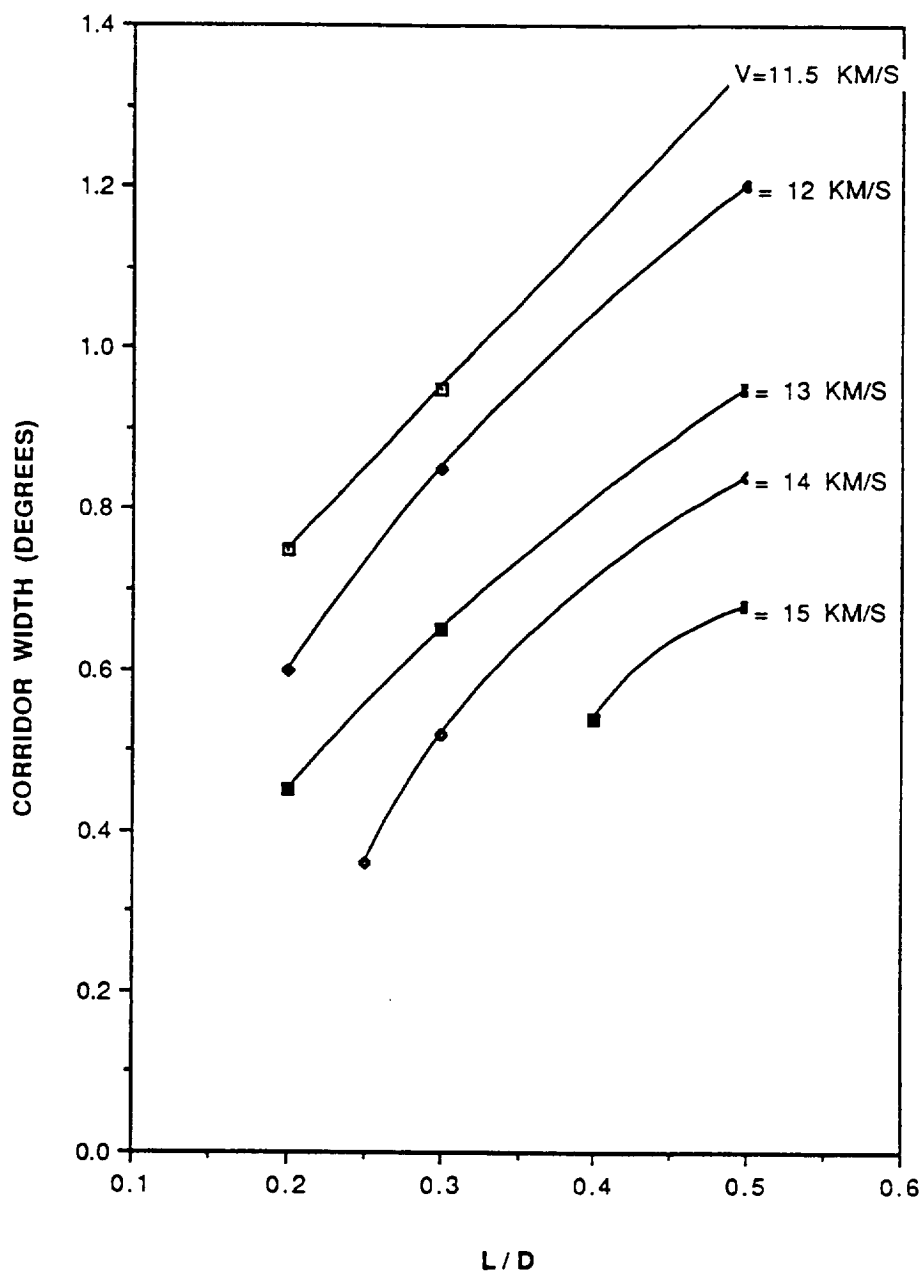
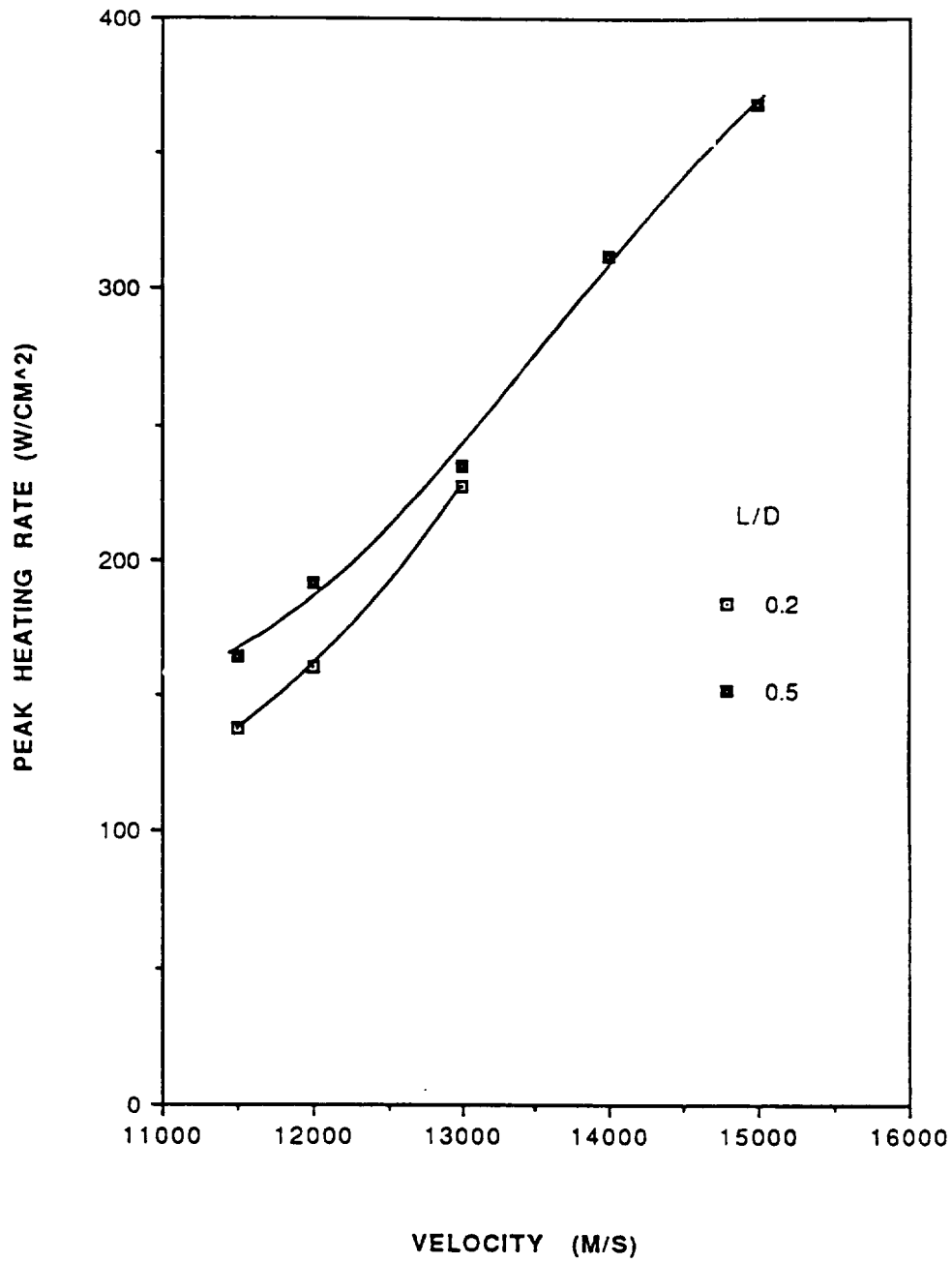
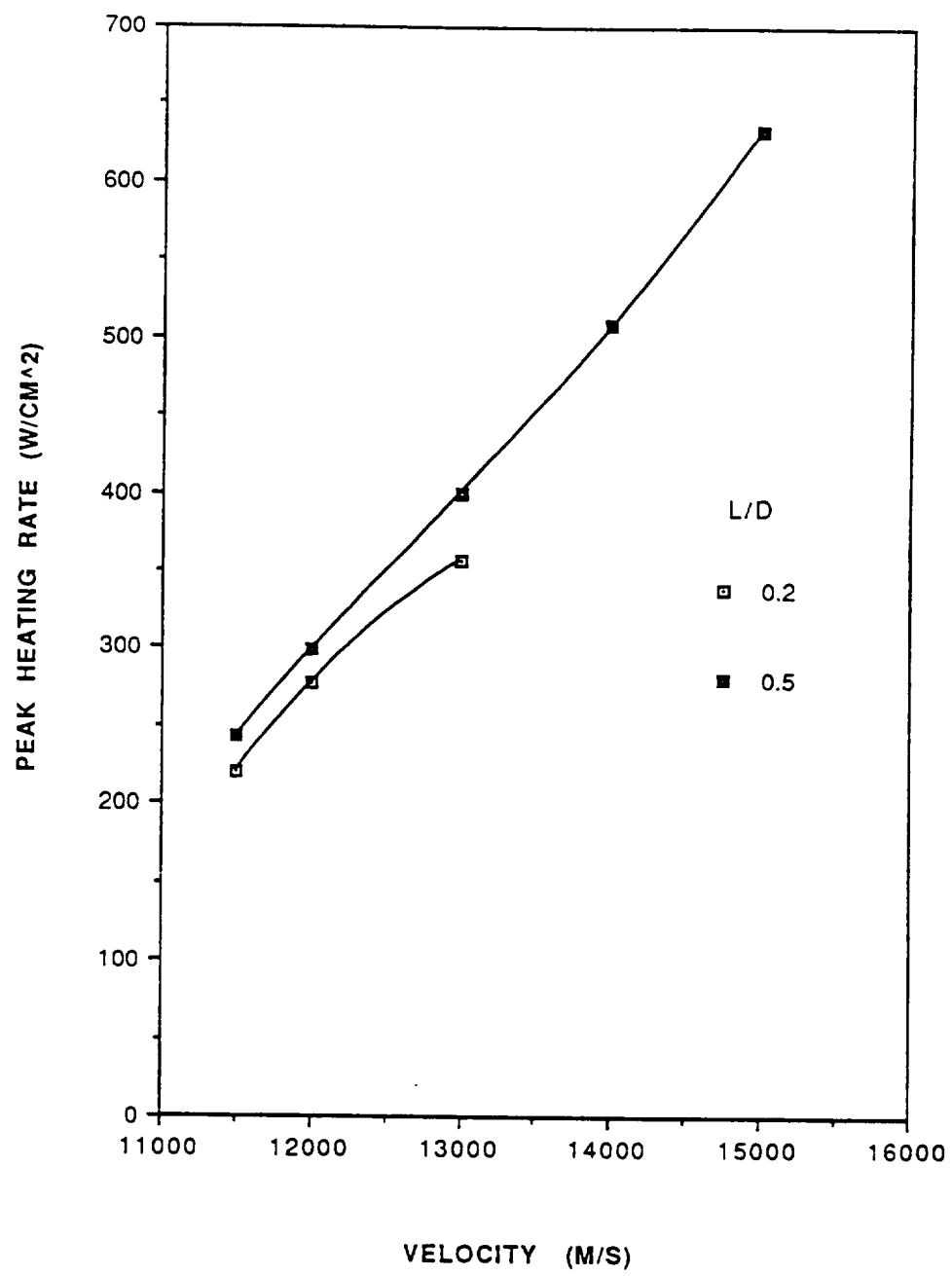


FIGURE 35. CORRIDOR WIDTH VS L/D FOR EARTH RETURN AEROCAPTURE



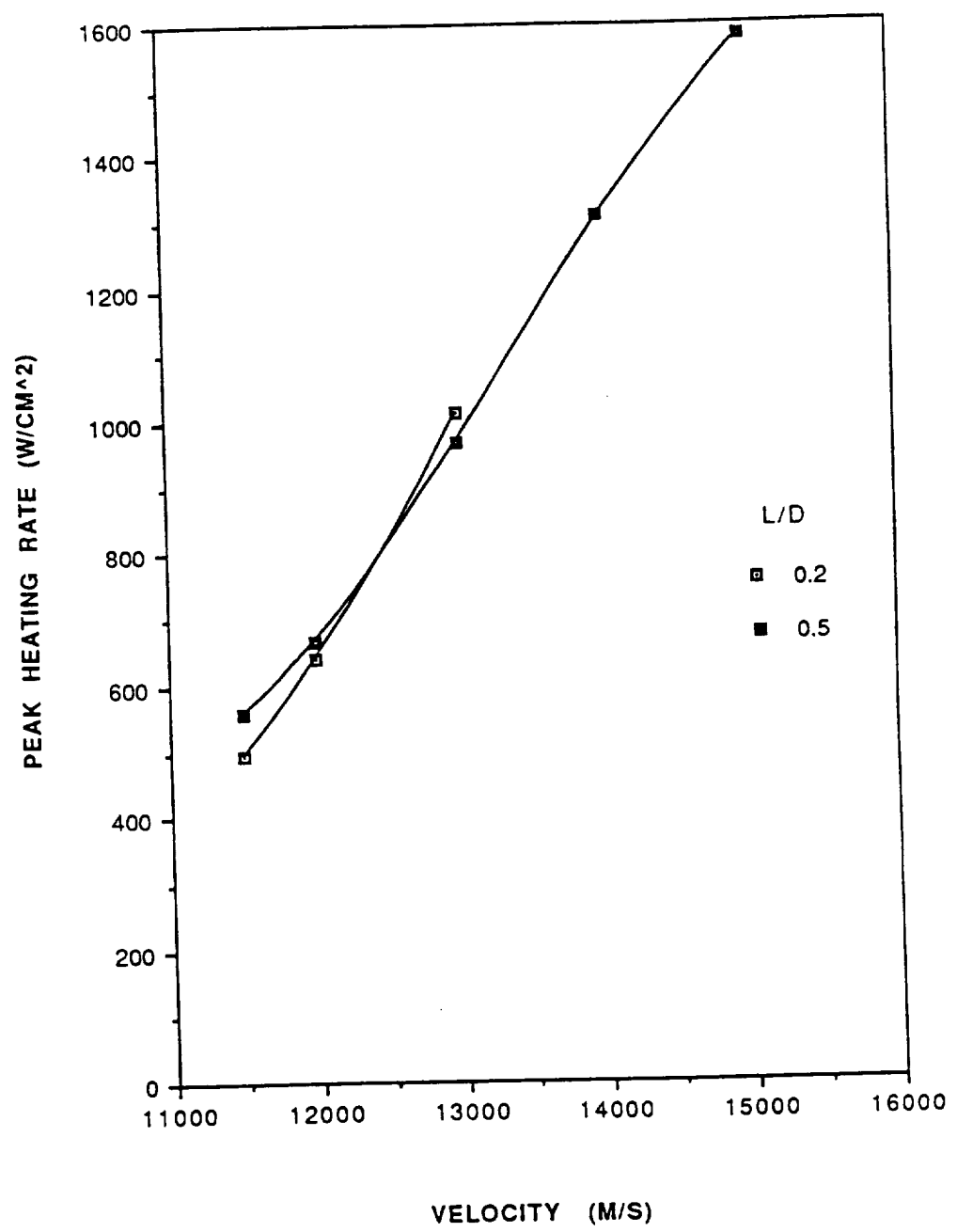
a) BALLISTIC COEFFICIENT = 50 KG/M²

FIGURE 36. PEAK STAGNATION-POINT HEATING RATE VS ENTRY VELOCITY FOR THE EARTH RETURN UNDERSHOOT TRAJECTORY



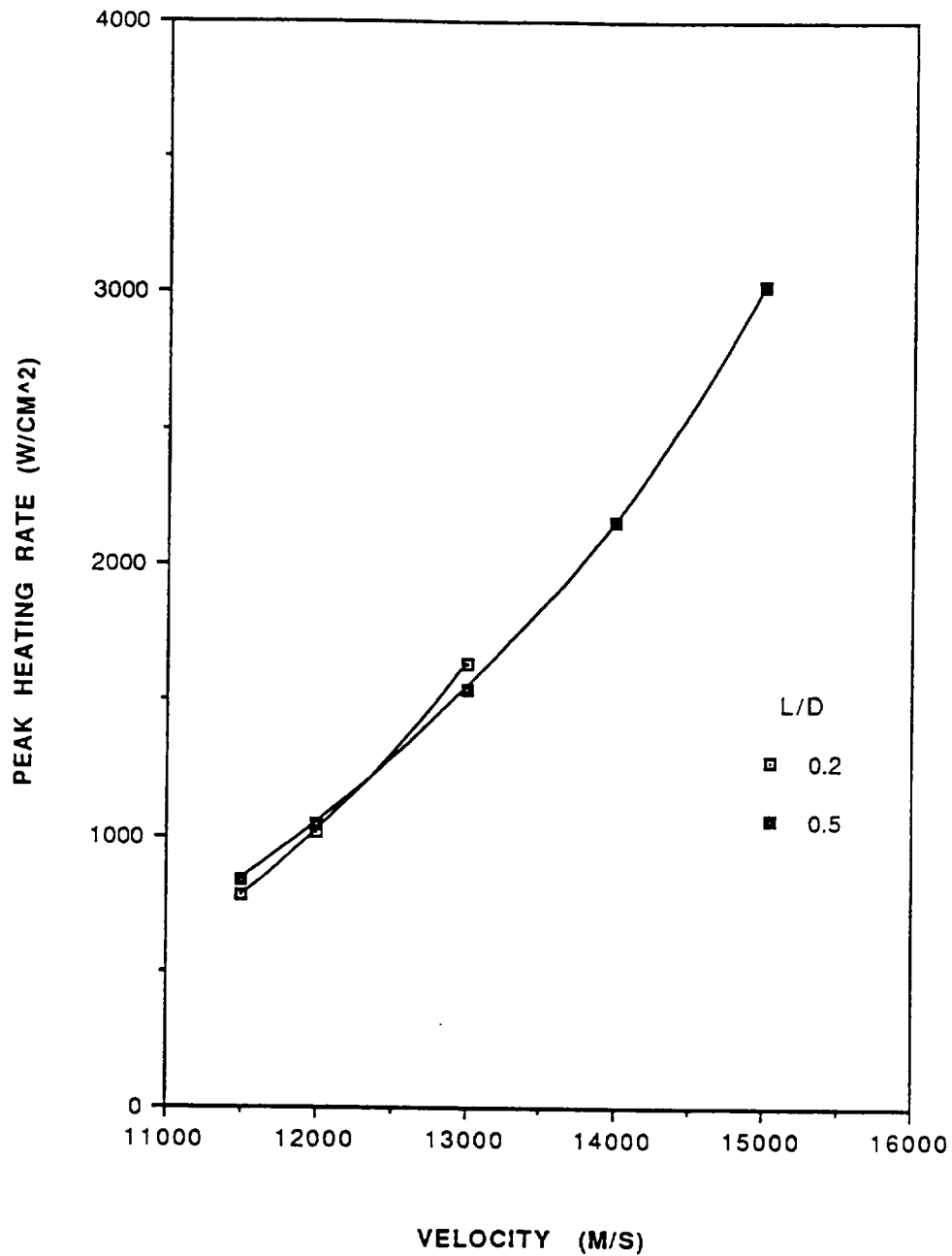
b) BALLISTIC COEFFICIENT = 100 KG/M^2

FIGURE 36. (CONTINUED)



c) BALLISTIC COEFFICIENT = 300 KG/M²

FIGURE 36. (CONTINUED)



d) BALLISTIC COEFFICIENT = 500 KG/M²

FIGURE 36. (CONCLUDED)

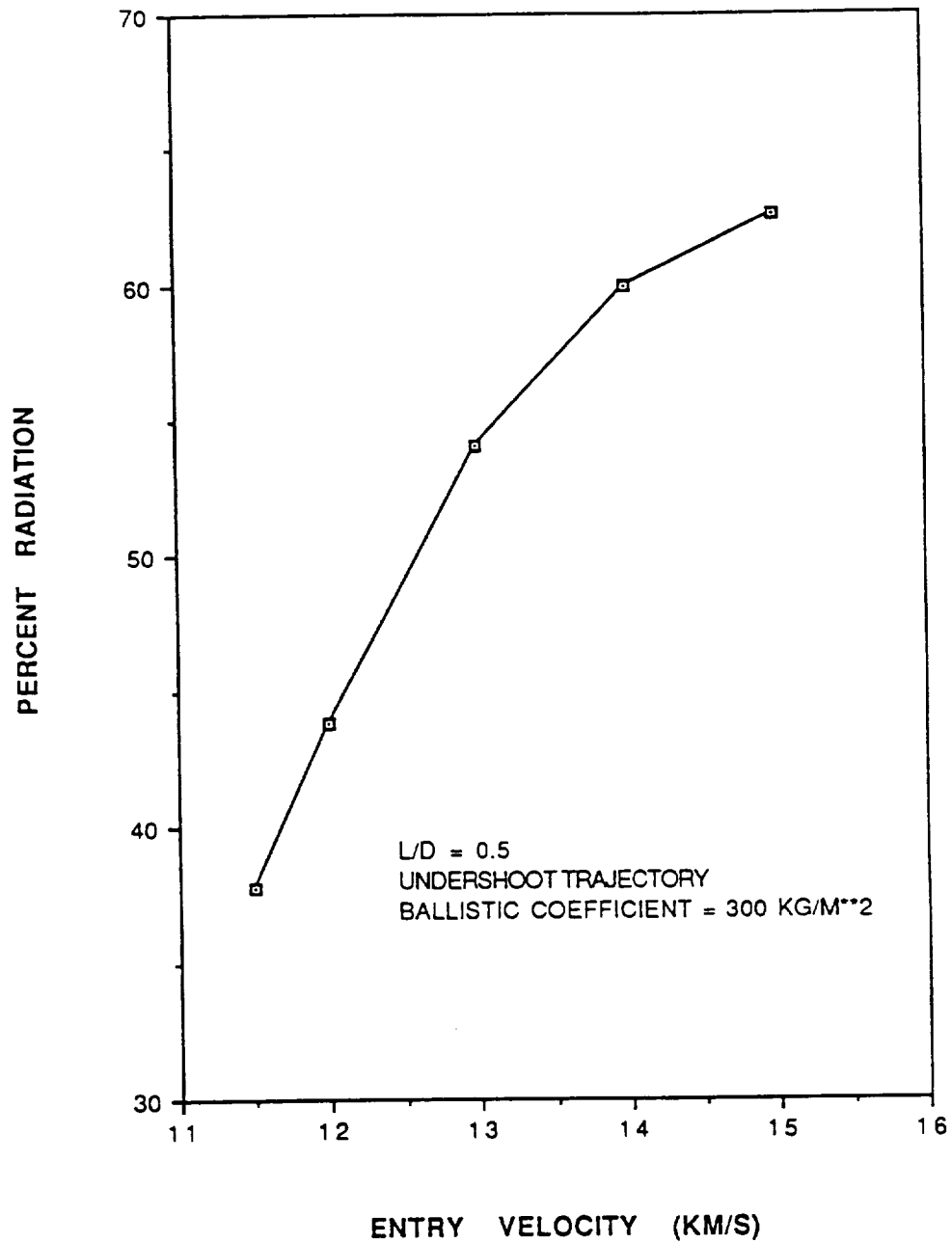


FIGURE 37. PERCENT OF PEAK HEATING
DUE TO RADIATION FOR THE EARTH RETURN
UNDERSHOOT TRAJECTORY

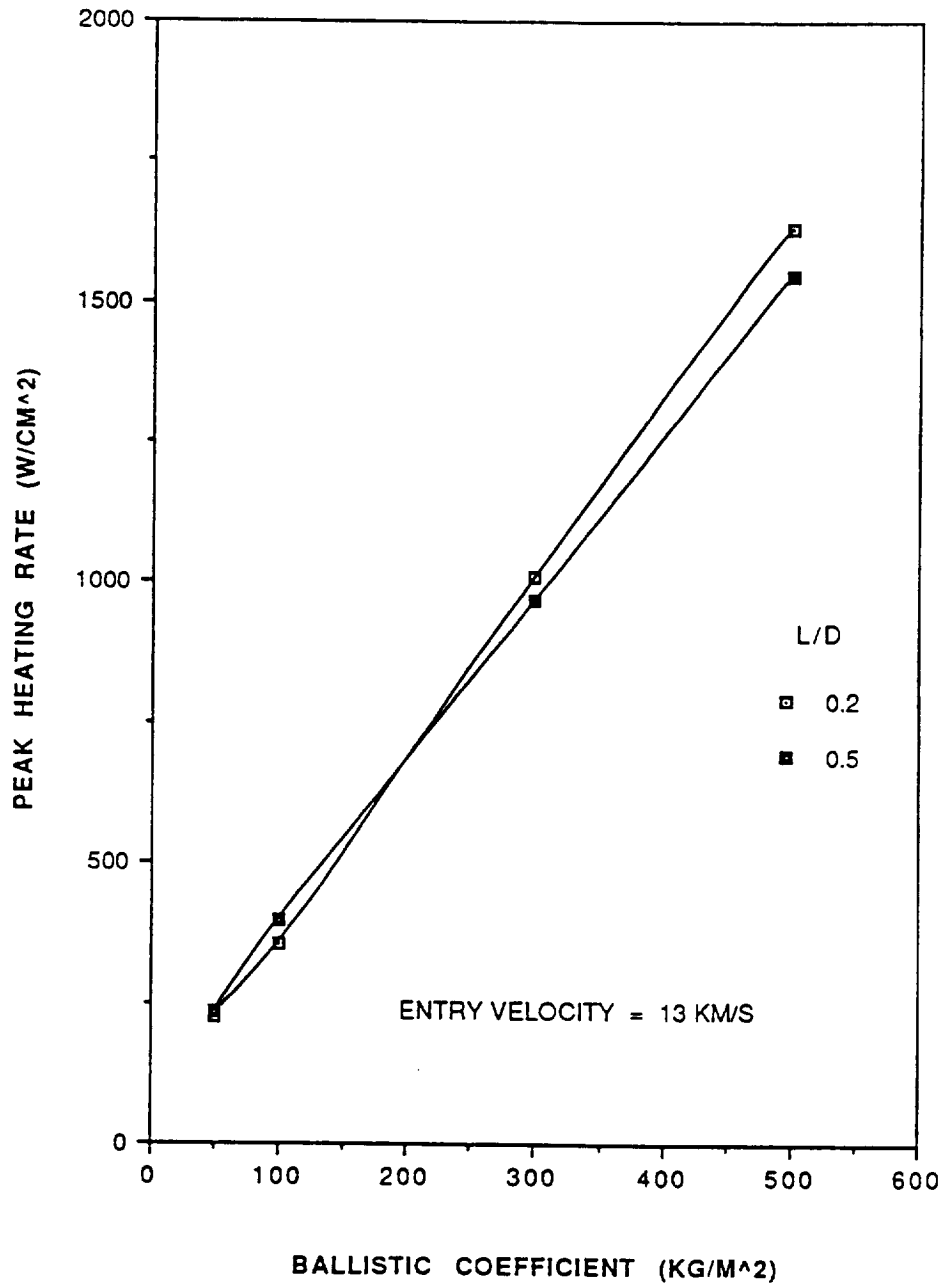


FIGURE 38. STAGNATION POINT PEAK HEATING RATE VS BALLISTIC COEFFICIENT FOR EARTH RETURN UNDERSHOOT TRAJECTORY

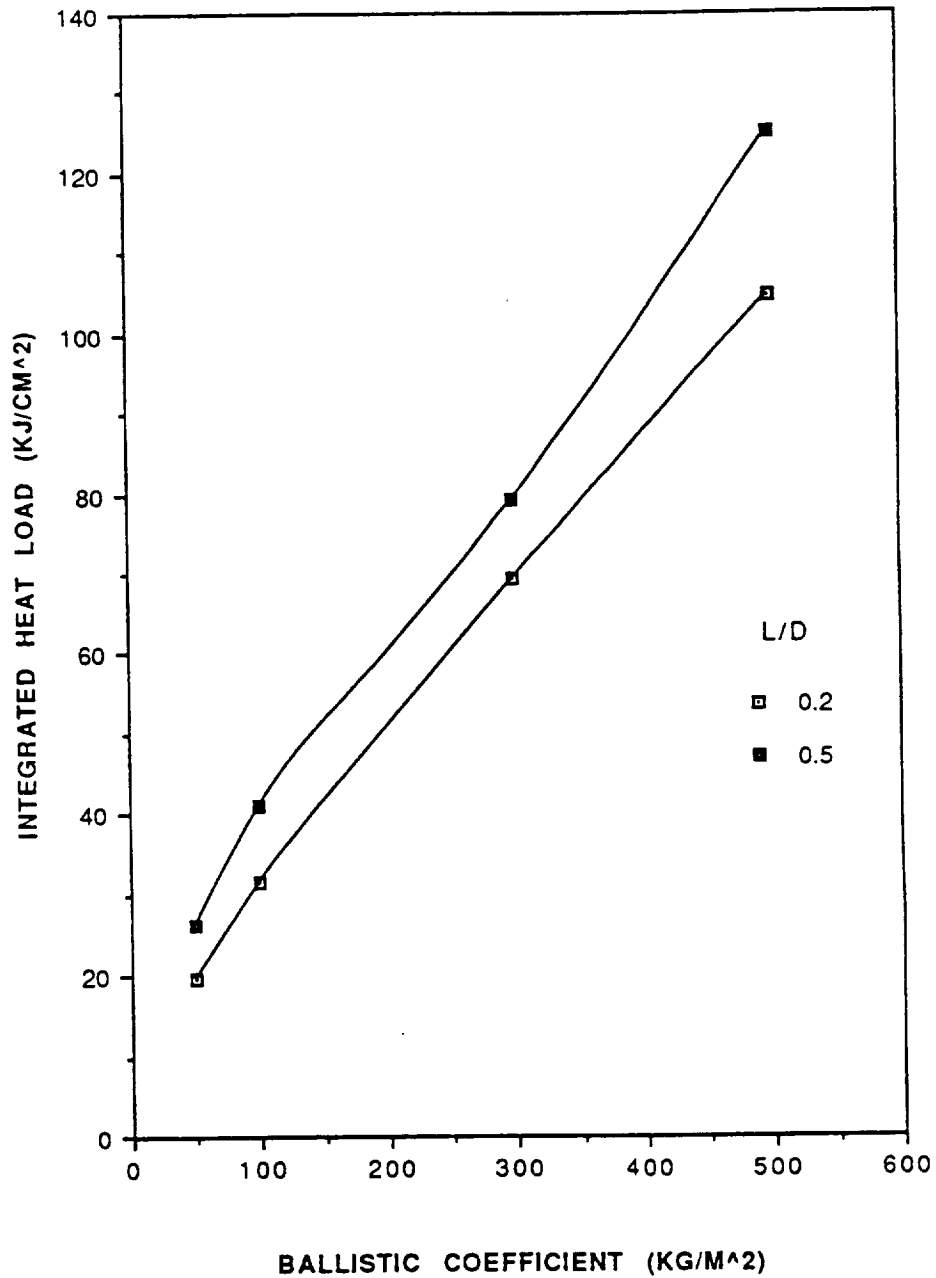
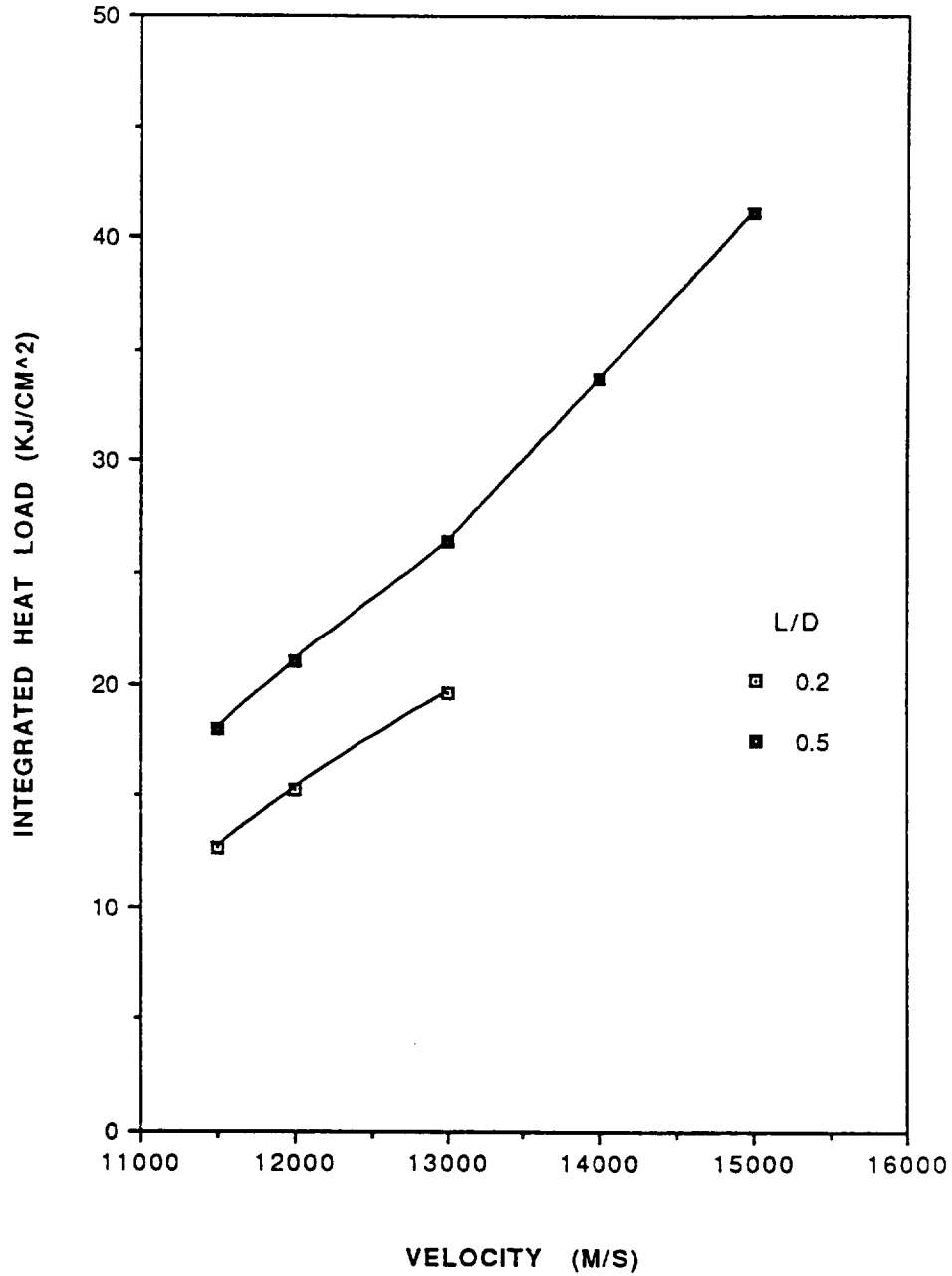
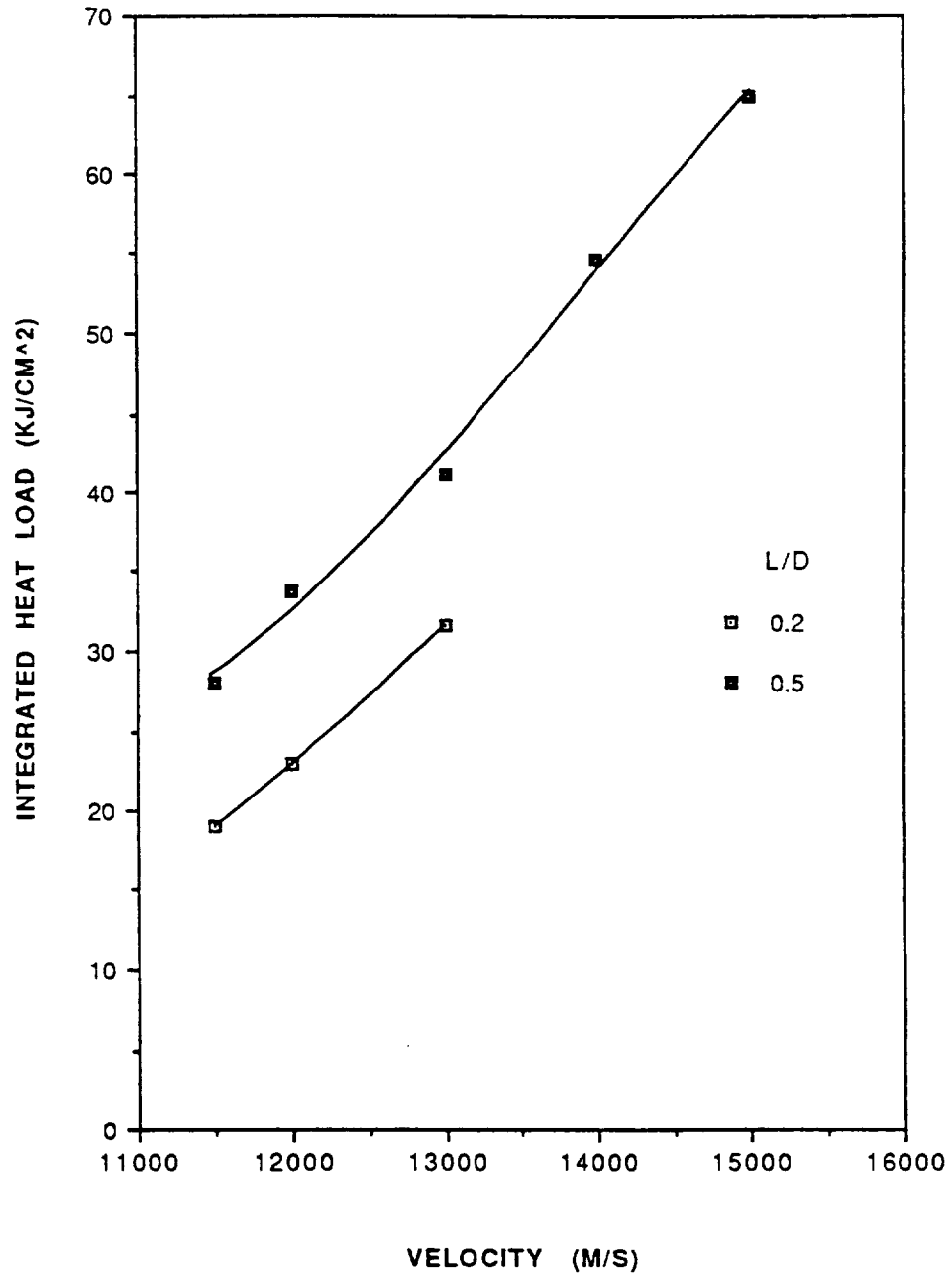


FIGURE 39. STAGNATION POINT INTEGRATED HEAT LOAD VS BALLISTIC COEFFICIENT FOR THE EARTH RETURN OVERSHOOT TRAJECTORY



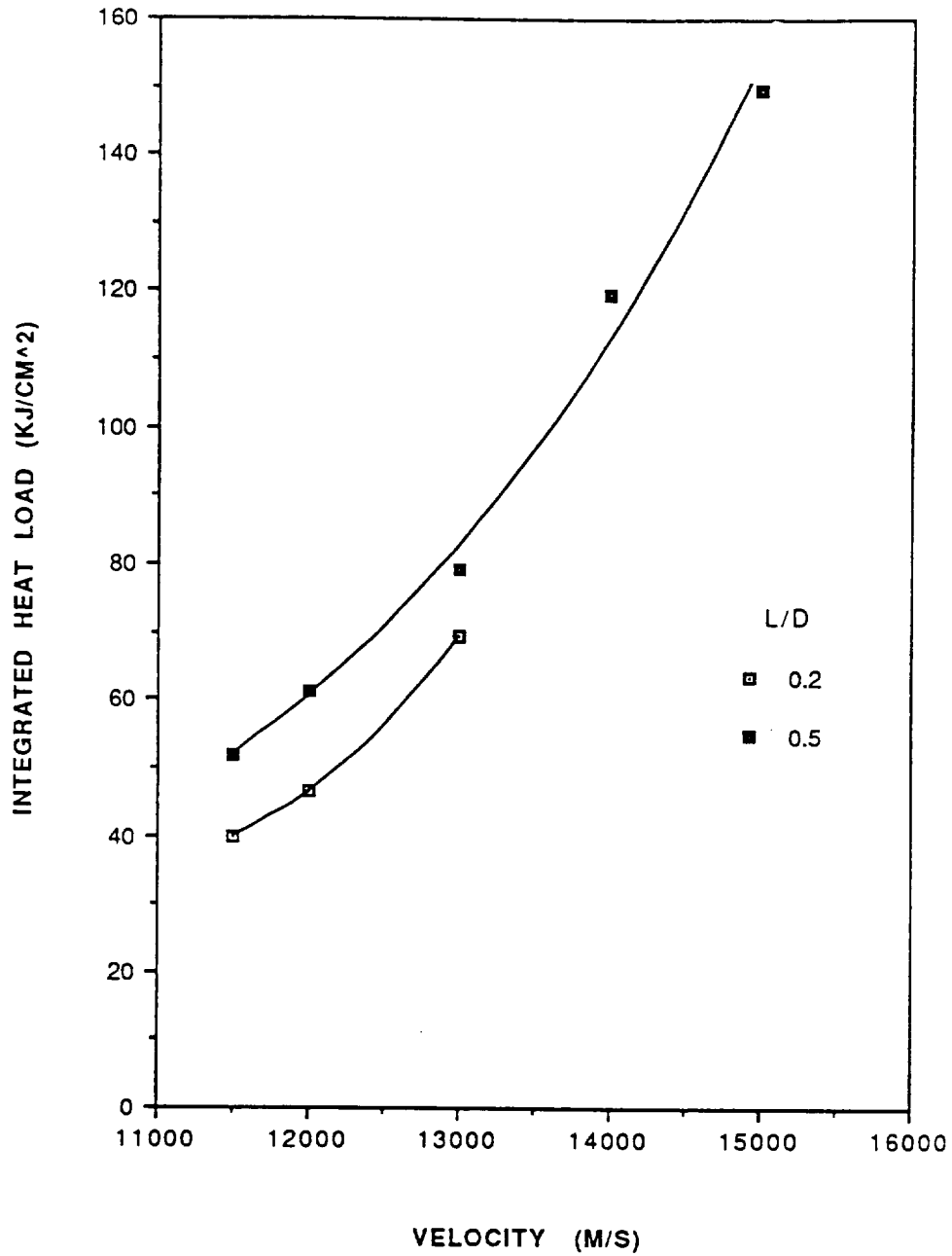
a) BALLISTIC COEFFICIENT = 50 KG/M²

FIGURE 40. STAGNATION-POINT INTEGRATED HEAT LOAD VS ENTRY VELOCITY FOR THE EARTH RETURN OVERSHOOT TRAJECTORY



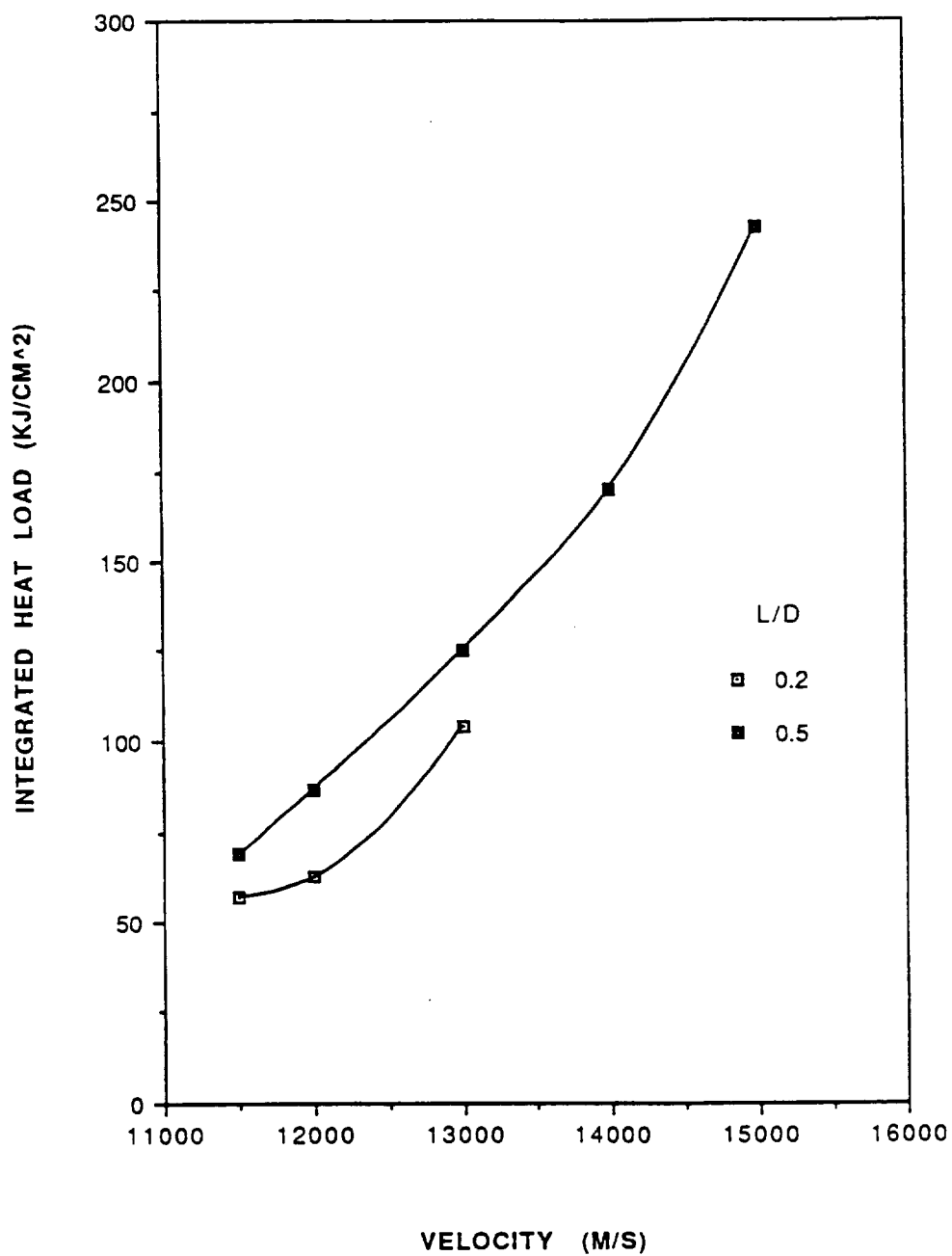
b) BALLISTIC COEFFICIENT = 100 KG/M²

FIGURE 40. (CONTINUED)



c) BALLISTIC COEFFICIENT = 300 KG/M²

FIGURE 40. (CONTINUED)



d) BALLISTIC COEFFICIENT = 500 KG/M²

FIGURE 40. (CONCLUDED)

APPENDIX 1. CONVECTIVE HEATING CALCULATIONS

Equation 8 is used to calculate the stagnation point convective heating rate. It is repeated below for ease of reference:

$$8) \quad q_c = C_1 (\rho_1 / r_n)^{1/2} V^{C_2} (1 - h_w/h_T)$$

This expression contains terms for the enthalpy at the wall, h_w , and the total enthalpy, h_T . The total enthalpy is calculated as the sum of the velocity squared divided by two plus a freestream enthalpy, h_1 :

$$10) \quad h_T = V^2 / 2 + h_1 .$$

At Mars, a constant freestream enthalpy of 137000 J/kg was employed, while at Earth a value of 260000 J/kg was used. The actual freestream enthalpy varies with altitude, but its contribution to the total enthalpy is quite small (under five percent) during the periods of significant heating. Therefore, its variation with altitude was neglected.

The wall enthalpy was calculated as a function of temperature using polynomial expressions derived by Prof. M.E. Tauber for air and carbon dioxide (personal communication of unpublished work, February 1989). The equations used at Earth and Mars respectively are:

$$11) \quad h_w = 940 T_w + 0.1043 (T_w)^2$$

$$12) \quad h_w = 608 T_w + 0.419 (T_w)^2 - 65.6 (10^{-6}) (T_w)^3$$

where T_w is the wall temperature which is calculated assuming a radiatively cooled surface:

$$13) \quad T_w = \left(q_s / (\epsilon \sigma) \right)^{0.25}.$$

ϵ is the surface emissivity which has an assumed value of 0.8, and σ is the Stefan-Boltzman constant, $5.67 (10^{-12}) \text{ W / cm}^2 / \text{K}^4$. To determine the wall temperature, the stagnation point convective heating rate is calculated using the first part of Equation 8) without the wall temperature correction:

$$14) \quad q_c = C1 (\rho_1 / r_n)^{1/2} V^3.$$

APPENDIX 2. COMPUTER ALGORITHM LOGIC

The basic logic used to determine the undershoot boundary is illustrated in Fig. A-1. The user supplies an input file which contains information on the vehicle aerodynamics and entry conditions along with an estimate of the undershoot boundary which must be shallower than the actual limit. The G load limit and the entry angle increment, Δ_γ , are also user supplied parameters. The vehicle flies lifting upward and the entry angle is incremented to steeper values in steps of Δ_γ on successive trajectory simulations until one of the constraints is violated (since a descending vehicle is considered to have a negative flight path angle, Δ_γ is actually subtracted from the current value on each successive run). The steepest entry angle which does not violate the G limit or minimum altitude is the undershoot boundary. A rollover maneuver is then imposed near the low spot in the trajectory during a repeat entry simulation at the undershoot angle; the flight path angle for the beginning and completion of this roll maneuver are user supplied inputs, designated A and C in Fig. A-2a. During this phase, the vehicle bank angle is based solely on the flight path angle. Once the vehicle slows to a user specified fraction, F, of the escape velocity (V_{escp}), a roll reversal begins to lift the aerobrake out of the atmosphere. During this phase, the bank angle is a function of the flight velocity (see Fig. A-2b). The algorithm calculates the orbital period of this undershoot trajectory with the roll maneuvers timed

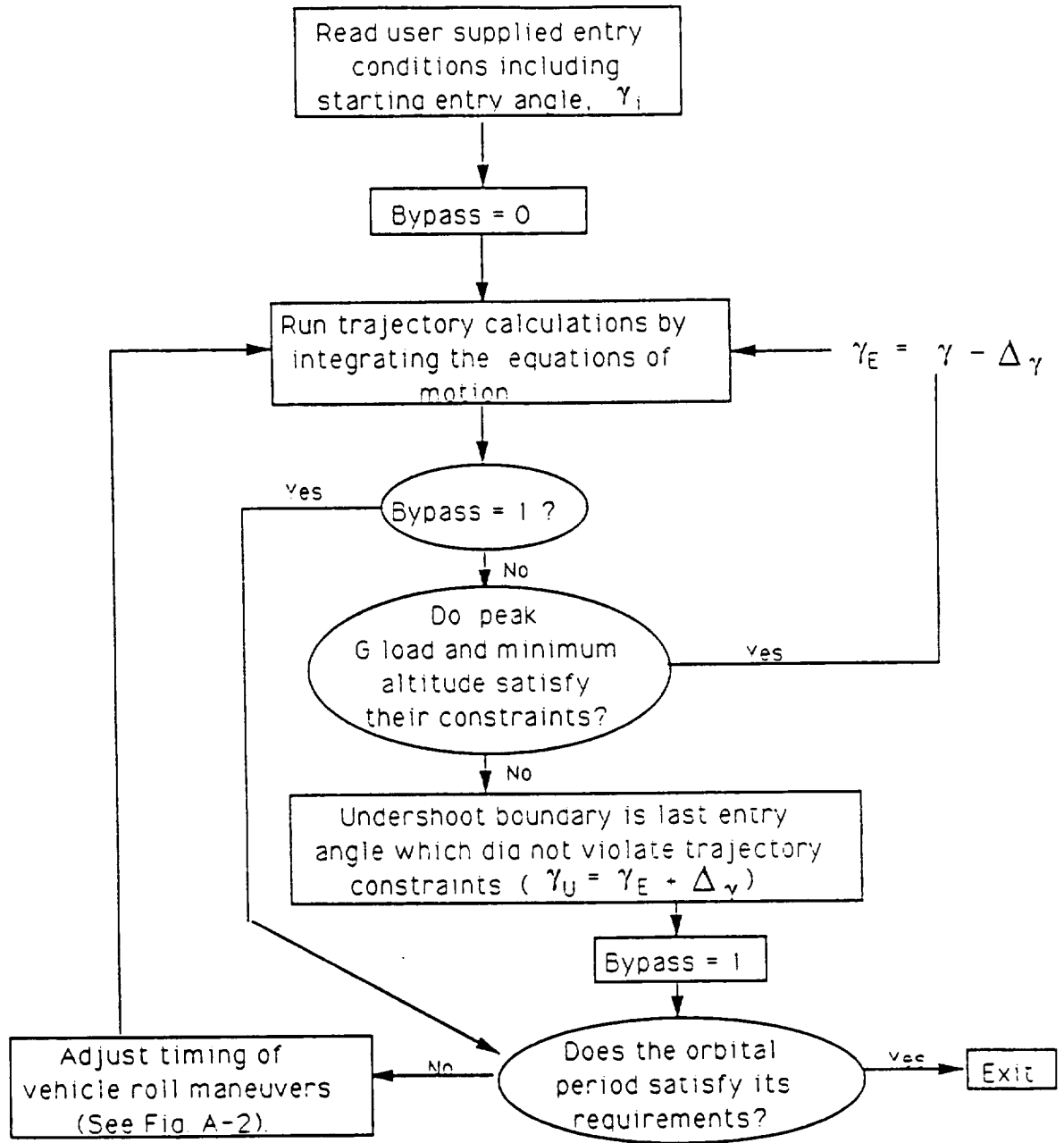


FIGURE A-1. UNDERSHOOT ALGORITHM FLOW CHART

as specified in the user supplied input file and compares this period with that of the specified target orbit.

If the actual orbital period is too long, the algorithm decreases the value of F by 0.01 and the simulation is run again. This process is repeated until the orbital period falls into the specified range. The strategy here is to maintain downward lift longer, thereby holding the vehicle in the atmosphere longer and dissipating more energy. The process is repeated for up to forty iterations. If it is not successful in adequately reducing the orbital period after this many steps, the vehicle is bouncing out of the atmosphere despite application of maximum downlift after the initial rollover. Therefore, it becomes necessary to execute the initial rollover earlier in the trajectory. To do this, the value of A , the flight path angle at which the roll maneuver begins, is changed by 0.1 degrees to a steeper angle in successive trajectory simulations until the orbital period is acceptable.

Conversely, if the orbital period is initially too short, the value of F is increased by 0.01 and the entry simulation is repeated. If this is not successful after 30 iterations, the initial rollover is delayed by increasing the value of the parameter A (to a less negative number) in steps of 0.1 degrees until the orbital period is satisfactory. If the period goes from too long to too short with one of these adjustments, the step size in either A or F is divided by two for the next iteration.

In most cases, the initial roll maneuver has been completed before the flight velocity falls below its threshold value, $F \times V_{\text{escp}}$. This

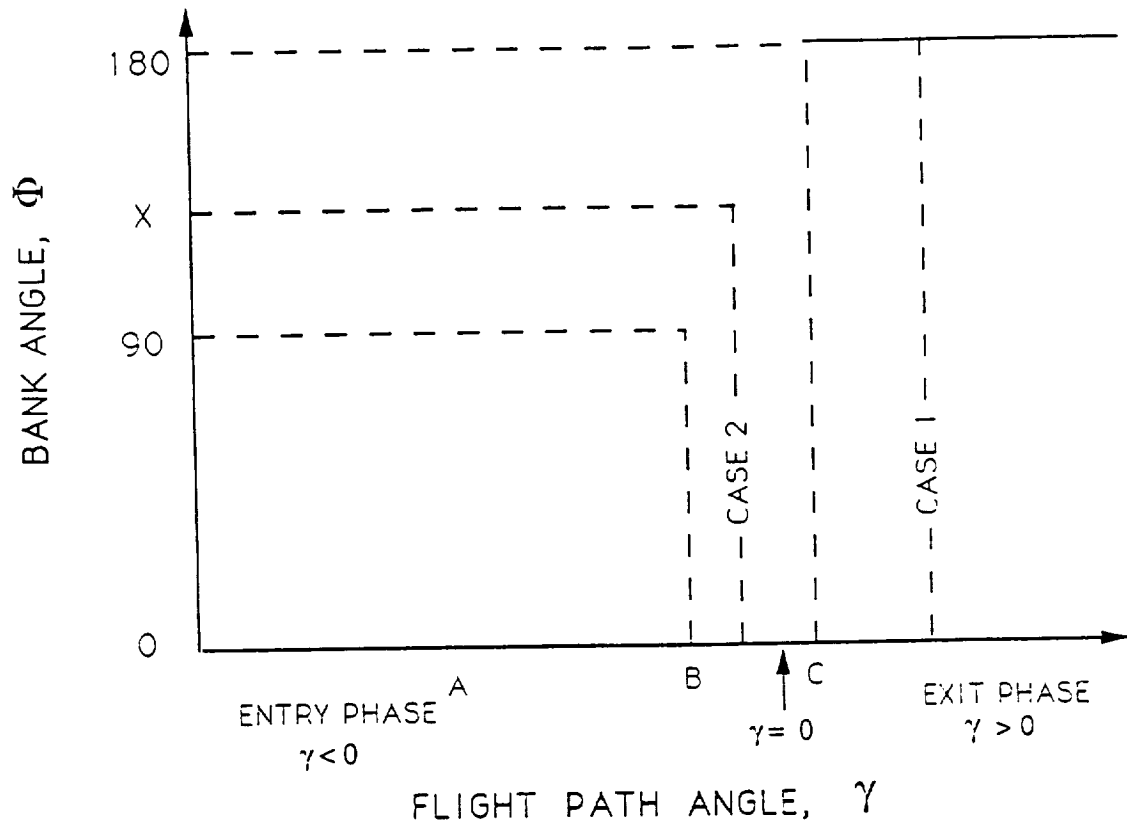


FIGURE A-2a. VARIATION OF BANK ANGLE WITH FLIGHT PATH ANGLE

Note: 1) For $A < \gamma < B$, $\phi = 90 - 90 \left(\frac{B - \gamma}{B - A} \right)$

2) For $B < \gamma < C$, $\phi = 90 - 90 \left(\frac{\gamma - B}{C - B} \right)$

3) For $\gamma > C$, $\phi = 180$

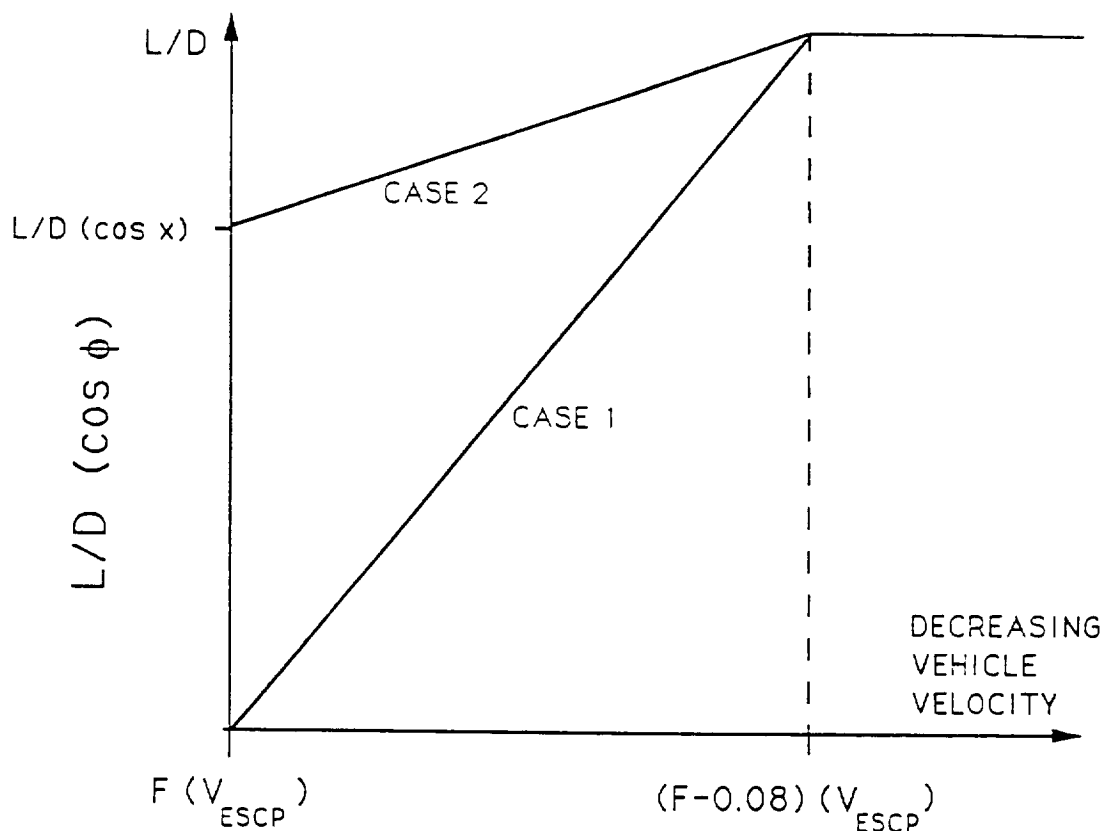


FIGURE A-2b. VARIATION OF BANK ANGLE WITH VEHICLE VELOCITY

Note: 1) For $(F-0.08)(V_{ESCP}) < V < F(V_{ESCP})$

$$L/D \cos \phi = L/D \cos \phi_v + \frac{F(V_{ESCP}) - V}{0.08(V_{ESCP})} (L/D - L/D \cos \phi_v)$$

Where ϕ_v is the vehicle bank angle when the velocity drops below its threshold value, and bank angle becomes a function of velocity. For Case 1, ϕ_v is 180 degrees, while for Case 2 it equals X.

2) For $V < (F-0.08)(V_{ESCP})$, $\phi = 0$

situation is depicted by Case 1 in Fig. A-2. The roll reversal begins with ϕ equal to 180 degrees. However, in some cases, the flight velocity drops below the threshold before the vehicle has completed its initial rollover. This situation is illustrated by Case 2 in Fig. A-2 where the roll reversal begins with ϕ equal to some value x which is less than 180 degrees.

The typical user-specified, initial values for A, C, and F are -1.0, 0.1, and 0.98 respectively. The parameter B is calculated as $C - 0.2$.

REPORT DOCUMENTATION PAGE

Form Approved
OMB No. 0704-0188

Public reporting burden for this collection of information is estimated to average 1 hour per response, including the time for reviewing instructions, searching existing data sources, gathering and maintaining the data needed, and completing and reviewing the collection of information. Send comments regarding this burden estimate or any other aspect of this collection of information, including suggestions for reducing this burden, to Washington Headquarters Services, Directorate for Information Operations and Reports, 1215 Jefferson Davis Highway, Suite 1204, Arlington, VA 22202-4302, and to the Office of Management and Budget, Paperwork Reduction Project (0704-0188), Washington, DC 20503.

1. AGENCY USE ONLY (Leave blank)		2. REPORT DATE August 1992	3. REPORT TYPE AND DATES COVERED Technical Memorandum	
4. TITLE AND SUBTITLE Physiologically Constrained Aerocapture for Manned Mars Missions			5. FUNDING NUMBERS 505-40-61	
6. AUTHOR(S) James Evans Lyne				
7. PERFORMING ORGANIZATION NAME(S) AND ADDRESS(ES) Ames Research Center Moffett Field, CA 94035-1000			8. PERFORMING ORGANIZATION REPORT NUMBER A-92149	
9. SPONSORING/MONITORING AGENCY NAME(S) AND ADDRESS(ES) National Aeronautics and Space Administration Washington, DC 20546-0001			10. SPONSORING/MONITORING AGENCY REPORT NUMBER NASA TM-103954	
11. SUPPLEMENTARY NOTES Point of Contact: Michael Tauber, Ames Research Center, MS 229-3, Moffett Field, CA 94035-1000 (415) 604-6086				
12a. DISTRIBUTION/AVAILABILITY STATEMENT Unclassified — Unlimited Subject Category 18			12b. DISTRIBUTION CODE	
13. ABSTRACT (Maximum 200 words) Aerobraking has been proposed as a critical technology for manned missions to Mars. The variety of mission architectures currently under consideration presents aerobrake designers with an enormous range of potential entry scenarios. Two of the most important considerations in the design of an aerobrake are the required control authority (lift-to-drag ratio) and the aerothermal environment which the vehicle will encounter. Therefore, this study examined the entry corridor width and stagnation-point heating rate and load for the entire range of probable entry velocities, lift-to-drag ratios, and ballistic coefficients for capture at both Earth and Mars. To accomplish this, a peak deceleration limit for the aerocapture maneuvers had to be established. Previous studies had used a variety of load limits without adequate proof of their validity. Existing physiological and space flight data were examined, and it was concluded that a deceleration limit of 5 G was appropriate. When this load limit was applied, numerical studies showed that an aerobrake with an L/D of 0.3 could provide an entry corridor width of at least 1 degree for all Mars aerocaptures considered with entry velocities up to 9 km/s. If 10 km/s entries are required, an L/D of 0.4 to 0.5 would be necessary to maintain a corridor width of at least 1 degree. For Earth return aerocapture, a vehicle with an L/D of 0.4 to 0.5 was found to provide a corridor width of 0.7 degree or more for all entry velocities up to 14.5 km/s. Aerodynamic convective heating calculations were performed assuming a fully catalytic, "cold" wall; radiative heating was calculated assuming that the shock layer was in thermochemical equilibrium. Heating rates were low enough for selected entries at Mars that a radiatively cooled thermal protection system might be feasible, although an ablative material would be required for most scenarios. Earth return heating rates were generally more severe than those encountered by the Apollo vehicles, and would require ablative heat shields in all cases.				
14. SUBJECT TERMS Aerocapture, Manned Mars missions, Deceleration limit			15. NUMBER OF PAGES 150	
			16. PRICE CODE A07	
17. SECURITY CLASSIFICATION OF REPORT Unclassified	18. SECURITY CLASSIFICATION OF THIS PAGE Unclassified	19. SECURITY CLASSIFICATION OF ABSTRACT	20. LIMITATION OF ABSTRACT	